A VIBRATORY SYSTEM FOR MEASURING RATES OF TURN

J. A. LINNETT

Thesis Submitted for the degree of

Doctor of Philosophy

University of Edinburgh

March 1968

ACKNOWLEDGEMENTS

The author gratefully acknowledges the advice of his supervisors, in particular Dr. A. D. S. Barr, at present Acting Head of the Department of Mechanical Engineering and Dr. J. D. Robson, formerly of this Department but now Rankine Professor of Mechanical Engineering at the University of Glasgow.

Special thanks are due also to Mr. George Smith for his advice and skill in the construction of the apparatus and to Miss Sally Birtwisle for her typing.

S Y N O P S I S

Vibratory rate sensing devices operate by measuring the vibrations induced by the Coriolis acceleration when a vibrating inertia is rotated. A double torsion rate sensor is investigated but it is shown to offer few advantages over the conventional tuning fork.

The equations of motion are developed for a more fundamental vibratory rate sensor consisting of a point mass with its motion constrained to one plane and controlled by linear springs and viscous dampers. Amplitude and phase angle relationships between the excited vibrations and the quadrature vibrations, induced by rotation and inherent coupling, demonstrate the possibility of measuring the rate of turn about an axis perpendicular to the plane of vibration by means of the phase angle in the regions where the coupling results in very little variation in amplitude. In addition the shape of the phase angle curve, unlike the amplitude curve, is shown to be independent of damping, thus making it possible to have a damping ratio high enough to give an acceptable transient response without affecting the sensitivity. This offers considerable advantages over the conventional vibratory rate sensor in which the rate is determined solely from the amplitude of the induced vibrations.

Two possible methods of using a second excitation source, in quadrature with the original one, are considered; it can be used

either to eliminate the quadrature vibrations at zero rate input, in which case the rate of turn can be measured by the amplitude ratio, or to eliminate the quadrature vibrations at all rates, in which case the rate of turn is measured by the amplitude and phase relationships between the two excitation forces.

Experiments carried out with a device approximating to the fundamental rate sensor demonstrate the validity of the derived theory.

CONTENTS

Page No:

CHAPTER 1

Introduction

1.1 The requirement for an alternative to the conventional gyroscope

The conventional rotating wheel gyroscope has played an increasingly important part in the navigation and guidance of vehicles since its first commerical use as a gyrocompass in ships at the turn of the century. Until the 1950's only relatively crude, and therefore inexpensive, gyroscopic devices were required for instruments and automatic guidance controls but recently the increasing speed of aircraft and rockets has demanded much more accurate control and, consequently, more sophisticated instruments. In particular, the development of inertial navigation has depended upon the availability of exceedingly accurate and sensitive gyroscopes.

Industry has been able to fulfill this demand for accurate instruments by continuous development of its manufacturing techniques, but the extremely small tolerances and the rigorous testing that is required in a modern gyroscope has resulted in a considerable escalation on its price. Consequently a lot of research effort has gone into the development of other devices capable of measuring rates of turn (see, for example the papers by Langford* and Stratton); one alternative to the conventional gyroscope is a device sensing rotation by means of a vibratory sensitive element.

* the references are listed alphabetically in the Bibliography.

The basic principle of a vibratory rate sensing device is that, if a mass vibrating in a straight line is subjected to an angular rate of turn about an axis perpendicular to that line, the resulting Coriolis acceleration generates an alternating reactive forcewhich induces motion in a direction perpendicular to both the original vibration line and the turning axis; in a linear spring-mass system the amplitude of the induced vibration is proportional to the rate of turn.

Vibratory devices appeared to offer excellent prospects for development into inexpensive, accurate and long lasting rate sensing instruments, the simplicity of the system and the lack of bearings seemed to be the main advantates. As a result, a considerable amount of effort was put into trying to produce a practical device of this type which would have an accuracy comparable to that of an inertial quality conventional gyroscope; the net result of all this work up to now can be judged by noting that no instrument of this type has been produced capable of giving this sort of accuracy.

1.2 The development of vibratory inertial sensors.

Although the Foucault pendulum (the original gyroscope) may be considered to be a vibratory device, the first attempt at making a small instrument employing a vibrating mass to measure rate of turn was probably made by Meredith in 1942, however his paper, published by Nature in 1949, points out that an order of flying insect known as the Diptera use a device of this kind; these insects have a pair of small organs, called halteres, which take the place of hind wings and vibrate at high frequency enabling them to fly in a stable manner (the mathematical theory is developed by Pringle).

The main disadvantage of the early instruments, which employed a single vibrator, was the difficulty of eliminating various errors, particularly those due to motion of the complete instrument. To overcome this problem most of the research has been concentrated on systems using balanced oscillators, the tuning fork being the most favoured device.

The developments in the United States led to the production of the Sperry Rate Gyrotron in 1953, the characteristics of which are described by Barnaby et al., Lyman and Morrow. In this country the majority of the work has been carried out by the Royal Aircraft Establishment at Farnborough and is covered in reports by Hobbs, Hunt, Pitt and Stratton. Some research has also been carried out in France and is reported by Mathey and Ettzeroglou.

The bibliography lists other reports and books covering various types of vibratory rate sensors and papers by Chatterton and Newton comparing vibratory and conventional rate sensors. The theory for the tuning fork is covered in the book by Arnold and Maunder and also in many of the papers listed; the well known paper by Fearnside and Briggs also discusses the possibility of instabilities occuring in this type of device.

As far as can be ascertained, all of the vibratory sensors that have been evaluated up to now have determined the rate of turn by measuring the amplitude of the vibration that has been induced by the Coriolis force; because the Coriolis force is comparatively small this has meant that any unwanted forces due to unbalance or other imperfections in the system have had to be reduced to a very low order, otherwise the measurement of very small rates of turn is impossible. Thus the instruments have been manufactured necessarily to very small tolerances and a thorough balancing procedure had to be carried out before it was possible to measure small rates.

The very small amplitudes that have to be measured and the difficulty in eliminating errors due to imperfections have been the main reasons why this type of instrument has not so far achieved the accuracy that was hoped for. The amount of research that has been carried out can be judged from the number of published papers, of which the bibliography doesn't claim to be a complete list, and the continued interest can be assessed by noting that at the Symposium on Gyros held in London in 1965, there was more discussion on the paper by Hunt and Hobbs than on most of the other papers that were presented.

1.3 Research at this University

The main difficulty in carrying out research into gyroscopic instruments at University level is the high cost of manufacturing any inertial sensor to the accuracy necessary for present day requirements. Therefore the main task must be to develop the basic principles and to test out the theory with relatively inexpensive apparatus which cannot be expected to have great accuracy or sensitivity.

Research on a double torsion type of vibratory rate sensor as an alternative to the tuning fork had been carried out here up to 1961 by McLean. A modified device of the same type was considered as it appeared to incorporate some improvements, however the conclusion was reached that this type of instrument did not have any significant advantages over the tuning fork (this is discussed in more detail in chapter 2). However this work did lead back to a consideration of the fundamental equations governing a vibratory rate sensing device, in particular the consideration that these instruments possessed two degrees of freedom; the theory, as it is usually presented, assumes that the amplitude to the forced sensing vibrations remains constant (it is normally maintained constant by a control system) this means that only one equation of motion is involved and the system effectively possesses only a single degree of freedom.

Consideration of the equations of motion for a fundamental vibratory rate sensor led to the theory described in the main part of this thesis and to the construction of a device capable of measuring down to rates of the order of 1,000 ^{o}/hr. In order to be of inertial quality a gyroscope must be capable of measuring down to about 1 min. of arc/hr. i.e. a sensitivity 6×10^4 greater than that achieved; however the device was not constructed with the object of producing a practical instrument so that a considerable improvement in accuracy and sensitivity should be possible.

CHAPTER 2

Preliminary Investigation and First Experimental Set-Up

2.1 Preliminary Investigations

The previous work carried out by McLean had concentrated on a double torsion type of vibrating gyro, fig,2.1.1., which differed from a conventional rotating wheel single axis rate gyroscope in that the rotor, instead of being rotated at constant angular velocity, was attached to a torsion shaft and excited at its natural frequency about the axis Oz. This meant that rotation about the input axis OY caused the system to vibrate about the output axis OX, the amplitude of the steady state vibration being proportioned to the imposed rate of turn about OY.

It is the Coriolis acceleration that is employed in a vibratory rate sensor and it seemed that McLeans device suffered from the disadvantage that a considerable proportion of the mass of the rotor, that adjacent to the OX axis, was subjected to very little Coriolis acceleration when rotation took place about OY. A dumbell shaped sensitive element where the mass was concentrated around the position of maximum Coriolis acceleration, viz. near the input axis OY, would appear to have considerable advantages.

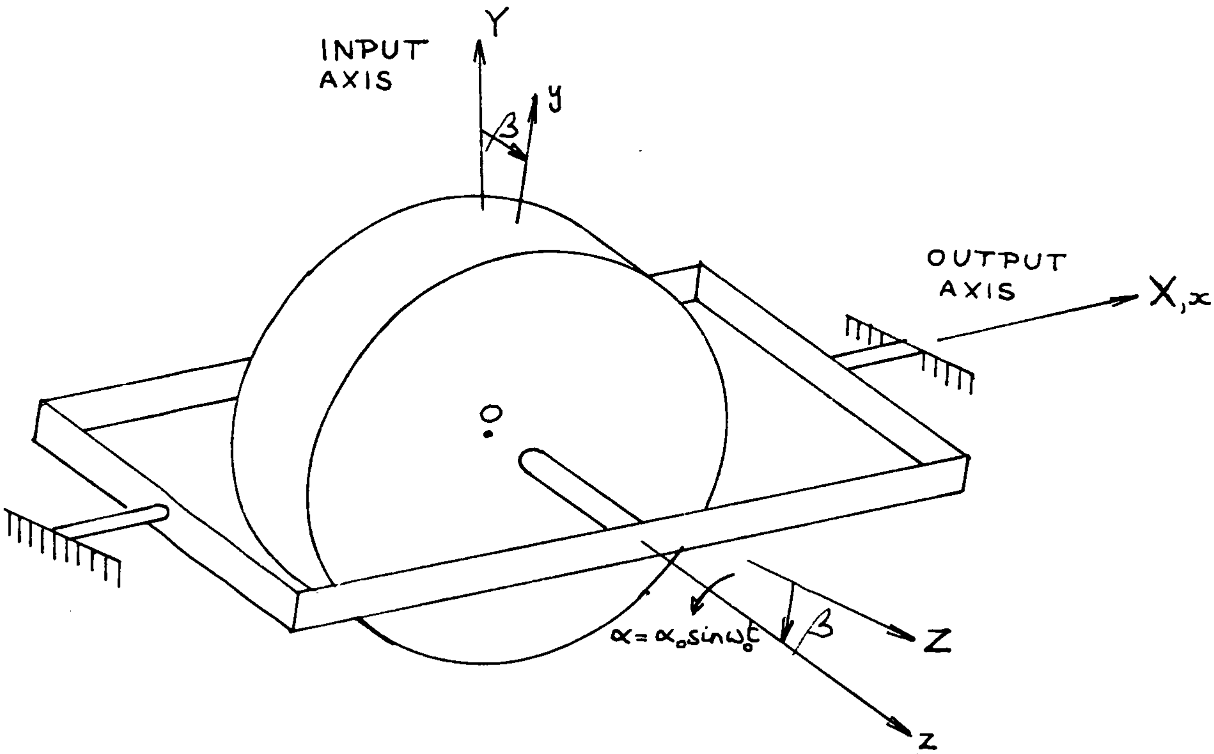

FIG. 2.1.1
Mcleans Rate Sensing Device

2.2 Theory

The device chosen is shown on the photograph, fig. 2.2.1., and diagrammatically in fig.2.2.2. An additional advantage of the design was that the conventional gimbal of McLeans device could be replaced by an internal gimbal, consisting of a clamping unit between the two shafts, with a consequent reduction in weight and output axis inertia. The sensitive element was vibrated about the Oz axis through an angle $\alpha = \alpha_0 \sin \omega_0 t$ at the natural frequency about that axis, ω_0, and the angular deflection, β about the OX axis, measured.

Taking axes OXYZ fixed to the vehicle and rotating at angular velocity

$$\bar{\Omega} = \Omega_1 \bar{I} + \Omega_2 \bar{J} + \Omega_3 \bar{K} \qquad (2.2.1)$$

(where $\bar{I}$, $\bar{J}$, and $\bar{K}$ are unit vectors along OX, OY and OZ respectively) and axes Oxyz rotating with the sensitive element through an angle β about OX, so that their angular velocity

$$\bar{\omega} = \omega_1 \bar{i} + \omega_2 \bar{j} + \omega_3 \bar{k} \qquad (2.2.2)$$

(where $\bar{i}$, $\bar{j}$, and $\bar{k}$ are unit vectors along Ox, Oy, and Oz respectively) for $\beta \ll 1$ is given by

$$\left.\begin{aligned} \omega_1 &= \Omega_1 + \dot{\beta} \\ \omega_2 &= \Omega_2 + \Omega_3 \beta \\ \omega_3 &= \Omega_3 - \Omega_2 \beta \end{aligned}\right\} \qquad (2.2.3)$$

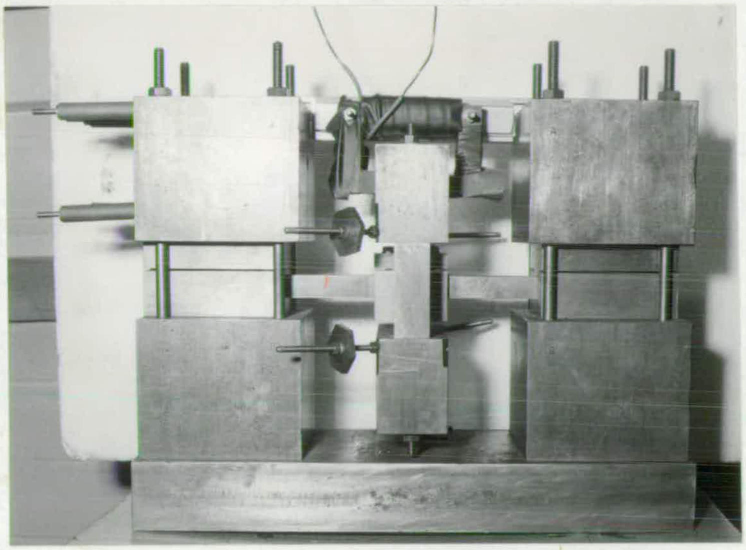

Fig. 2.2.1 Double torsion vibratory rate sensor

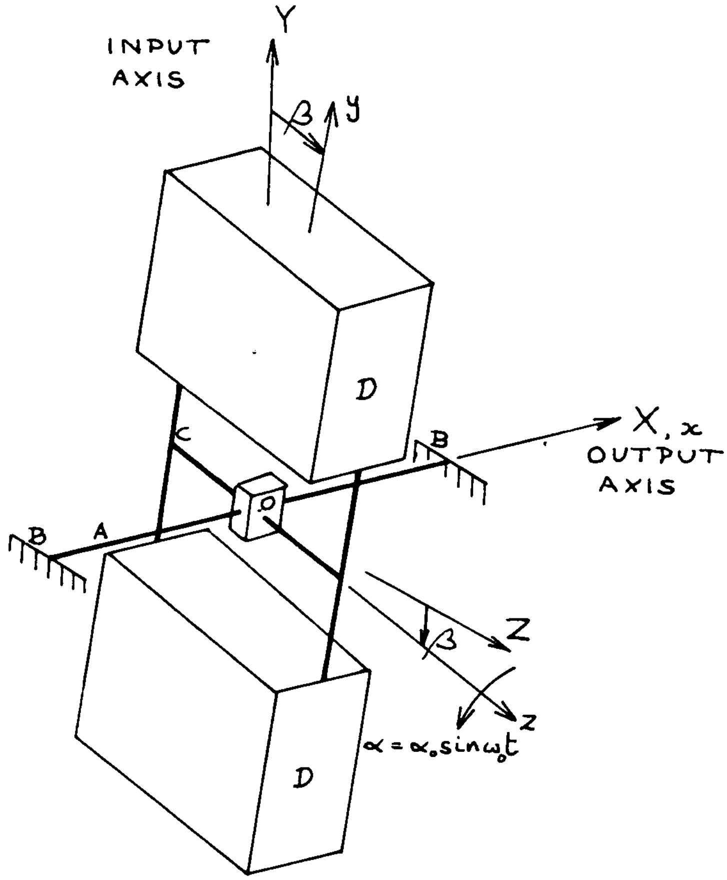

FIG. 2.2.2

Double Torsion Vibratory Rate Sensor

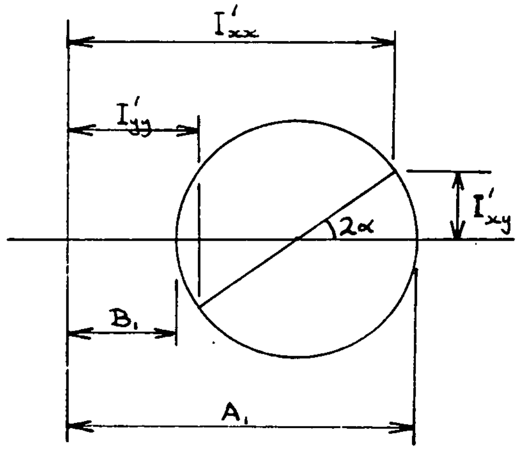

FIG. 2.2.3

Mohr Circle for Rotation of the Sensitive Element about Oz

If the sensitive element has principal moments of inertia A_1, B_1; C_1, the moment and product of inertia, w.r.t.Oxyz, due to rotation α about the axis Oz are determined from the Mohr circle, fig 2.2.3, to be:

$$\left.\begin{aligned} I'_{xx} &= \frac{A_1 + B_1}{2} + \frac{A_1 - B_1}{2}\cos 2\alpha \\ I'_{yy} &= \frac{A_1 + B_1}{2} - \frac{A_1 - B_1}{2}\cos 2\alpha \\ I'_{xy} &= -\frac{A_1 - B_1}{2}\sin 2\alpha \end{aligned}\right\} \qquad (2.2.4)$$

$$\left.\begin{aligned} \text{also} \quad I'_{zz} &= C_1 \\ \text{and} \quad I'_{yz} &= I'_{zx} = 0 \end{aligned}\right\} \qquad (2.2.5)$$

The angular velocity of the sensitive element, assuming that all the rotation relative to OXYZ takes place about OX, is $\bar{\omega} + \dot{\alpha}\,\bar{k}$ so that, from Arnold and Maunder equation 35 page 91, its relative angular momentum $\bar{h}' = h'_1\bar{i} + h'_2\bar{j} + h'_3\bar{k}$ has components:

$$\left.\begin{aligned} h'_1 &= I'_{xx}(\Omega_1 + \dot{\beta}) + F\alpha(\Omega_2 + \Omega_3\beta) \\ h_2 &= I'_{yy}(\Omega_2 + \Omega_3\beta) + F\alpha(\Omega_1 + \dot{\beta}) \\ h_3 &= I'_{zz}(\Omega_3 - \Omega_2\beta + \dot{\alpha}) \end{aligned}\right\} \qquad (2.2.6)$$

where $F = A_1 - B_1$ (2.2.7)

From Arnold and Maunder equations 33 page 90 the torque about the output axis is given by:

$$T_1 = \dot{h}_1 - h_2\omega_3 + h_3\omega_2 \qquad (2.2.8)$$

where h_1, h_2 and h_3 include the angular momentem of the clamping unit, i.e.

$$\left.\begin{aligned} h_1 &= h_1' + A_2\,(\Omega_1+\dot{\beta}) \\ h_2 &= h_2' + B_2\,(\Omega_2+\Omega_3\beta) \\ h_3 &= h_3' + C_2\,(\Omega_3-\Omega_2\beta) \end{aligned}\right\} \qquad (2.2.9)$$

where A_2, B_2 and C_2 are the principal moments of inertia of the clamping unit about Ox, Oy and Oz respectively.

If the output shaft has viscous damping constant c and stiffness k, from equation (2.2.8) we have:

$$\begin{aligned} -k\beta - c\dot{\beta} = &\Big\{(I_{xx}'+A_2)(\dot{\Omega}_1+\ddot{\beta}) + \left(\frac{dI_{xx}'}{dt}\right)(\Omega_1+\dot{\beta}) \\ &+ F\alpha(\dot{\Omega}_2+\Omega_3\dot{\beta}+\dot{\Omega}_3\beta) + F\dot{\alpha}(\Omega_2+\Omega_3\beta)\Big\} \\ &-\Big\{(I_{yy}'+B_2)(\Omega_2+\Omega_3\beta)(\Omega_3-\Omega_2\beta) \\ &+ F\alpha(\Omega_1+\dot{\beta})(\Omega_3-\Omega_2\beta)\Big\} \\ &+\Big\{(I_{zz}'+C_2)(\Omega_3-\Omega_2\beta)(\Omega_2+\Omega_3\beta) \\ &+ I_{zz}'\dot{\alpha}\,(\Omega_2+\Omega_3\beta)\Big\} \qquad (2.2.10) \end{aligned}$$

Assuming that $\alpha \ll 1$, from (2.2.4):

$$\left.\begin{aligned} I_{xx}' &\doteqdot A_1 \\ I_{yy}' &\doteqdot B_1 \\ \frac{dI_{xx}'}{dt} &= -(A_1 - B_1)\sin 2\alpha\,.\,\dot{\alpha} \doteqdot -2F\alpha\dot{\alpha} \end{aligned}\right\} \qquad (2.2.11)$$

so that, taking $A = A_1 + A_2$, $B = B_1 + B_2$ and $C = C_1 + C_2$ (the principal moments of inertia of the sensitive element and clamping unit combined about

Ox, Oy and Oz when the system is not vibrating) and rearranging (2.2.10):

$$A\ddot{\beta} + \{c - 2F\alpha\dot{\alpha}\}\dot{\beta} + \{k + F\alpha\dot{\Omega}_3 + F\dot{\alpha}\Omega_3 - B\Omega_3^2 + B\,\Omega_2^2 + F\alpha\Omega_1\Omega_2 + C\,\Omega_3^2 - C\Omega_2^2 + C_1\dot{\alpha}\Omega_3\}\beta + \{B\Omega_2\Omega_3 - C\Omega_2\Omega_3\}\beta^2 + F\alpha\Omega_2\beta\dot{\beta}$$
$$= -A\dot{\Omega}_1 + 2F\alpha\dot{\alpha}\,\Omega_1 - F\alpha\dot{\Omega}_2 - F\dot{\alpha}\Omega_2 + B\Omega_2\Omega_3 + F\alpha\,\Omega_3\Omega_1 - C\Omega_3\Omega_2 - C_1\dot{\alpha}\,\Omega_2 \qquad (2.2.12)$$

If $k \gg$ second order terms in α and Ω and if we can neglect second order terms in α and β on the L.H.S., equation (2.2.12) reduces to:

$$A\ddot{\beta} + c\dot{\beta} + k\beta$$
$$= -A\dot{\Omega}_1 + (B - C)\Omega_2\Omega_3 + F\alpha\Omega_3\Omega_1 - (F + C_1)\dot{\alpha}\Omega_2 - F\alpha\dot{\Omega}_2 + 2F\alpha\dot{\alpha}\Omega_1 \qquad (2.2.13)$$

Examining the solution for the case when $\bar{\Omega}$ is constant, so that $\dot{\Omega}_1 = \dot{\Omega}_2 = \dot{\Omega}_3 = 0$ and assuming that a pick-up sensitive to oscillatory motion only is employed, so that the constant forcing functions (i.e. those not containing α) can be neglected, we have:

$$A\ddot{\beta} + c\dot{\beta} + k\beta$$
$$= F\alpha\Omega_3\Omega_1 - (F + C_1)\dot{\alpha}\Omega_2 + 2F\alpha\dot{\alpha}\Omega_1$$
$$= F\alpha_0\Omega_3\Omega_1 \sin\omega_0 t - (F + C_1)\alpha_0\omega_0\Omega_2 \cos\omega_0 t + F\alpha_0^2\omega_0\Omega_1 \sin 2\omega_0 t \qquad (2.2.14)$$

This is a standard second order linear differential equation having a steady state solution:

$$\beta = \frac{F\alpha_0\Omega_3\Omega_1 \sin(\omega_0 t - \varphi) - (F+C_1)\alpha_0\omega_0\Omega_2\cos(\omega_0 t - \varphi)}{A\sqrt{(\omega_0^2-\omega_n^2)^2 + (2\zeta\omega_0\omega_n)^2}}$$

$$+ \frac{F\alpha_0^2\omega_0\Omega_1 \sin(2\omega_0 t - \psi)}{A\sqrt{(4\omega_0^2-\omega_n^2)^2 + (4\zeta\omega_0\omega_n)^2}} \qquad (2.2.15)$$

where $\omega_n = \sqrt{\frac{k}{A}}$ the undamped natural frequency of the system about OX

$\zeta = \frac{c}{2\sqrt{Ak}}$ the damping ratio

$$\varphi = \arctan\left(-\frac{2\zeta\omega_0\omega_n}{\omega_0^2-\omega_n^2}\right)$$

$$\psi = \arctan\left(-\frac{4\zeta\omega_0\omega_n}{4\omega_0^2-\omega_n^2}\right)$$

From (2.2.14) it can be seen that, for $\zeta \ll 1$, the maximum response to the first term will occur when $\omega_n \doteqdot \omega_0$ i.e. when the undamped natural frequency about OX is approximately equal to that about Oz.

For the case $\omega_n = \omega_0$:

$$\varphi = \frac{\pi}{2} \quad \text{and} \quad \psi = \arctan\left(-\tfrac{4}{3}\zeta\right)$$

$$\therefore \beta = -\frac{F\alpha_0\Omega_3\Omega_1}{2A\zeta\omega_0^2}\cos\omega_0 t - \frac{(F+C_1)\alpha_0\Omega_2}{2A\zeta\omega_0}\sin\omega_0 t$$

$$+ \frac{F\alpha_0^2\Omega_1}{3A\omega_0\sqrt{1+\left(\frac{4}{3}\zeta\right)^2}}\sin\left[2\omega_0 t - \arctan\left(-\tfrac{4}{3}\zeta\right)\right] \qquad (2.2.16)$$

<u>Notes on the steady state response to a constant $\overline{\Omega}$</u>

1. β depends upon Ω_1 and Ω_3 as well as the value of Ω_2 in which we are interested.

2. The first term in $\Omega_3 \Omega_1$ has a factor ω_o^2 in its denominator which will make it less significant than the second term.

3. The third term in Ω_1 will not be very significant if $\omega_n = \omega_o$; also it contains α_o^2 in the numerator which will be very small. In any case it is possible to attenuate this signal by employing a filter tuned to the frequency ω_o.

4. The first two terms are 90° out of phase, so it is possible to discriminate between them by measuring the in-phase and quadrature signals of the output β.

5. The second term has its amplitude proportional to Ω_2 and the direction of rotation can be determined by noting whether the signal is in-phase or 180° out of phase with the input α; therefore the device should be capable of being used to determine the magnitude and direction of the rate of rotation about OY.

2.3 <u>Experimental Set-Up</u>

Only a general description of the device itself will be given as it didn't prove too successful and is not the subject of the main part of this report. Referring to the photograph, fig. 2.2.1 and the letters on the diagrammatic sketch, fig. 2.2.2: the square sectioned output shaft and clamping unit A was made in one piece, the shaft being clamped at B by heavy blocks to a baseplate with provision for altering the clamping position to adjust the natural frequency; the 'H' shaped sensitive element unit, C, was square sectioned and clamped at the centre of the horizontal member into the clamping unit; two heavy blocks, D, were attached to the top and bottom of the uprights to provide the main sensing masses.

Initially the device was excited to oscillate about the Oz axis by the electromagnet shown in fig.2.2.1 but an alternative method, consisting of a Goodmans moving coil vibrator attached to the four legs at the top left of fig. 2.2.1 with a rod passing through one of the clamping blocks onto the upper mass D, was also employed later to give larger amplitudes. The torsional oscillations about Oz and OX were measured initially by strain gauges attached to the appropriate shafts but a more satisfactory method for laboratory purposes was to use two Bruel and Kjaer accelerometers mounted on the outer faces of the blocks D and aligned along OX and Oz.

The necessary power for the electromagnet or the vibrator was supplied by a Goodmans power oscillator and, when the accelerometers were being used, the signals could be displayed directly onto a Solartron solarscope CD1014, the amplitudes being measured by a Philips GM6012 valve voltmeter.

The device itself was attached to a Bryans gyro instrument test table mk.4A, capable of being rotated at up to 3 rpm.

The power leads to the vibrator or electromagnet and the output leads from the accelerometers were brought via an overhead cantilever and no slip rings were employed; this limited the number of rotations that the table could be allowed to perform.

2.4 Results

The main difficulty that has been experienced with vibratory rate sensing devices has been the unwanted coupling that exists between the forced vibrations of the sensitive element and the output shaft, resulting in output signals when the device is not rotating (zero signals). In this device the coupling could be caused, for example, by a mass unbalance in the sensitive element, non-orthogonality of the shafts or the misalignment of the excitor. It can be shown that the inertia coupling effects (proportional to acceleration) can be balanced out by the addition of a suitable mass to the sensitive element but there is also the possibility of damping coupling (proportional to velocity) and stiffness coupling (proportional to displacement).

Consequently the device was first tested rigidly attached to a bench and a balancing operation carried out by means of adjustable weights attached to the blocks D (fig.2.2.2). It was found possible to reduce the zero signals but not eliminate them entirely.

The device was then mounted on the turntable and here a major difficulty became apparent, viz. that the response of the sensitive element to the exciting force varied considerably with the turntable orientation; this was due to the fact that the turntable itself was not very rigid and consequently its receptance varied slightly with the turntable position. In combination with the very low damping ratio of the device, this meant that the position of the resonance peak varied with turntable orientation causing the varying response.

By mounting the device on a rubber pad it was possible to minimise this effect a little and it could be demonstrated that the output accelerometer signal increased fairly linearly with time; however, the graphs obtained were not sufficiently consistent to make them worth including in this report.

The main characteristics of the system that could be measured or calculated were:

Fundamental frequency $\omega_o = 140$ Hz $\doteqdot 880$ rads/sec

Damping ratio $\zeta \doteqdot 0.0028$

Moments of inertia of the sensitive element
$$\begin{cases} A_1 \doteqdot 0.105 \text{ lb in sec}^2 \\ B_1 \doteqdot 0.031 \text{ lb in sec}^2 \\ C_1 \doteqdot 0.080 \text{ lb in sec}^2 \end{cases}$$

Substituting these values into equation (2.2.16) the expected response of the system would be:

$$\begin{aligned} \beta = & -1.63 \times 10^{-4} \Omega_3 \Omega_1 \alpha_o \cos\omega_o t \\ & -0.298 \Omega_2 \alpha_o \sin\omega_o t \\ & +5.55 \times 10^{-4} \Omega_1 \alpha_o{}^2 \sin 2\omega_o t \end{aligned} \qquad (2.4.1)$$

It can be seen that, except in exceptional circumstances, the second term should predominate and $\dfrac{\beta}{\alpha_o} \doteqdot -0.298\Omega_2 \sin\omega_o t$ (2.4.2)

2.5 Conclusions

It was apparent that the system would need substantial modifications to make it work successfully so it didn't seem worth while pursuing this line, particularly when the results of the work on torsion oscillator gyroscopes at the R.A.E. by Hunt and Hobbs were available: they show that only two basic types of instrument of this type appear to have any practical possibility of success, and both of those require a sensitive element consisting of two bodies oscillating in anti-phase, supported at a nodal point.

However, several things had been learnt from these experiments, and other reports on this type of instrument, which eventually suggested a more fundamental line of research. As stated previously, the main difficulty in constructing an instrument of this type with sufficient accuracy has been the coupling effects causing unwanted zero signals, therefore it seemed that a comprehensive study of the effects of the various types of coupling was required.

The other aspect that seemed worth investigating was the relationship between the output oscillations and the exciting force: the work in this chapter, and most of the other papers, assumes that the exciting force is controlled to keep the forced amplitude constant; this effectively reduces the system to one with only a single degree of freedom as only one equation is involved (in this case the torque equations about the output axis derived from (2.2.8) in which α_o is assumed constant). In fact the system possesses two degrees of freedom and if the amplitude of the exciting force, rather that the amplitude of α, remained constant a further equation involving T_3, the torque about the axis Oz (fig.2.2.2) would be involved. Rather than develop the second equation in this case, it seemed preferable to deal with this aspect for a more fundamental system, along with the effects of coupling.

CHAPTER 3

Theory of the Fundamental System

3.1 General Theory

Consider a point mass m constrained to move in the plane Oxy of a rectangular set of axes Oxyz, which are rotating in space at an angular velocity $\bar{\Omega} = \Omega_1\bar{i} + \Omega_2\bar{j} + \Omega_3\bar{k}$ about a non-accelerating origin O (fig.3.1.1). When displaced from O the mass is subjected to a restoring force:

$$-(c\dot{x} + kx + c_i\ddot{y} + c_d\dot{y} + c_s y)\bar{i}$$

$$-(c\dot{y} + ky + c_i\ddot{x} + c_d\dot{x} + c_s x)\bar{j}$$

where

- c is the damping coefficient
- k is the spring constant

  } assumed equal in the two directions

- c_i is the inertia coupling coefficient
- c_d is the damping coupling coefficient
- c_s is the spring coupling coefficient

  } equal in the two directions for a conservative coupled system.

The mass is excited by a force $(P_1 e^{j\omega t})\bar{i}$ of constant amplitude P_1 and at frequency ω.

The absolute acceleration $\bar{a}$ of the mass at position $\bar{r} = x\bar{i} + y\bar{j} + z\bar{k}$ w.r.t. Oxyz is given, in vector form, by:

$$\bar{a} = \frac{\partial^2 \bar{r}}{\partial t^2} + \left[\frac{d\bar{\Omega}}{dt} \times \bar{r} + \bar{\Omega} \times (\bar{\Omega} \times \bar{r})\right] + 2\bar{\Omega} \times \frac{\partial \bar{r}}{\partial t} \qquad (3.1.1)$$

where $\dfrac{\partial \bar{r}}{\partial t} = \dot{x}\bar{i} + \dot{y}\bar{j} + \dot{z}\bar{k}$

and $\dfrac{\partial^2 \bar{r}}{\partial t^2} = \ddot{x}\bar{i} + \ddot{y}\bar{j} + \ddot{z}\bar{k}$

represent the velocity and acceleration of the mass relative

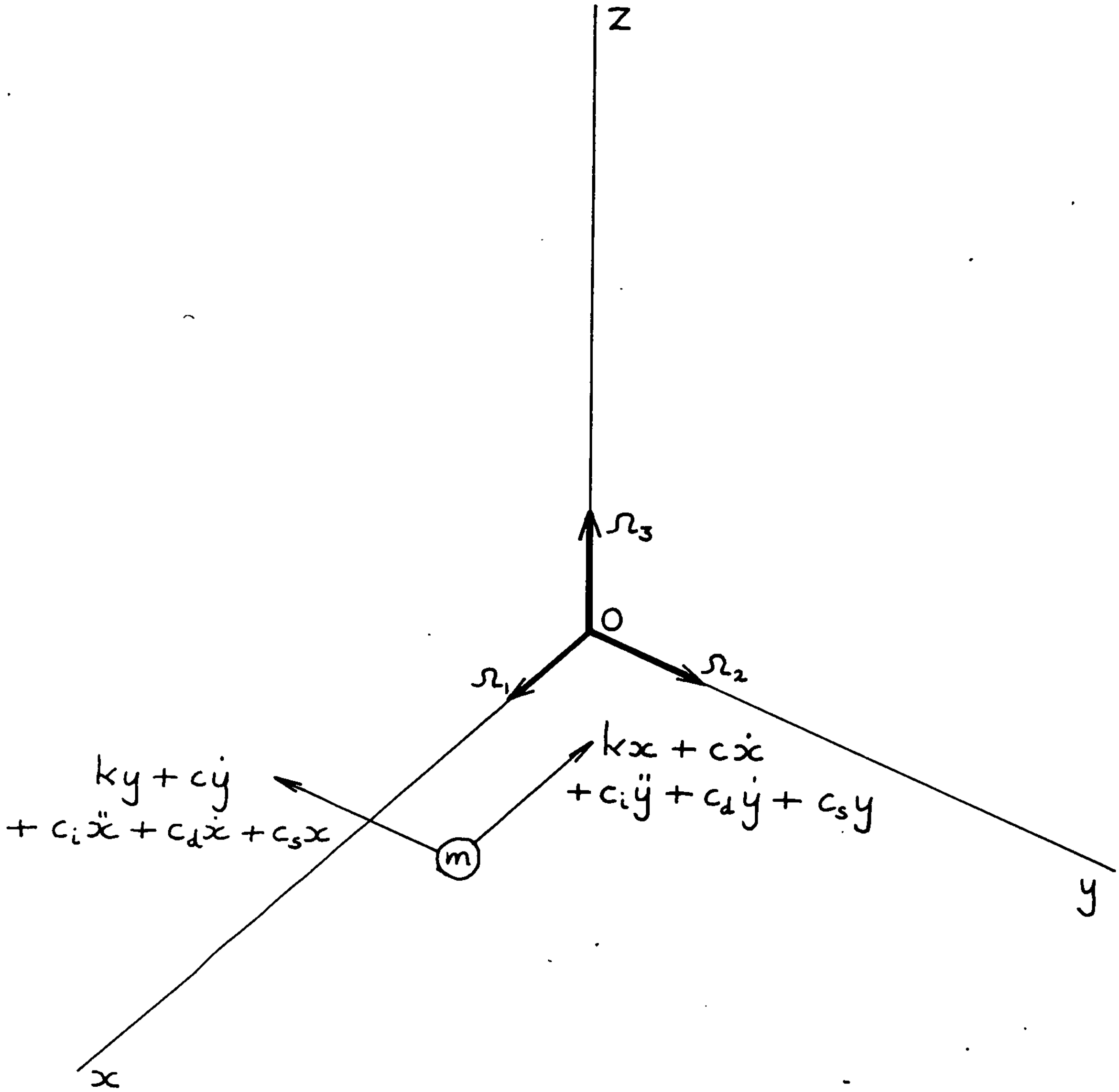

Fig 3.1.1 The Fundamental System

to Oxyz. In components; with $z = \dot{z} = \ddot{z} = 0$,

$\bar{a} = a_1\bar{i} + a_2\bar{j} + a_3\bar{k}$ becomes :

$$\left.\begin{aligned} a_1 &= \ddot{x} + \left[-y\dot{\Omega}_3 - x(\Omega_2^{\,2} + \Omega_3^{\,2}) + y\Omega_1\Omega_2\right] - 2\dot{y}\Omega_3 \\ a_2 &= \ddot{y} + \left[x\dot{\Omega}_3 - y(\Omega_3^{\,3} + \Omega_1^{\,2}) + x\Omega_1\Omega_2\right] + 2\dot{x}\Omega_3 \\ a_3 &= \left[(y\dot{\Omega}_1 - x\dot{\Omega}_2) + \Omega_3(y\Omega_2 + x\Omega_1)\right] + 2(\dot{y}\Omega_1 - \dot{x}\Omega_2) \end{aligned}\right\} \quad (3.1.2)$$

Applying Newtons second law for motion along Ox and Oy, the equations of motion become:

$$\left.\begin{aligned} P_1 e^{j\omega t} - (c\dot{x} + kx + c_i\ddot{y} + c_d\dot{y} + c_s y) &= ma_1 \\ - (c\dot{y} + ky + c_i\ddot{x} + c_d\dot{x} + c_s x) &= ma_2 \end{aligned}\right\} \quad (3.1.3)$$

Substituting for a_1 and a_2 from (3.1.2) and rearranging:

$$\left.\begin{aligned} & m\ddot{x} + c\dot{x} + \left[k - m(\Omega_2^{\,2} + \Omega_3^{\,2})\right]x \\ & \quad + c_i\ddot{y} + (c_d - 2m\Omega_3)\dot{y} + \left[c_s - m(\dot{\Omega}_3 - \Omega_1\Omega_2)\right]y \\ & \quad = P_1 e^{j\omega t} \\ & m\ddot{y} + c\dot{y} + \left[k - m(\Omega_3^{\,2} + \Omega_1^{\,2})\right]y \\ & \quad + c_i\ddot{x} + (c_d + 2m\Omega_3)\dot{x} + \left[c_s + m(\dot{\Omega}_3 + \Omega_1\Omega_2)\right]x \\ & \quad = 0 \end{aligned}\right\} \quad (3.1.4)$$

Putting (3.1.4) into the generalised form by dividing through by m we have:

$$\left.\begin{aligned} & \ddot{x} + 2\zeta\omega_n\dot{x} + \left[\omega_n^{\,2} - (\Omega_2^{\,2} + \Omega_3^{\,2})\right]x \\ & \quad + u_i\ddot{y} + (\omega_n u_d - 2\Omega_3)\dot{y} + \left[\omega_n^2 u_s - (\dot{\Omega}_3 - \Omega_1\Omega_2)\right]y \\ & \quad = \omega_n^{\,2} X_s e^{j\omega t} \\ & \ddot{y} + 2\zeta\omega_n\dot{y} + \left[\omega_n^{\,2} - (\Omega_3^{\,2} + \Omega_1^{\,2})\right]y \\ & \quad + u_i\ddot{x} + (\omega_n u_d + 2\Omega_3)\dot{x} + \left[\omega_n^{\,2} u_s + (\dot{\Omega}_3 + \Omega_1\Omega_2)\right]x \\ & \quad = 0 \end{aligned}\right\} \quad (3.1.5)$$

where $\omega_n = \sqrt{\frac{k}{m}}$ the uncoupled undamped natural frequency

$\zeta = \frac{c}{2\sqrt{mk}}$ the damping ratio

$u_i = \frac{c_i}{m}$ the non-dimensional inertia coupling ratio

$u_d = \frac{c_d}{\omega_n m}$ the non-dimensional damping coupling ratio

$u_s = \frac{c_s}{\omega_n^2 m}$ the non-dimensional stiffness coupling ratio

$X_s = \frac{P_1}{k}$ The deflection due to a static force P_1

From equations (3.1.5) we are interested in determining the variation of x and y with $\bar{\Omega}$.

3.2 Uncoupled system rotating about Oz under free vibration

In this case u_i, u_d, u_s, Ω_1, Ω_2 and X_s are all zero and equations (3.1.5) reduce to:

$$\left.\begin{aligned} \ddot{x} + 2\zeta\omega_n\dot{x} + (\omega_n^2 - \Omega_3^2)x - 2\Omega_3\dot{y} - \dot{\Omega}_3 y &= 0 \\ \ddot{y} + 2\zeta\omega_n\dot{y} + (\omega_n^2 - \Omega_3^2)y + 2\Omega_3\dot{x} + \dot{\Omega}_3 x &= 0 \end{aligned}\right\} \quad (3.2.1)$$

For an undamped system with Ω_3 constant we have:

$$\left.\begin{aligned} \ddot{x} + (\omega_n^2 - \Omega_3^2)x - 2\Omega_3\dot{y} &= 0 \\ \ddot{y} + (\omega_n^2 - \Omega_3^2)y + 2\Omega_3\dot{x} &= 0 \end{aligned}\right\} \quad (3.2.2)$$

Putting
$$\left.\begin{aligned} x &= x_o e^{\lambda t} \\ y &= y_o e^{\lambda t} \end{aligned}\right\} \quad (3.2.3)$$

into (3.2.2) gives:

$$\left.\begin{aligned}(\lambda^2 + \omega_n^2 - \Omega_3^2)x_o - (2\Omega_3\lambda)y_o &= 0\\ (\lambda^2 + \omega_n^2 - \Omega_3^2)y_o + (2\Omega_3\lambda)x_o &= 0\end{aligned}\right\} \quad (3.2.4)$$

yielding the characteristic equation :

$$(\lambda^2 + \omega_n^2 - \Omega_3^2)^2 + (2\Omega_3\lambda)^2 = 0 \quad (3.2.5)$$

i.e. $\lambda^2 \pm j(2\Omega_3)\lambda + (\omega_n^2 - \Omega_3^2) = 0$

or $\lambda = \mp j\Omega_3 \pm \sqrt{-\Omega_3^2 - (\omega_n^2 - \Omega_3^2)}$

$= j(\mp\Omega_3 \pm \omega_n)$

i.e. the four roots of (3.2.5) are :

$$\lambda_{1,2} = \pm j(\Omega_3 - \omega_n) \text{ and } \lambda_{3,4} = \pm j(\Omega_3 + \omega_n) \quad (3.2.6)$$

Substituting in (3.2.4): for $\lambda_{1,3}$, $\left(\frac{y_o}{x_o}\right)_{1,3} = +j$

for $\lambda_{2,4}$, $\left(\frac{y_o}{x_o}\right)_{2,4} = -j$

so that the solution to equations (3.2.2) is:

$$\left.\begin{aligned}x &= A_1e^{\lambda_1 t} + A_2e^{\lambda_2 t} + A_3e^{\lambda_3 t} + A_4e^{\lambda_4 t}\\ y &= j\left\{A_1e^{\lambda_1 t} - A_2e^{\lambda_2 t} + A_3e^{\lambda_3 t} - A_4e^{\lambda_4 t}\right\}\end{aligned}\right\} \quad (3.2.7)$$

which can be written :

$$\left.\begin{aligned}x &= B_1 \cos(\Omega_3 - \omega_n)t + B_2 \sin(\Omega_3 - \omega_n)t\\ &\quad + B_3 \cos(\Omega_3 + \omega_n)t + B_4 \sin(\Omega_3 + \omega_n)t\\ y &= -B_1 \sin(\Omega_3 - \omega_n)t + B_2 \cos(\Omega_3 - \omega_n)t\\ &\quad - B_3 \sin(\Omega_3 + \omega_n)t + B_4 \cos(\Omega_3 + \omega_n)t\end{aligned}\right\} \quad (3.2.8)$$

where A_{1-4} and B_{1-4} are initial value constants. If, at time $t = 0$, the mass is passing through the origin with unit velocity along Ox (i.e. $\dot{x}=1$, $x=y=\dot{y}=0$ when $t = 0$) equations (3.2.8) become:

$$\left.\begin{aligned} x &= \frac{1}{2\omega_n}\left\{-\sin(\Omega_3-\omega_n)t+\sin(\Omega_3+\omega_n)t\right\} \\ y &= \frac{1}{2\omega_n}\left\{-\cos(\Omega_3-\omega_n)t+\cos(\Omega_3+\omega_n)t\right\} \end{aligned}\right\} \quad (3.2.9)$$

or

$$\left.\begin{aligned} x &= \frac{1}{\omega_n}\cos\Omega_3 t\,\sin\omega_n t \\ y &= -\frac{1}{\omega_n}\sin\Omega_3 t\,\sin\omega_n t \end{aligned}\right\} \quad (3.2.10)$$

i.e. the mass vibrates at frequency ω_n along a straight line which is rotating at angular velocity $-\Omega_3$ about Oz as shown in fig. 3.2.1 ; this is the expected result viz. that the mass will continue to vibrate in the same straight line in space.

From equations (3.2.8) it can be seen that the natural frequencies of the rotating system are $|\Omega_3-\omega_n|$ and $|\Omega_3+\omega_n|$. Plotting the non-dimensional ratios $\frac{|\Omega_3-\omega_n|}{\omega_n} = |\ell_3-1|$ and $\frac{|\Omega_3+\omega_n|}{\omega_n} = |\ell_3+1|$ against $\frac{\Omega_3}{\omega_n} = \ell_3$ on fig. 3.2.2 shows how the natural frequencies vary with the rate of turn.

For a damped system equations (3.2.1) can be solved, but it is apparent that, for $\zeta \ll 1$, the two natural frequencies will be very close to those obtained in the undamped case and the amplitude will decrease exponentially with time.

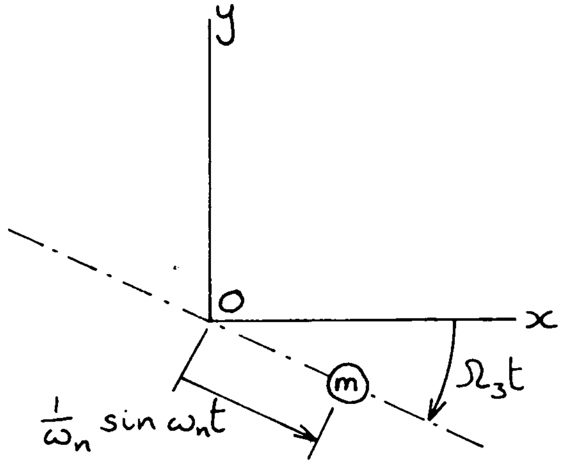

Fig 3.2.1 Undamped system under free vibration

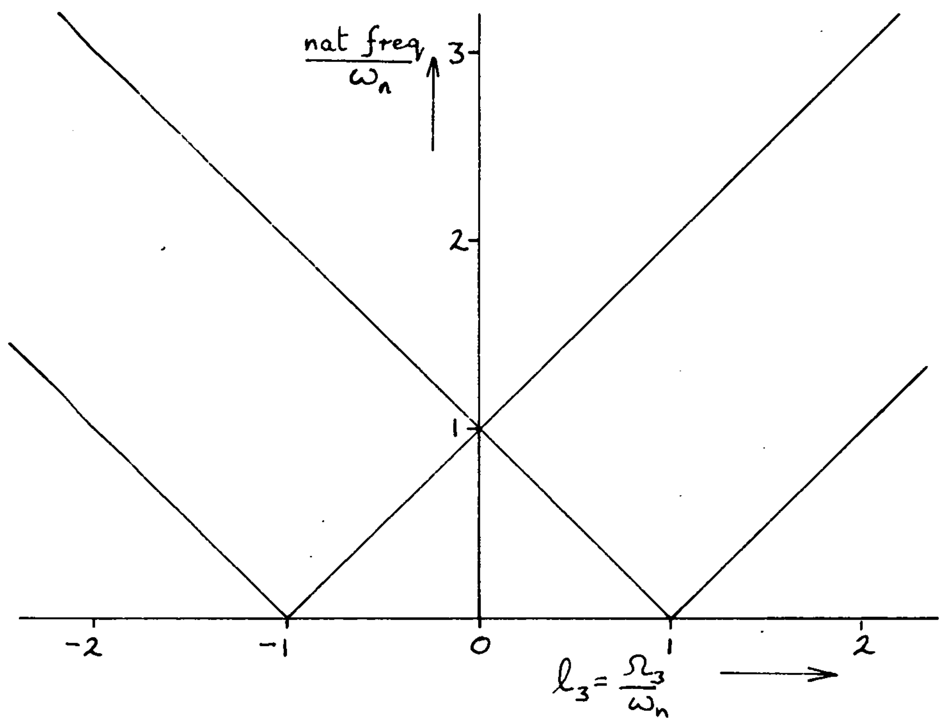

Fig 3.2.2 Variation of the undamped natural frequency with rate of turn

3.3 Uncoupled system rotating at a constant angular velocity about Oz under forced vibration

In this case u_i, u_d, u_s, Ω_1, Ω_2 and $\dot{\Omega}_3$ are all zero and equations (3.1.5) reduce to:

$$\left.\begin{aligned} \ddot{x} + 2\zeta\omega_n\dot{x} + (\omega_n^2 - \Omega_3^2)x - 2\Omega_3\dot{y} &= \omega_n^2 X_s e^{j\omega t} \\ \ddot{y} + 2\zeta\omega_n\dot{y} + (\omega_n^2 - \Omega_3^2)y + 2\Omega_3\dot{x} &= 0 \end{aligned}\right\} \qquad (3.3.1)$$

The steady state solution will be of the form:

$$\left.\begin{aligned} x &= Xe^{j\omega t} \\ y &= Ye^{j\omega t} \end{aligned}\right\} \qquad (3.3.2)$$

which, substituted in equations(3.3.1), gives:

$$\left.\begin{aligned} \left[(-\omega^2 + \omega_n^2 - \Omega_3^2) + j(2\zeta\omega\omega_n)\right]X - j(2\omega\Omega_3)Y &= \omega_n^2 X_s \\ \left[(-\omega^2 + \omega_n^2 - \Omega_3^2) + j(2\zeta\omega\omega_n)\right]Y + j(2\omega\Omega_3)X &= 0 \end{aligned}\right\} \qquad (3.3.3)$$

Non-dimensionalising by putting $r = \frac{\omega}{\omega_n}$, the frequency ratio, and $\ell_3 = \frac{\Omega_3}{\omega_n}$ we have:

$$\left.\begin{aligned} \left[-(r^2 + \ell_3^2 - 1) + j(2\zeta r)\right]X - j(2r\ell_3)Y &= X_s \\ \left[-(r^2 + \ell_3^2 - 1) + j(2\zeta r)\right]Y + j(2r\ell_3)X &= 0 \end{aligned}\right\} \qquad (3.3.4)$$

From the second of these equations:

$$\frac{Y}{X} = \frac{j(2r\ell_3)}{(r^2 + \ell_3^2 - 1) - j(2\zeta r)} \qquad (3.3.5)$$

$$= \frac{2r\ell_3}{(r^2 + \ell_3^2 - 1)^2 + (2\zeta r)^2}\left\{(-2\zeta r) + j(r^2 + \ell_3^2 - 1)\right\} \qquad (3.3.6)$$

i.e. the modulus

$$\left|\frac{Y}{X}\right| = \frac{2r|\ell_3|}{\sqrt{(r^2 + \ell_3^2 - 1)^2 + (2\zeta r)^2}} \qquad (3.3.7)$$

and, for ℓ_3 positive, the phase angle $\angle\frac{Y}{X} = \pi - \arctan\left(\frac{r^2+\ell_3^2-1}{2\zeta r}\right)$ (3.3.8)

and, for ℓ_3 negative, the phase angle $\angle\frac{Y}{X} = 2\pi - \arctan\left(\frac{r^2+\ell_3^2-1}{2\zeta r}\right)$ (3.3.9)

The main interest is the variation of $\left|\frac{Y}{X}\right|$ and $\angle\frac{Y}{X}$ with ℓ_3 and it can be seen that, for $\ell_3 \ll \zeta$:

$$\left|\frac{Y}{X}\right| \rightarrow \left\{\frac{2r}{\sqrt{(r^2-1)^2 + (2\zeta r)^2}}\right\}|\ell_3| \tag{3.3.10}$$

$$\left.\begin{aligned} &\text{and } \angle\frac{Y}{X} \rightarrow \pi - \arctan\frac{(r^2-1)}{2\zeta r} \quad \text{if } \ell_3 > 0 \\ &\text{or} \qquad \rightarrow 2\pi - \arctan\frac{(r^2-1)}{2\zeta r} \quad \text{if } \ell_3 < 0 \end{aligned}\right\} \tag{3.3.11}$$

From (3.3.10) it is apparent that, for low values of ℓ_3, $\left|\frac{Y}{X}\right|$ varies linearly with $|\ell_3|$ and therefore provides a simple means for determining its value.

$$\text{As } \ell_3 \rightarrow \infty, \left|\frac{Y}{X}\right| \rightarrow 0 \text{ and } \angle\frac{Y}{X} \rightarrow \frac{\pi}{2} \tag{3.3.12}$$

$$\text{\& as } \ell_3 \rightarrow -\infty, \left|\frac{Y}{X}\right| \rightarrow 0 \text{ and } \angle\frac{Y}{X} \rightarrow \frac{3\pi}{2} \tag{3.3.13}$$

The peak value of $\left|\frac{Y}{X}\right|$, as ℓ_3 varies, occurs when:

$\dfrac{(r^2+\ell_3^2-1)^2 + (2\zeta r)^2}{\ell_3^2}$ is a minimum; i.e., differentiating w.r.t. ℓ_3, when

$$\ell_3^2\left\{2(r^2+\ell_3^2-1)(2\ell_3)\right\} = \left\{(r^2+\ell_3^2-1)^2 + (2\zeta r)^2\right\}2\ell_3$$

$$\text{i.e. } \ell_3 = \sqrt[4]{(r^2-1)^2 + (2\zeta r)^2} \tag{3.3.14}$$

$$\text{and this gives } \left|\frac{Y}{X}\right|_{max} = \frac{2r}{\sqrt{2\left[\left\{(r^2-1)^2 + (2\zeta r)^2\right\}^{\frac{1}{2}} + (r^2-1)\right]}} \tag{3.3.15}$$

To illustrate the variation of $\left|\frac{Y}{X}\right|$ and $\angle\frac{Y}{X}$ with ℓ_3, typical curves are drawn on figs. 3.3.1 and 3.3.2, the figures chosen being $\zeta = 0.1$ and $r = 0.9$, 1.0 and 1.1 (the curves were drawn from

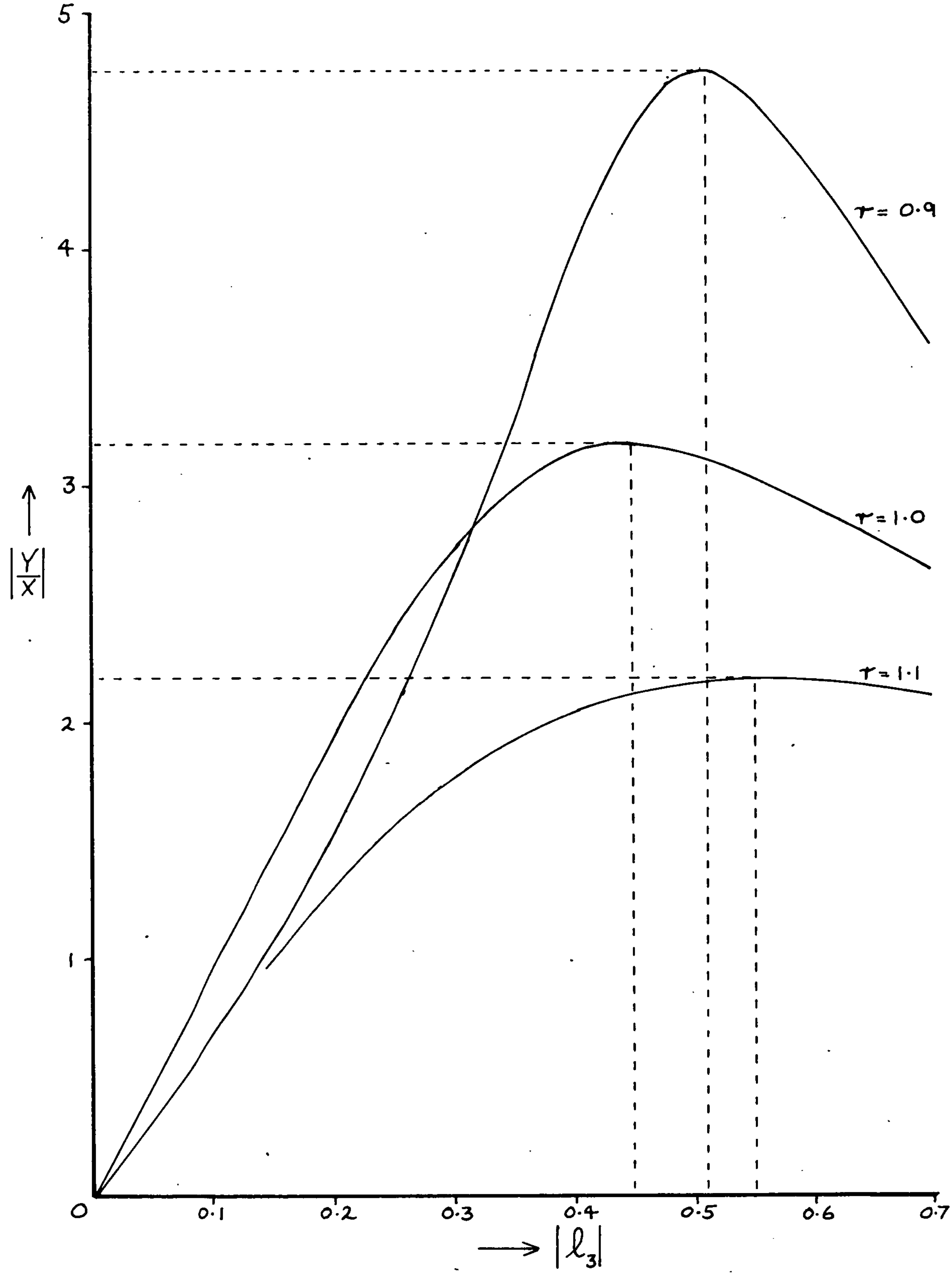

Fig 3.3.1 Variation of $\left|\frac{Y}{X}\right|$ with l_3 for $\zeta = 0·1$ and $r = 0·9$, $1·0$ and $1·1$

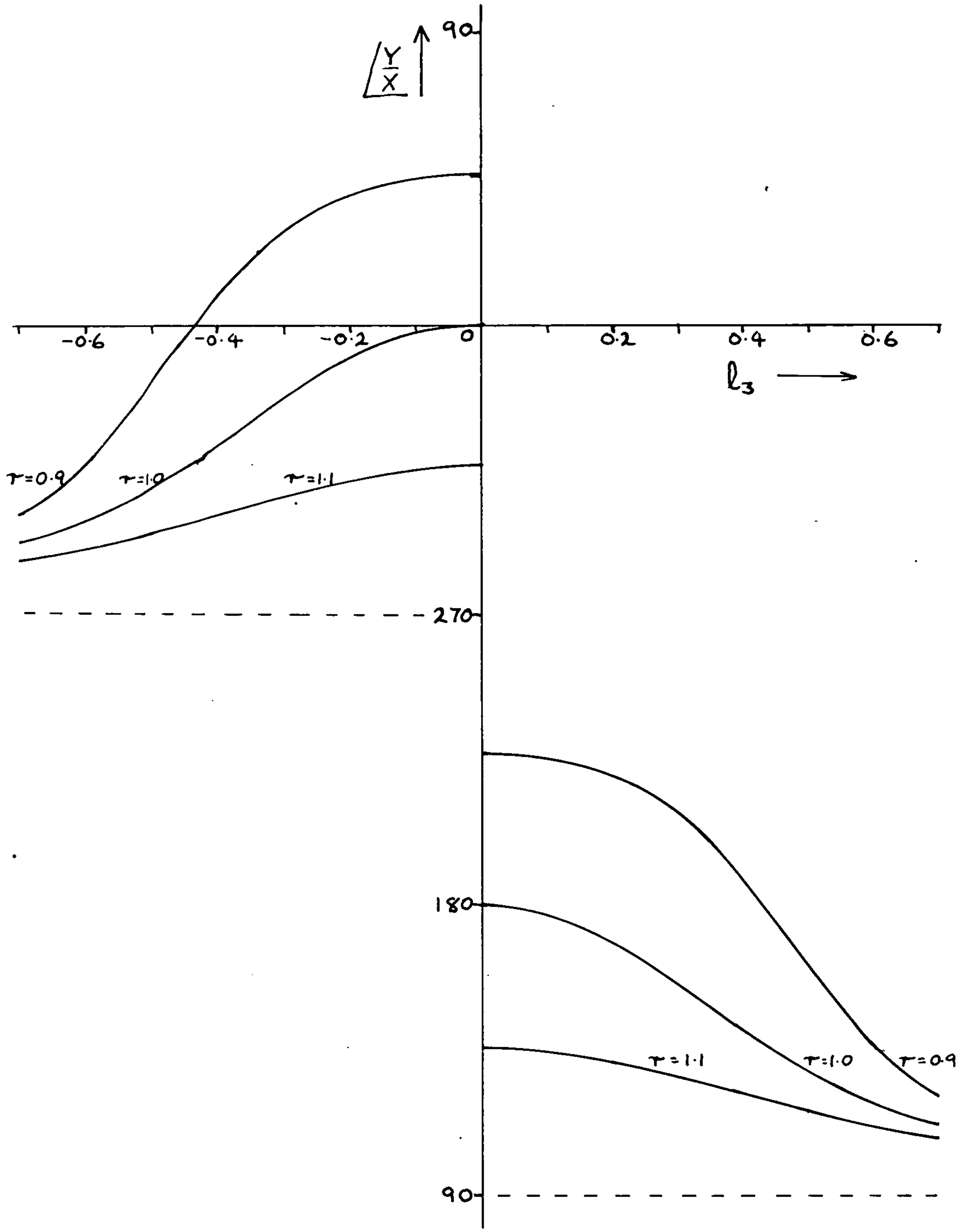

Fig 3.3.2 Variation of $\angle\frac{Y}{X}$ with l_3 for $\zeta = 0{\cdot}1$ and $\tau = 0{\cdot}9, 1{\cdot}0$ and $1{\cdot}1$

computer calculations as described in Chapter 4). It can be seen that $\left|\frac{Y}{X}\right|_{max}$ decreases with increasing r but that the maximum sensitivity to small values of ℓ_3, i.e. the maximum slope of the $\left|\frac{Y}{X}\right|$ against $|\ell_3|$ curve, occurs when r = 1; from equation (3.3.10) the value of this maximum sensitivity is:

$$\left(\frac{\left|\frac{Y}{X}\right|}{|\ell_3|}\right)_{\substack{max\ for\\ |\ell_3| \ll \zeta}} = \frac{1}{\zeta} \qquad (3.3.16)$$

From fig. 3.3.2 and equations (3.3.11) it is apparent that there is a step change of 180° in the phase angle curve as ℓ_3 passes through zero (it is indeterminate when $\ell_3 = 0$ as $\left|\frac{Y}{X}\right| = 0$) and this provides a means of determining the direction of rotation.

So far the investigation has been concerned with the variation of $\frac{Y}{X}$ with ℓ_3 but, returning to equations(3.3.4) and substituting from equation (3.3.5) it is possible to determine the variation of $\frac{Y}{X_s}$ and $\frac{X}{X_s}$ with ℓ_3. Substituting for X from (3.3.5) into (3.3.4) we have:

$$\frac{Y}{X_s} = \frac{-j(2r\ell_3)}{\left\{(r^2+\ell_3^2-1) - j(2\zeta r)\right\}^2 + \left\{j(2r\ell_3)\right\}^2} \qquad (3.3.17)$$

This is a more complicated expression to evaluate than the one for $\frac{Y}{X}$ and the use of a digital computer, as described in Chapter 4, is desirable; however it is possible to see from (3.3.17) that, for the regions of primary interest, $|\ell_3| \ll \zeta$:

$$\frac{Y}{X_s} \longrightarrow \frac{-j(2r\ell_3)}{\left\{(r^2-1) + j(2\zeta r)\right\}^2} \qquad (3.3.18)$$

i.e. $\left|\frac{Y}{X_s}\right| \longrightarrow \frac{2r}{(r^2-1)^2+(2\zeta r)^2}\left|\ell_3\right|$ (3.3.19)

The maximum sensitivity for low ℓ_3 now occurs when

$$r^2 = \tfrac{1}{3}\left\{(1-2\zeta^2) \pm 2\sqrt{1-\zeta^2+\zeta^4}\right\} \qquad (3.3.20)$$

its value is plotted on figure 3.3.3 and compared with the maximum sensitivity of $\left|\frac{Y}{X}\right|$; it can be seen that is is greater for $\zeta < 0.53$.

The variation of $\frac{X}{X_s}$ with ℓ_3 is obtained by substituting from (3.3.5) into (3.3.17) viz:

$$\frac{X}{X_s} = -\frac{\left\{(r^2+\ell_3^{\,2}-1) - j(2\zeta r)\right\}}{\left\{(r^2+\ell_3^{\,2}-1) - j(2\zeta r)\right\}^2 + \left\{j(2r\ell_3)\right\}^2} \qquad (3.3.21)$$

In this case for $|\ell_3| \ll \zeta$

$$\frac{X}{X_s} \longrightarrow -\frac{1}{(r^2-1) - j(2\zeta r)} \doteq \frac{1}{(1-r^2) + j(2\zeta r)} \qquad (3.3.22)$$

$$\left.\begin{array}{ll} \text{or} & \left|\frac{X}{X_s}\right| \longrightarrow \frac{1}{\sqrt{(1-r^2)^2+(2\zeta r)^2}} \\ \text{and} & \angle\frac{Y}{X_s} \longrightarrow -\arctan\left(\frac{2\zeta r}{1-r^2}\right) \end{array}\right\} \qquad (3.3.23)$$

which is the expected response of a single degree of freedom system to forced vibration.

Plots of $\frac{Y}{X_s}$ and $\frac{X}{X_s}$ against ℓ_3 and a more detailed discussion of the results are dealt with in Chapter 4.

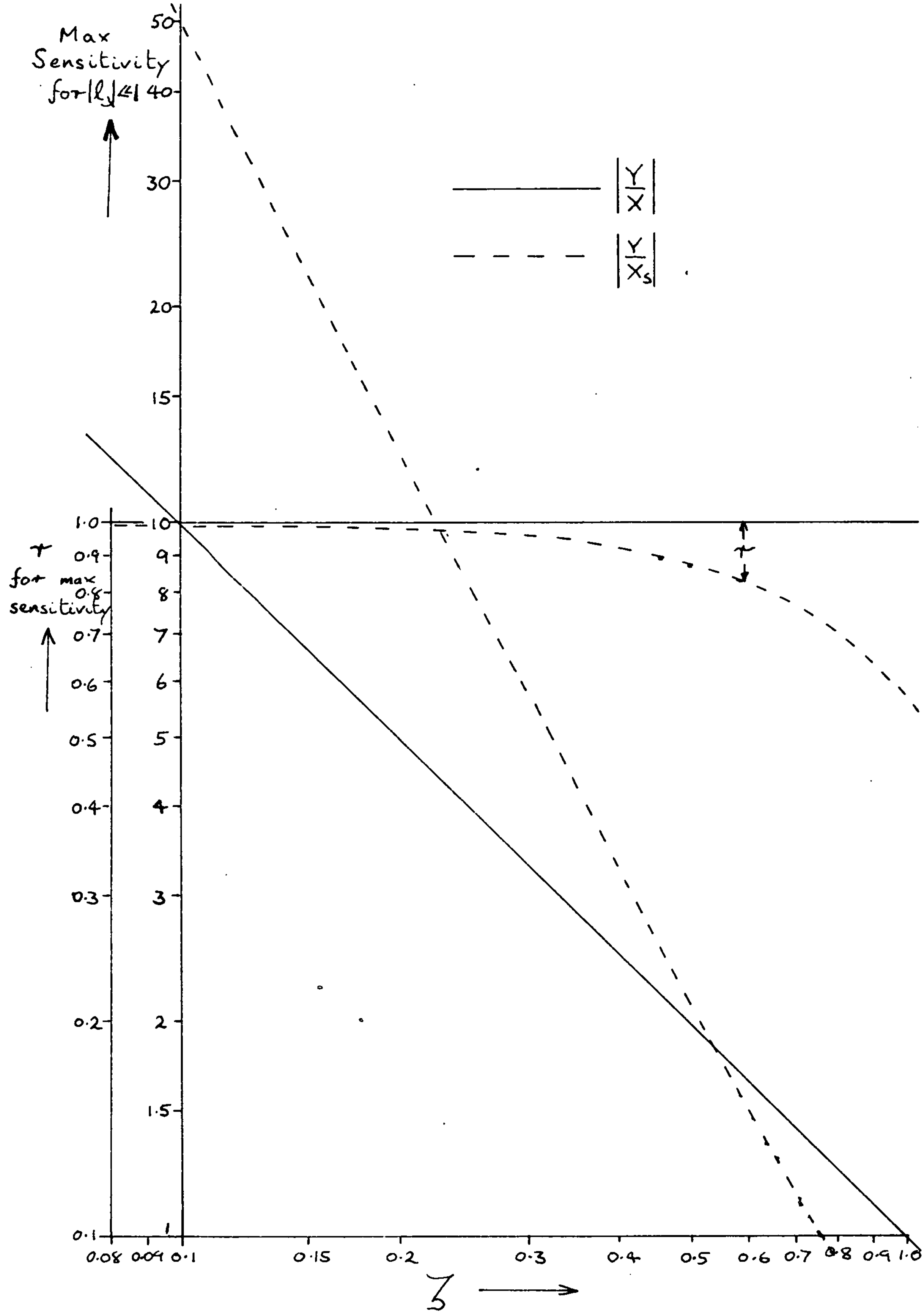

Fig 3.3.3 Maximum Sensitivity $\left|\frac{Y}{X}\right| / |\ell_3|$ and $\left|\frac{Y}{X_s}\right| / |\ell_3|$ and the value of τ at which it occurs for $|\ell_3| \ll 1$

3.4. The effect of coupling on the system rotating at constant angular velocity about Oz under forced vibration

In this case Ω_1, Ω_2 and $\dot{\Omega}_3$ are zero and equations (3.1.5) become:

$$\left.\begin{aligned} &\ddot{x} + 2\zeta\omega_n\dot{x} + (\omega_n^2 - \Omega_3^2)x \\ &\qquad + u_i\ddot{y} + (\omega_n u_d - 2\Omega_3)\dot{y} + \omega_n^2 u_s y = \omega_n^2 X_s e^{j\omega t} \\ &\ddot{y} + 2\zeta\omega_n\dot{y} + (\omega_n^2 - \Omega_3^2)y \\ &\qquad + u_i\ddot{x} + (\omega_n u_d + 2\Omega_3)\dot{x} + \omega_n^2 u_s x = 0 \end{aligned}\right\} \qquad (3.4.1)$$

For the steady state solution we again use the substitution (3.3.2) and non-dimensionalise [cf. equations (3.3.3) and (3.3.4)] to give:

$$\left.\begin{aligned} &\left[-(r^2+\ell_3^2-1) + j(2\zeta r)\right]X + \left[(-u_i r^2+u_s) + jr(u_d-2\ell_3)\right]Y = X_s \\ &\left[-(r^2+\ell_3^2-1) + j(2\zeta r)\right]Y + \left[(-u_i r^2+u_s) + jr(u_d+2\ell_3)\right]X = 0 \end{aligned}\right\} \qquad (3.4.2)$$

From the second equation:

$$\frac{Y}{X} = -\frac{(-u_i r^2 + u_s) + jr(u_d + 2\ell_3)}{-(r^2 + \ell_3^2 - 1) + j(2\zeta r)} \qquad (3.4.3)$$

and by substituting in the first equation the variation of $\frac{Y}{X_s}$ and $\frac{X}{X_s}$ as ℓ_3 varies can be determined; however the analysis is rather complicated so a computer program was considered advisable to analyse these equations. As these results are the main point of interest, the construction of the computer program and the analysis of the theoretical results are dealt with in Chapter 4.

3.5 Transient response of the uncoupled system

Consider the effect of a change in Ω_3 with u_i, u_d, u_s, Ω_1 and Ω_2 all zero. Equation (3.1.5) reduces to:

$$\left.\begin{aligned} \ddot{x} + 2\zeta\omega_n\dot{x} + (\omega_n^2 - \Omega_3^2)x - 2\Omega_3\dot{y} - \dot{\Omega}_3 y &= \omega_n^2 X_s e^{j\omega t} \\ \ddot{y} + 2\zeta\omega_n\dot{y} + (\omega_n^2 - \Omega_3^2)y + 2\Omega_3\dot{x} + \dot{\Omega}_3 x &= 0 \end{aligned}\right\} \quad (3.5.1)$$

These equations are very difficult to solve as they stand if Ω_3 varies with time; however, as we are mainly interested in small values of Ω_3, we can make the assumptions for this investigation that Ω_3^2 can be neglected and that the amplitude of x remains constant during the change [justified by equation (3.3.23)]. It is then only necessary to consider the second of equations (3.5.1) with $x = X'e^{j\omega t}$ (3.5.2)

then, considering the response of y to a suddenly applied Ω_3, we have:

$$\ddot{y} + 2\zeta\omega_n\dot{y} + \omega_n^2 y = -\,j(2\omega\Omega_3)X'e^{j\omega t} \quad (3.5.3)$$

This now a second order linear differential equation with constant coefficients, the solution being the sum of the particular integral:

$$y = \frac{-j(2\omega\Omega_3)X'e^{j\omega t}}{(\omega_n^2 - \omega^2) + j(2\zeta\omega\omega_n)} = \frac{-j(2r\,\ell_3)}{(1-r^2) + j(2\zeta r)}X'e^{j\omega t} \quad (3.5.4)$$

[cf. equation (3.3.5)]

and the complementary function which, for $\zeta < 1$, is of the form

$$y = Y_1 e^{-\zeta\omega_n t}\cos\left(\omega_n\sqrt{1-\zeta^2}\;t - \varphi_1\right) \quad (3.5.5)$$

where Y_1 and φ_1 are initial value constant.

This means that the transient amplitude, given by (3.5.5), decreases as $Y_1 e^{-\zeta\omega_n t}$ leaving the steady state response (3.5.4)

As the primary concern here is with values of r close to unity and small values of ζ, consider the general solution for r = 1, and $\zeta \ll 1$, then, taking $x = X'\cos\omega t$, from (3.5.4) and (3.5.5) we have:

$$y = Y_1 e^{-\zeta\omega_n t}\cos(\omega_n t - \varphi_1) - \frac{\ell_3}{\zeta}X'\cos\omega_n t \qquad (3.5.6)$$

and if $y = \dot{y} = 0$ when $t = 0$; $\varphi_1 = 0$ and $Y_1 = \frac{\ell_3}{\zeta}X'$

i.e. $$y = \left\{e^{-\zeta\omega_n t} - 1\right\}\frac{\ell_3}{\zeta}X'\cos\omega_n t \qquad (3.5.7$$

i.e. there is an exponential lag of time constant $\frac{1}{\zeta\omega_n}$ in the response of $|y|$ to ℓ_3.

3.6 Response of the uncoupled system to a constant $\bar{\Omega}$

In this case u_i, u_d, u_s and $\dot{\Omega}_3$ are all zero and equations (3.1.5) reduce to:

$$\left.\begin{aligned}\ddot{x} + 2\zeta\omega_n\dot{x} + \left[\omega_n^2 - (\Omega_2^2 + \Omega_3^2)\right]x - 2\Omega_3\dot{y} + \Omega_1\Omega_2 y &= \omega_n^2 X_s e^{j\omega t}\\ \ddot{y} + 2\zeta\omega_n\dot{y} + \left[\omega_n^2 - (\Omega_3^2 + \Omega_1^2)\right]y + 2\Omega_3\dot{x} + \Omega_1\Omega_2 x &= 0\end{aligned}\right\} \qquad (3.6.1)$$

By comparison with equation (3.1.5) it can be seen that the terms in $\Omega_1\Omega_2$ have the same effect on the system as a stiffness coupling ratio

$$u_s \equiv \frac{\Omega_1\Omega_2}{\omega_n^2} = \ell_1\ell_2 \qquad (3.6.2)$$

where $\ell_1 = \frac{\Omega_1}{\omega_n}$ and $\ell_2 = \frac{\Omega_2}{\omega_n}$

so the result can be computed in the same way. However, by comparison with equations (3.4.2), the steady state solution of equations (3.6.1) is given by:

$$\left.\begin{aligned}\left[-(r^2+\ell_2^{\,2}+\ell_3^{\,2}-1) + j(2\zeta r)\right]X + \left[\ell_1\ell_2 - j(2r\ell_3)\right]Y &= X_s \\ \left[-(r^2+\ell_3^{\,2}+\ell_1^{\,2}-1) + j(2\zeta r)\right]Y + \left[\ell_1\ell_2 + j(2r\ell_3)\right]X &= 0\end{aligned}\right\} \quad (3.6.3)$$

From the second equation:

$$\frac{Y}{X} = \frac{\ell_1\ell_2+j(2r\ell_3)}{(r^2+\ell_3^{\,2}+\ell_1^{\,2}-1) - j(2\zeta r)} \qquad (3.6.4)$$

from which it is apparent that the response to $\ell_1\ell_2$ is 90° out of phase with the response to ℓ_3 and could therefore be descriminated against. The $\ell_1^{\,2}$ term in the denominator will affect the position of the resonance peak; however, for the most interesting cases when $\overline{\Omega}$ is small (ℓ_1, ℓ_2 and $\ell_3 \ll \zeta$), the terms in ℓ^2 and $\ell_1\ell_2$ become insignificant and the ℓ_3 term will be predominant.

3.7 Response of the uncoupled system to a sinusoidal input

As for the transient response in Section 3.5, the complete equations (3.1.5) are effectively impossible to solve in the general case for sinusoidally varying rotation of the form $\overline{\Omega} = \overline{\Omega}' \sin\omega' t$, where $\overline{\Omega}' = \Omega_1'\overline{i} + \Omega_2'\overline{j} + \Omega_3'\overline{k}$ is a constant, as time dependent co-efficients of x and y are involved. However, if it can be assumed $\overline{\Omega}'$ is sufficiently small, so that the amplitude of x remains constant in the form $x = X' \sin\omega t$, from the second of equations (3.1.5) we have:

$$\begin{aligned}\ddot{y} + 2\zeta\omega_n\dot{y} + \left[\omega_n^{\,2} - (\Omega_1'^{\,2} + \Omega_3'^{\,2})\sin^2\omega' t\right]y \\ = -2\omega\Omega_3' X' \sin\omega' t \cos\omega t - \omega'\Omega_3' X' \cos\omega' t \sin\omega t \\ -\Omega_1'\Omega_2' X' \sin^2\omega' t \sin\omega t\end{aligned} \qquad (3.7.1)$$

or $$\ddot{y}+2\zeta\omega_n\dot{y}+\left[\left(\omega_n^2-\frac{\Omega_1'^2+\Omega_3'^2}{2}\right)+\frac{\Omega_1'^2+\Omega_3'^2}{2}\cos 2\omega' t\right]y$$

$$= -\omega\Omega_3' X'\left\{\sin(\omega+\omega')t - \sin(\omega-\omega')t\right\}$$
$$-\tfrac{1}{2}\omega'\Omega_3' X'\left\{\sin(\omega+\omega')t + \sin(\omega-\omega')t\right\} - \tfrac{1}{2}\Omega_1'\Omega_2' X' \sin\omega t$$
$$+\tfrac{1}{4}\Omega_1'\Omega_2' X'\left\{\sin(\omega+2\omega')t + \sin(\omega-2\omega')t\right\} \qquad (3.7.2)$$

This is a modified non-homogeneous form of Mathieu's equation and the variable coefficient of y on the LHS indicates the possibility of instability if $\omega' \doteqdot \omega_n$ (or more unlikely, when $\omega' \doteqdot \frac{1}{2}\omega_n$, $\frac{1}{3}\omega_n$ etc.), depending upon the values of Ω_1', Ω_3' and ζ. If $\omega' \not\doteqdot \omega_n$, as $\overline{\Omega}'$s is small, the solution to equation (3.7.2) should approximate to that of the reduced linear equation with the LHS: $\ddot{y} + 2\zeta\omega_n\dot{y} + \omega_n^2 y$

Confining our attention to the case when $\omega = \omega_n$ and $\zeta < 0.2$ (giving a high resonance peak), by examining the RHS of the reduced equation (3.7.2) it can be seen that, if ω' is not very small, the dominating response will be due to the term $-\frac{1}{2}\Omega_1'\Omega_2' \cdot X' \sin\omega_n t$ as this is the only one varying near the resonant frequency; i.e. the steady state response for $\omega' \not\ll \omega_n$ becomes:

$$y \doteqdot \frac{\frac{1}{2}\Omega_1'\Omega_2' X' \cos\omega_n t}{2\zeta\omega_n^2} = \frac{l_1' l_2'}{4\zeta} X' \cos\omega_n t \qquad (3.7.3)$$

where $l_1' = \dfrac{\Omega_1'}{\omega_n}$ and $l_2' = \dfrac{\Omega_2'}{\omega_n}$

For the case when $\omega' \ll \omega_n$ with $\omega = \omega_n$ the steady state response, from (3.7.2), approximates to:

$$y = -\left(\frac{\ell_3' X' \sin\omega' t}{\zeta}\right)\sin\omega_n t$$
$$+\left(\frac{\omega' \ell_3' X' \cos\omega' t}{2\zeta\omega_n}\right)\cos\omega_n t$$
$$+\left(\frac{\ell_1' \ell_2' X'}{4\zeta}\right)\cos\omega_n t$$
$$-\left(\frac{\ell_1' \ell_2'}{4\zeta} X' \cos 2\omega' t\right)\cos\omega_n t \qquad (3.7.4)$$

and, as ℓ_1', ℓ_2', ℓ_3' and ω' are all very small, the first term should predominate, i.e. the steady state value $|y_{ss}|$ will be proportional to $\ell_3 = \ell_3' \sin\omega' t$

To summarise for sinsuoidal response if $\omega = \omega_n$; $|y|$ will follow ℓ_3 for $\omega' \ll \omega_n$, but for higher values of ω' the output due to ℓ_3 is sharply attenuated and $|y|$ will approach a constant value proportional to $\ell_1' \ell_2'$: in addition there is the possibility of an instability if $\omega' \rightarrow \omega_n$ (or $\frac{1}{2}\omega_n$; $\frac{1}{3}\omega_n$ etc., but these are considered unlikely).

3.8 The effect of an accelerating origin O

If the origin has acceleration $\overline{A} = A_1\overline{i} + A_2\overline{j} + A_3\overline{k}$ the absolute accelerations a_1, a_2 and a_3 given by equation (3.1.2) contain additional terms A_1, A_2 and A_3 respectively; therefore, comparing with equations (3.1.5), for the uncoupled system the equations of motion become:

$$
\left.\begin{aligned}
&\ddot{x} + 2\zeta\omega_n\dot{x} + \left[\omega_n^{\,2} - (\Omega_2^{\,2} + \Omega_3^{\,2})\right]y \\
&\qquad - 2\Omega_3\dot{y} - (\dot{\Omega}_3 - \Omega_1\Omega_2)y \qquad = \omega_n^{\,2}X_s e^{j\omega t} - A_1 \\
&\ddot{y} + 2\zeta\omega_n y + \left[\omega_n^{\,2} - (\Omega_3^{\,2} + \Omega_1^{\,2})\right]y \\
&\qquad + 2\Omega_3\dot{x} + (\dot{\Omega}_3 + \Omega_1\Omega_2)x \qquad = -A_2
\end{aligned}\right\} \tag{3.8.1}
$$

If the system is not rotating and is subjected to a constant acceleration $\bar{A}$ the steady state solution for x and y will contain additional constant terms in A_1 and A_2; i.e. if x and y are measured by pick-offs sensitive to oscillatory motion only, the results will not be affected. However, if the system is rotating and accelerating, then A_1 and A_2 will be time dependent and can be considered as additional forcing terms: for example if $\bar{A}$ is constant, or the system is in a constant gravitational field, and $\bar{\Omega}$ is constant, then A_1 and A_2 will vary at frequency Ω, but as long as $\omega \neq \omega_n$ and $\Omega \neq \omega_n$ the steady state motion due to $\bar{A}$ should be negligible.

3.9 The effect of applying an additional exciting force in the direction Oy

If an exciting force $P_2 e^{j(\omega t + \psi)}$, at the same frequency ω as the force in the x direction, but leading it by an angle ψ, is applied in the direction Oy, equations (3.1.5) become modified to:

$$
\begin{aligned}
&\ddot{x} + 2\zeta\omega_n\dot{x} + \left[\omega_n^{\,2} - (\Omega_2^{\,2} + \Omega_3^{\,2})\right]x \\
&\qquad + u_i\ddot{y} + (\omega_n u_d - 2\Omega_3)\dot{y} + \left[\omega_n^{\,2}u_s - (\dot{\Omega}_3 - \Omega_1\Omega_2)\right]y \\
&\qquad = \omega_n^{\,2}X_s e^{j\omega t}
\end{aligned} \tag{3.9.1a}
$$

$$\ddot{y} + 2\zeta\omega_n\dot{y} + \left[\omega_n^{\,2} - (\Omega_3^{\,2} + \Omega_1^{\,2})\right] y$$
$$+ u_i\ddot{x} + (\omega_n u_d + 2\Omega_3)\dot{x} + \left[\omega_n^{\,2} u_s + (\dot{\Omega}_3 + \Omega_1\Omega_2)\right] x$$
$$= \omega_n^{\,2} Y'_s e^{j(\omega t + \psi)} \qquad (3.9.1b)$$

where $Y'_s = \frac{P_2}{k}$ the deflection due to a static force P_2.

Considering the case when $\bar{\Omega} = \Omega_3 \bar{k}$ = constant; by comparison with equations (3.4.2) the steady state solution is given by:

$$\left.\begin{aligned} &\left[-(r^2 + \ell_3^{\,2} - 1) + j(2\zeta r)\right] X + \left[(-u_i r^2 + u_s) + jr(u_d - 2\ell_3)\right] Y \\ &\quad = X_s \\ &\left[-(r^2 + \ell_3^{\,2} - 1) + j(2\zeta r)\right] Y + \left[(-u_i r^2 + u_s) + jr(u_d + 2\ell_3)\right] X \\ &\quad = Y'_s e^{j\psi} = Y_s \quad \text{(say)} \end{aligned}\right\} \qquad (3.9.2)$$

The additional exciting force can be employed in two ways viz. (a) to cancel out the zero errors due to u_i, u_d and u_s, i.e. to make $Y = 0$ when $\ell_3 = 0$ or (b) to keep all the vibrations along Ox (i.e. $Y = 0$) for all values of ℓ_3. Considering these two cases separately.

a) <u>Making $Y = 0$ when $\ell_3 = 0$</u>

From equations (3.9.2), if $X = X_o$ and $Y = 0$ when $\ell_3 = 0$:

$$\left.\begin{aligned} \left[-(r^2 - 1) + j(2\zeta r)\right] X_o &= X_s \\ \left[(-u_i r^2 + u_s) + jru_d\right] X_o &= Y_s \end{aligned}\right\} \qquad (3.9.3)$$

i.e.

$$Y_s = \left[\frac{(-u_i r^2 + u_s) + jru_d}{-(r^2 - 1) + j(2\zeta r)}\right] X_s \qquad (3.9.4)$$

Substituting this value into (3.9.2) and eliminating X_s we have:

$$\Big\{\Big[-(r^2+\ell_3{}^2-1) + j(2\zeta r)\Big]\Big[-(r^2-1) + j(2\zeta r)\Big] - \Big[(-u_i r^2+u_s) + jru_d\Big]\Big[(-u_i r^2+u_s)+jr(u_d-2\ell_3)\Big]\Big\}Y$$
$$= \Big\{\Big[(-u_i r^2+u_s) + jru_d\Big]\Big[-(r^2+\ell_3{}^2-1) + j(2\zeta r)\Big] - \Big[-(r^2-1) + j(2\zeta r)\Big]\Big[(-u_i r^2+u_s) + jr(u_d+2\ell_3)\Big]\Big\}X$$

If u_i, u_d and u_s are all small ($\ll 1$) by ignoring 2nd order of small quantities this equation reduces to:

$$\frac{Y}{X} = \frac{-\ell_3{}^2\Big[(-u_i r^2+u_s)+jru_d\Big] - j2r\ell_3\Big[-(r^2-1)+j(2\zeta r)\Big]}{\Big[-(r^2+\ell_3{}^2-1) + j(2\zeta r)\Big]\Big[-(r^2-1) + j(2\zeta r)\Big]} \qquad (3.9.5)$$

and if ℓ_3 is sufficiently small to make $\ell_3{}^2 u_i$ etc $\ll \ell_3$

$$\frac{Y}{X} = \frac{j(2r\ell_3)}{(r^2+\ell_3{}^2-1) - j(2\zeta r)} \qquad (3.9.6)$$

This is identical to equation (3.3.5) which represents the solution when u_i, u_d and u_s are all zero, so the effects of the coupling, provided it is sufficiently small, can be cancelled out by the exciting force in the direction Oy.

b) <u>Making $Y = 0$ for all values of ℓ_3</u>

From equations (3.9.2), if $Y = 0$:

$$\left.\begin{aligned}\Big[-(r^2+\ell_3{}^2-1) + j(2\zeta r)\Big]X &= X_s\\ \Big[(-u_i r^2 + u_s) + jr(u_d + 2\ell_3)\Big]X &= Y_s\end{aligned}\right\} \qquad (3.9.7)$$

Eliminating X we have:

$$\frac{Y_s}{X_s} = \frac{(-u_i r^2+u_s)+jr(u_d+2\ell_3)}{-(r^2+\ell_3{}^2-1) + j(2\zeta r)} \qquad (3.9.8)$$

which is identical to the value $-\frac{Y}{X}$ obtained in equation (3.4.3). In consequence the results can be obtained from those to be computed in Chapter 4 by noting that:

$$\left|\frac{Y_s}{X_s}\right| = \frac{Y_s'}{X_s} = \frac{P_2}{P_1} \equiv \left|\frac{Y}{X}\right|_{\text{computed}} \qquad (3.9.9)$$

$$\text{and} \angle\frac{Y_s}{X_s} = \psi \equiv \pi + \angle\frac{Y}{X} \qquad (3.9.10)$$

3.10 The effect of a small difference in stiffness and damping between the x and y directions

If the stiffnesses in the directions Ox and Oy are k_1 and k_2 respectively and the damping coefficients c_1 and c_2 respectively, the modified equations of motion, by comparing with equation (3.1.4), become:

$$\left.\begin{aligned} & m\ddot{x} + c_1\dot{x} + \left[k_1 - m(\Omega_3^2 + \Omega_2^2)\right]x \\ & \quad + c_i\ddot{y} + (c_d - 2m\Omega_3)\dot{y} + \left[c_s - m(\dot{\Omega}_3 - \Omega_1\Omega_2)\right]y \\ & \quad = P_1 e^{j\omega t} \\ & m\ddot{y} + c_2\dot{y} + \left[k_2 - m(\Omega_1^2 + \Omega_3^2)\right]y \\ & \quad + c_i\ddot{x} + (c_d + 2m\Omega_3)\dot{x} + \left[c_3 + m(\dot{\Omega}_3 + \Omega_1\Omega_2)\right]x \\ & \quad = 0 \end{aligned}\right\} \qquad (3.10.1)$$

Putting (3.10.1) into the generalised form and examining the frequency response for the case when $\bar{\Omega} = \Omega_3\bar{k}$ is constant, by comparison with (3.4.2) we have:

$$\left.\begin{aligned} & \left[-(r_1^2 + \ell_{31}^2 - 1) + j(2\zeta_1 r_1)\right]X + \left[(-u_i r_1^2 + u_{s1}) + jr_1(u_{d1} - 2\ell_{31})\right]Y = X_s \\ & \left[-(r_2^2 + \ell_{32}^2 - 1) + j(2\zeta_2 r_2)\right]Y + \left[(-u_i r_2^2 + u_{s2}) + jr_2(u_{d2} + 2\ell_{32})\right]X = 0 \end{aligned}\right\} \qquad (3.10.2)$$

$$\text{where}\quad\left\{\begin{array}{llll}
r_1 = \dfrac{\omega}{\omega_{n1}} = \omega\Big/\sqrt{\dfrac{k_1}{m}} & ; & r_2 = \dfrac{\omega}{\omega_{n2}} = \omega\Big/\sqrt{\dfrac{k_2}{m}} \\[2ex]
\ell_{31} = \dfrac{\Omega_3}{\omega_{n1}} = \Omega_3\Big/\sqrt{\dfrac{k_1}{m}} & ; & \ell_{32} = \dfrac{\Omega_3}{\omega_{n2}} = \Omega_3\Big/\sqrt{\dfrac{k_2}{m}} \\[2ex]
\zeta_1 = c_1\big/2\sqrt{mk_1} & ; & \zeta_2 = c_2\big/2\sqrt{mk_2} \\[2ex]
u_{d1} = \dfrac{c_d}{\omega_{n1} m} = \dfrac{c_d}{\sqrt{mk_1}} & ; & u_{d2} = \dfrac{c_d}{\omega_{n2} m} = \dfrac{c_d}{\sqrt{mk_2}} \\[2ex]
u_{s1} = \dfrac{c_s}{\omega_{n1}^2 m} = \dfrac{c_s}{k_1} & ; & u_{s2} = \dfrac{c_s}{\omega_{n2}^2 m} = \dfrac{c_s}{k_2}
\end{array}\right.$$

From the second of equations (3.10.2)

$$\frac{Y}{X} = -\frac{(-u_i r_2^2 + u_{s2}) + j r_2 (u_{d2} + 2\ell_{32})}{-(r_2^2 + \ell_{32}^2 - 1) + j(2\zeta_2 r_2)} \tag{3.10.3}$$

which differs from equation (3.4.2) for $\frac{Y}{X}$ only in the additional subscript 2; i.e. the results obtained will be unaffected as long as the stiffness considered is that in the direction Oy. The expressions for $\frac{Y}{X_s}$ and $\frac{X}{X_s}$ will involve terms with subscript 1 and therefore will not be identical to the results obtained in Chapter 4; however, as the primary concern will be with $\frac{Y}{X}$, it is not considered necessary to examine the other solutions here.

Considering the cases, discussed in section 3.9, with the additional forcing terms in the direction Oy. In case (a) by comparing with equations (3.9.3) to (3.9.6):

$$\frac{Y}{X} = \frac{j\,(2 r_2 \ell_{32})}{(r_2^2 + \ell_{32}^2 - 1) + j(2\zeta_2 r_2)} \tag{3.10.4}$$

again only involving terms with subscript 2. In case (b) however, by comparing with equations (3.9.7) and (3.9.8):

$$\frac{Y_s}{X_s} = \frac{(-u_i r_2^{\,2} + u_{s2}) + jr_2(u_{d2} + 2\ell_{32})}{-(r_1^{\,2} + \ell_{31}^{\,2} - 1) + j(2\zeta_1 r_1)} \tag{3.10.5}$$

this is now K times the value $\frac{Y}{X}$ obtained in (3.10.3) where

$$K = \frac{-(r_2^{\,2} + \ell_{32}^{\,2} - 1) + j(2\zeta_2 r_2)}{-(r_1^{\,2} + \ell_{31}^{\,2} - 1) + j(2\zeta_1 r_1)} \tag{3.10.6}$$

As the main concern is with values of r close to unity

let $\left\{\begin{aligned} r_1 &= 1 + \delta_1 \\ r_2 &= 1 + \delta_2 \end{aligned}\right\}$ where δ_1 and δ_2 are small quantities ($\ll 1$)

then if $|\ell_3| \ll \zeta$

$$K \doteq \frac{-\delta_2 + j\zeta_2}{-\delta_1 + j\zeta_1} \tag{3.10.7}$$

i.e. for small differences between δ_1 and δ_2 and between ζ_1 and ζ_2:

$$|K| = \sqrt{\frac{\delta_2^{\,2} + \zeta_2^{\,2}}{\delta_1^{\,2} + \zeta_1^{\,2}}} \doteq 1 \tag{3.10.8}$$

$$\begin{aligned} \text{and } \angle K &= \left(\pi - \arctan\frac{\zeta_2}{\delta_2}\right) - \left(\pi - \arctan\frac{\zeta_1}{\delta_1}\right) \\ &= \arctan\left(\frac{\zeta_1}{\delta_1}\right) - \arctan\left(\frac{\zeta_2}{\delta_2}\right) \end{aligned} \tag{3.10.9}$$

From (3.10.8) and (3.10.9) it can be seen that the effect of the small differences on $\left|\frac{Y_s}{X_s}\right|$ is negligible but could significantly affect the value of $\angle\frac{Y_s}{X_s}$ as :

$$\angle\frac{Y_s}{X_s} = \pi + \angle\frac{Y}{X} + \angle K \tag{3.10.10}$$

3.11 Summary

This chapter has been concerned with a basic linear damped spring mass system and it has been shown that it is possible to measure Ω_3, the rate of turn about an axis perpendicular to the plane of vibration of the mass Oxy. It appears from section 3.2 that a method employing a free vibration system could not be made to work practicably as the damping would have to be negligible and any unwanted coupling would make the calculations very difficult; therefore a forced vibration system will be required.

For small values of Ω_3, it has been shown in section 3.3 that both $\left|\frac{Y}{X}\right|$ and $\left|\frac{Y}{X_s}\right|$ vary linearly with the magnitude of Ω_3 whilst the phase angles $\angle\frac{Y}{X}$ and $\angle\frac{Y}{X_s}$ provide a means of determining the sign of Ω_3. The factors which might affect the response have been shown to be the various couplings, c_i, c_d and c_s (section 3.4), rotations Ω_1 and Ω_2 about the other two axes (section 3.6), oscillatory variations in the rotation $\overline{\Omega}$ (section 3.7) and an accelerating origin (section 3.8). The transient response will be affected by the value of the damping ratic ζ (section 3.5) and this might be the deciding factor in the choice of its numerical value.

The advantage of applying an additional exciting force has been discussed in section 3.9, it can be employed either to cancel out the effects of c_i, c_d and c_s or to provide an alternative method of determing Ω_3 by measuring the magnitude ratio $\frac{P_2}{P_1}$ and the phase angle between the two exciting forces; a mismatch of the natural frequencies in the two directions Ox and Oy is shown in section 3.10 to have little effect on the results, except in this last case, provided that they are referred to the parameters in the direction Oy.

Before going on to consider how this basic system can be realised in a practical device, the variation of $\frac{Y}{X}$, $\frac{Y}{X_s}$ and $\frac{X}{X_s}$ with Ω_3 will be considered in more detail in the next chapter.

CHAPTER 4

The theoretical steady state vibration of the fundamental system due to a constant angular rate of rotation about Oz

4.1 The equations (3.4.2) in computer language

As stated in section 3.4, a computer program was considered desirable to evaluate, from equations (3.4.2), the steady state response of the fundamental damped-spring-mass system, **fig.3.1.1**, to a constant angular rate of rotation $\overline{\Omega} = \Omega_3 \overline{k}$. We require to determine and analyse the variation in the modulus and phase angle (argument) of $\frac{Y}{X}$, $\frac{Y}{X_s}$ and $\frac{X}{X_s}$ for different values of ℓ_3 when r, ζ, u_i, u_d and u_s have particular values.

In order to conform to the computer language (Atlas Autocode) it is necessary to redefine some of the symbols:

$$\left.\begin{array}{lll} \text{Let } d & \equiv & \zeta \\ u(1) & \equiv & u_i \\ u(2) & \equiv & u_d \\ u(3) & \equiv & u_s \\ \text{and } \ell & \equiv & \ell_3 \end{array}\right\} \qquad (4.1.1)$$

As several factors in equations (3.4.2) keep on recurring, it is convenient to evaluate these initially:

$$\left.\begin{array}{llll} \text{Let } v(1) & = (u(3) - u(1)r^2) & \equiv & (u_s - u_i r^2) \\ v(2) & = (u(2) + 2\ell)r & \equiv & (u_d + 2\ell_3)r \\ v(3) & = (u(2) - 2\ell)r & \equiv & (u_d - 2\ell_3)r \\ v(4) & = (r^2 + \ell^2 - 1) & \equiv & (r^2 + \ell_3^2 - 1) \\ \text{and } v(5) & = -2dr & \equiv & -2\zeta r \end{array}\right\} \qquad (4.1.2)$$

Equations (3.4.2) now become:

$$\left.\begin{aligned} -\left[v(4) + jv(5)\right]X + \left[v(1) + jv(3)\right]Y &= X_s \\ -\left[v(4) + jv(5)\right]Y + \left[v(1) + jv(2)\right]X &= 0 \end{aligned}\right\} \quad (4.1.3)$$

From the second equation:

$$\frac{Y}{X} = \frac{v(1) + jv(2)}{v(4) + jv(5)} \quad (4.1.4)$$

Substituting for X from (4.1.4) into (4.1.3) we have:

$$\begin{aligned} \frac{Y}{X_s} &= \frac{v(1) + jv(2)}{\left[v(1)+jv(2)\right]\left[v(1)+jv(3)\right] - \left[v(4)+jv(5)\right]^2} \\ &= \frac{v(1) + jv(2)}{v(6) + jv(7)} \end{aligned} \quad (4.1.5)$$

$$\left.\begin{aligned} \text{where } v(6) &= v(1)^2 - v(2)v(3) - v(4)^2 + v(5)^2 \\ \text{and } v(7) &= v(1)\left[v(2) + v(3)\right] - 2v(4)v(5) \end{aligned}\right\} \quad (4.1.6)$$

and from (4.1.4) and (4.1.5) we have:

$$\frac{X}{X_s} = \frac{v(4) + jv(5)}{v(6) + jv(7)} \quad (4.1.7)$$

In the computer language:

$$\left.\begin{aligned} \text{radius } (a,b) &\equiv \sqrt{a^2 + b^2} \\ \text{and arctan } (a,b) &\equiv \arctan\left(\frac{b}{a}\right) \end{aligned}\right\} \quad (4.1.8)$$

so the results required are:

$$\text{from}(4.1.4) \quad \left\{\begin{aligned} \text{mod } \frac{Y}{X} &= \text{radius}(v(1),v(2))/\text{radius}(v(4),v(5)) \\ \text{arg } \frac{Y}{X} &= \text{arctan}(v(1),v(2)) - \text{arctan}(v(4),v(5)) \end{aligned}\right\} \quad (4.1.9)$$

$$\text{from}(4.1.5) \quad \left\{\begin{aligned} \text{mod } \frac{Y}{X_s} &= \text{radius}(v(1),v(2))/\text{radius}(v(6),v(7)) \\ \text{arg } \frac{Y}{X_s} &= \text{arctan}(v(1),v(2)) - \text{arctan}(v(6),v(7)) \end{aligned}\right\} \quad (4.1.10)$$

$$\text{from}(4.1.7) \quad \left\{\begin{aligned} \text{mod } \frac{X}{X_s} &= \text{radius}(v(4),v(5))/\text{radius}(v(6),v(7)) \\ \text{arg } \frac{X}{X_s} &= \text{arctan}(v(4),v(5)) - \text{arctan}(v(6),v(7)) \end{aligned}\right\} \quad (4.1.11)$$

The basic procedure in evolving the program was to declare d, u(1), u(2) and u(3) and then vary ℓ for a range of values of r.

4.2 A typical computer program

```
***A

JOB

ENG 002/0000C161/LINNETT C/1

OUTPUT

0 LINE PRINTER 1000 LINES

EXECUTION 3 MINUTES
COMPILER AA
```

upper case delimiters

```
BEGIN
INTEGER h,i,j,k,n,f
REAL d,l,m,r,s,li,ri
REAL ARRAY u(1:3),v(1:7),a(1:3),b(1:3)
read(f,ri,s,h,li,m,n)
CYCLE j=1,1,f
read(d,u(1),u(2),u(3))
CAPTIONøøDAMPING øøø RATIO øøø =ø ; print fl(d,3)
CAPTIONøøINERTIA øø COUPLING ø=ø; print fl(u(1),3)
CAPTIONøøDAMPING øø COUPLING ø=ø; print fl(u(2),3)
CAPTIONøSTIFFNESS ø COUPLING ø=ø; print fl(u(3),3)
CAPTION øøøøø 1 øøøøøøø MOD(Y/X)øøø ARG(Y/X)øøøø MOD(Y/Xs)øø
CAPTION ARG(Y/Xs)øøøø MOD(X/Xs)øø ARG(X/Xs)
CYCLE i=0,1,h
r=ri+s*i
COMMENT r is increased from ri by s for h cycles
CAPTION øø r ø=ø ; print fl(r,4); newline
```

```
v(1)=u(3)-u(1)*r²

v(5)=-2d*r

CYCLE k=0,1,n

l=li+m*k

COMMENT l is increased from li by m for n cycles

v(2)=(u(2)+2l)r

v(3)=(u(2)-2l)r

v(4)=r²+l²-1
v(6)=v(1)²-v(2)*v(3)-v(4)²+v(5)²
v(7)=v(1)(v(2)+v(3))-2v(4)*v(5)
a(1)=radius(v(1),v(2))
a(2)=radius(v(4),v(5))
a(3)=radius(v(6),v(7))
IF v(1)=0 AND v(2)=0 THEN -> 2

b(1)=arctan(v(1),v(2))
->3
2:b(1)=π/2
COMMENT b(1) -> π/2 if v(1) = 0+ and v(2) = 0+

3:b(2)=arctan(v(4),v(5))

b(3)=arctan(v(6),v(7))

b(1)=57.3 b(1)

b(2)=57.3 b(2)

b(3)=57.3 b(3)

IF a(2) < 1α-9 OR a(3) < 1α-9 THEN ->4

print (l,1,4); spaces(3)

print fl(a(1)/a(2),3); spaces(3)

print (b(1)-b(2),3,1); spaces(5)

print fl(a(1)/a(3),3); spaces(3)

print (b(1)-b(3),3,1); spaces(5)
print fl(a(2)/a(3),3); spaces(3)
```

```
print (b(2)-b(3),3,1); newline
4:REPEAT
REPEAT

REPEAT

END OF PROGRAM
```

```
9 0.95 0.05 2 -0.015 0.001 30

0.1 0.01 0.002 0
0.1 0.01 0.005 0
0.1 0.01 0.01  0
0.1 0    0.01  0
0.2 0.01 0.01  0
0.4 0.01 0.01  0
0.1 0.05 0.01  0
0.1 0.01 0.02  0
0.1 0.05 0.02  0

***Z
```

A section of the print-out from this program is shown in fig. 4.2.1.

DAMPING RATIO = 1.000⏨-1
INERTIA COUPLING = 5.000⏨-2
DAMPING COUPLING = 1.000⏨-2
STIFFNESS COUPLING = 0.000⏨-40

L	MOD(Y/X)	ARG(Y/X)	MOD(Y/XS)	ARG(Y/XS)	MOD(X/XS)	ARG(X/XS)
R = 9.5000⏨-1						
-0.0150	2.294⏨-1	-40.1	1.022⏨0	-105.0	4.456⏨0	-65.0
-0.0140	2.261⏨-1	-42.1	1.009⏨0	-107.0	4.462⏨0	-64.9
-0.0130	2.230⏨-1	-44.3	9.964⏨-1	-109.0	4.467⏨0	-64.8
-0.0120	2.204⏨-1	-46.5	9.855⏨-1	-111.1	4.472⏨0	-64.7
-0.0110	2.180⏨-1	-48.7	9.759⏨-1	-113.3	4.477⏨0	-64.6
-0.0100	2.160⏨-1	-51.0	9.678⏨-1	-115.5	4.481⏨0	-64.5
-0.0090	2.143⏨-1	-53.3	9.611⏨-1	-117.7	4.485⏨0	-64.4
-0.0080	2.130⏨-1	-55.7	9.560⏨-1	-120.0	4.488⏨0	-64.4
-0.0070	2.121⏨-1	-58.0	9.524⏨-1	-122.4	4.491⏨0	-64.3
-0.0060	2.115⏨-1	-60.4	9.504⏨-1	-124.7	4.494⏨0	-64.3
-0.0050	2.113⏨-1	297.2	9.500⏨-1	232.9	4.496⏨0	-64.2
-0.0040	2.115⏨-1	294.8	9.512⏨-1	230.6	4.498⏨0	-64.2
-0.0030	2.121⏨-1	292.4	9.540⏨-1	228.2	4.499⏨0	-64.2
-0.0020	2.130⏨-1	290.0	9.584⏨-1	225.8	4.500⏨0	-64.2
-0.0010	2.143⏨-1	287.6	9.644⏨-1	223.5	4.500⏨0	-64.1
-0.0000	2.159⏨-1	285.3	9.719⏨-1	221.2	4.501⏨0	-64.1
0.0010	2.179⏨-1	283.0	9.808⏨-1	218.9	4.500⏨0	-64.1
0.0020	2.203⏨-1	280.8	9.913⏨-1	216.6	4.500⏨0	-64.2
0.0030	2.230⏨-1	278.6	1.003⏨0	214.4	4.499⏨0	-64.2
0.0040	2.260⏨-1	276.4	1.016⏨0	212.2	4.498⏨0	-64.2
0.0050	2.293⏨-1	274.3	1.031⏨0	210.1	4.496⏨0	-64.2
0.0060	2.329⏨-1	272.3	1.046⏨0	208.0	4.494⏨0	-64.3
0.0070	2.368⏨-1	270.4	1.063⏨0	206.0	4.491⏨0	-64.3
0.0080	2.409⏨-1	268.5	1.081⏨0	204.1	4.488⏨0	-64.4
0.0090	2.453⏨-1	266.6	1.100⏨0	202.2	4.485⏨0	-64.4
0.0100	2.500⏨-1	264.9	1.120⏨0	200.4	4.481⏨0	-64.5
0.0110	2.548⏨-1	263.2	1.141⏨0	198.6	4.477⏨0	-64.6
0.0120	2.599⏨-1	261.6	1.162⏨0	196.9	4.472⏨0	-64.7
0.0130	2.652⏨-1	260.0	1.185⏨0	195.2	4.467⏨0	-64.8
0.0140	2.707⏨-1	258.5	1.208⏨0	193.6	4.462⏨0	-64.9
0.0150	2.764⏨-1	257.0	1.232⏨0	192.1	4.456⏨0	-65.0

Fig. 4.2.1 Section of the computer print-out

4.3 The solutions with zero coupling

The variation of $\left|\frac{Y}{X}\right|$ and $\angle\frac{Y}{X}$ with ℓ_3 for $\zeta = 0.1$, $r = 0.9$, 1.0 and 1.1, and $u_i = u_d = u_s = 0$ has already been plotted in figures 3.3.1 and 3.3.2. From equations (3.3.15) it was shown that the $\left|\frac{Y}{X}\right|$ against $|\ell_3|$ curve rose to a single peak, the height of which decreased with increasing r, but that the maximum slope for $\ell_3 \ll 1$ was $\frac{1}{\zeta}$ and occured when $r = 1$ [see equation (3.3.16)].

Considering the variation of $\frac{X}{X_s}$, $\frac{Y}{X_s}$ and $\frac{Y}{X}$ with ℓ_3 for various values of r: for r = 0, i.e. a constant exciting force $P_1\bar{i}$, equations (3.3.4) give:

$$\left.\begin{aligned} \frac{X}{X_s} &= \frac{1}{1 - \ell_3^2} \\ \text{and } \frac{Y}{X} &= 0 \text{ if } \ell_3 \neq 1 \end{aligned}\right\} \qquad (4.3.1)$$

$$\text{If } \ell_3 = 1, \; \frac{Y}{X} = \lim_{r \to 0}\left\{ - \frac{2r}{-r^2 + j(2\zeta r)}\right\} = j\left(\frac{1}{\zeta}\right) \qquad (4.3.2)$$

As expected, equations (4.3.1) and (4.3.2) reveal that the modulus curves plotted against $|\ell_3|$ for r = 0 go to a peak at the critical speed $|\ell_3| = 1$, the peak being infinite in the case of $\left|\frac{X}{X_s}\right|$ and $\left|\frac{Y}{X_s}\right|$.

The modulus curves for $0 < |\ell_3| < 2.0$ and $0 < r < 1.6$ are plotted on figures 4.3.1 - 4.3.3 for $\zeta = 0.1$. From figures 4.3.1 and 4.3.2 it can be seen that, except in the cases when r = 0 or $\ell_3 = 0$, the curves for $\left|\frac{X}{X_s}\right|$ and $\left|\frac{Y}{X_s}\right|$ against $|\ell_3|$ or r have two peaks; for $\zeta \ll 1$ these peaks occur at approximately the two undamped natural frequencies of the system [cf. fig.3.3.2]. Figure 4.3.3 shows the single peak in the variation of $\left|\frac{Y}{X}\right|$ with $|\ell_3|$, this occurs close to the lower of the two undamped natural frequencies for $\zeta \ll 1$ [cf.eqn.(3.3.14)].

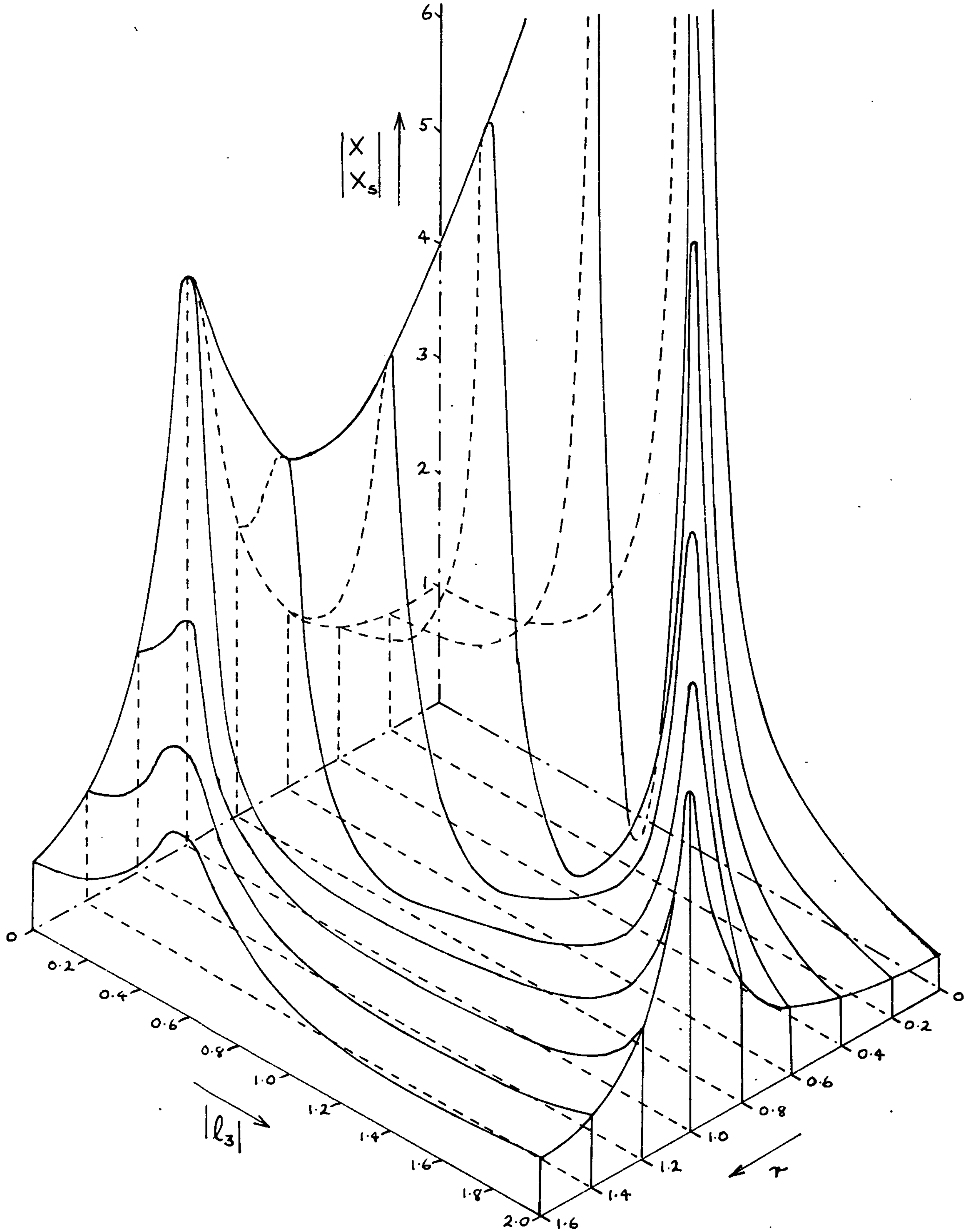

Fig 4.3.1 Variation of $\left|\frac{X}{X_s}\right|$ with $|l_3|$ and r for $\zeta = 0.1$

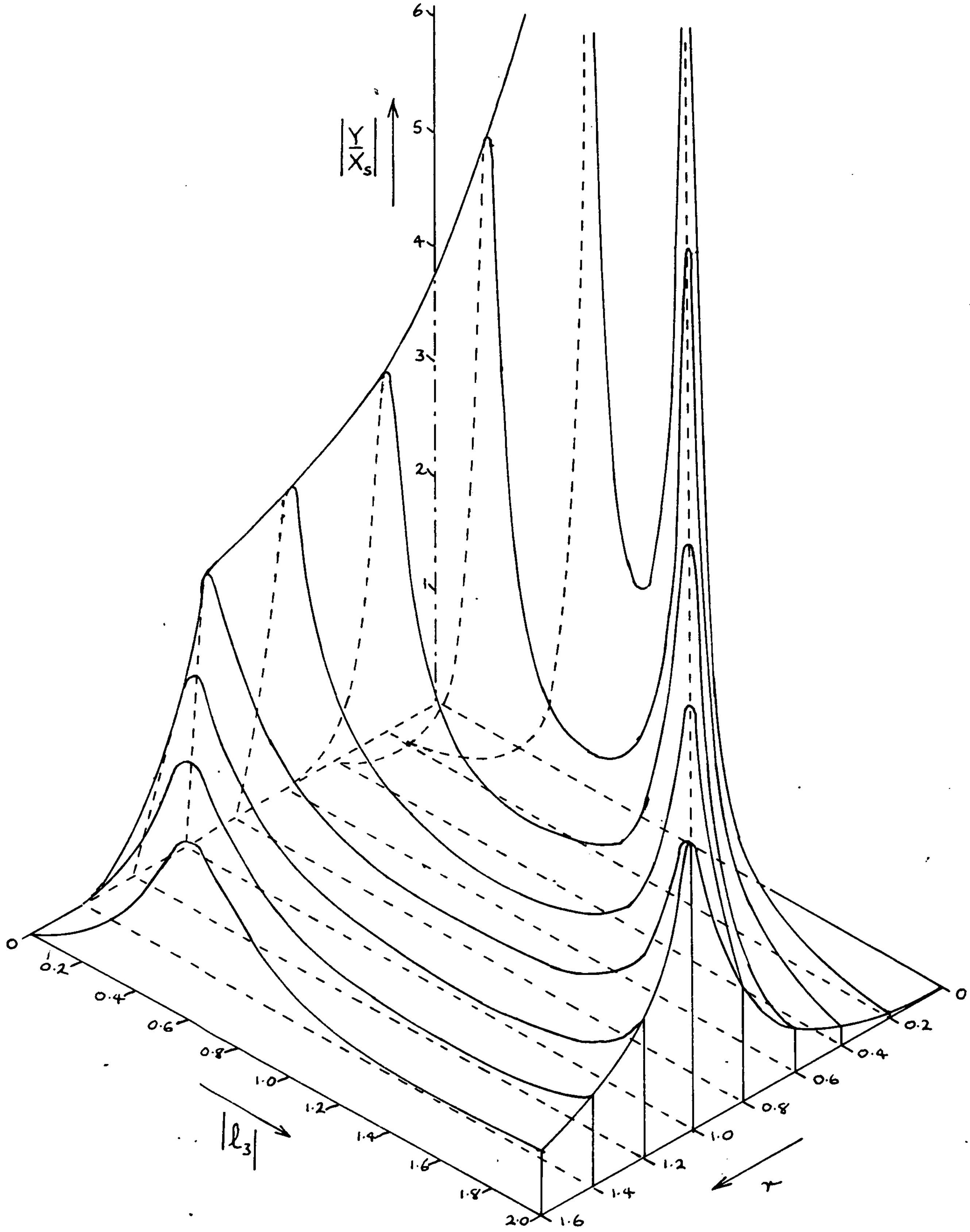

Fig. 4.3.2 Variation of $\left|\frac{Y}{X_s}\right|$ with $|\ell_3|$ and r for $\zeta = 0.1$

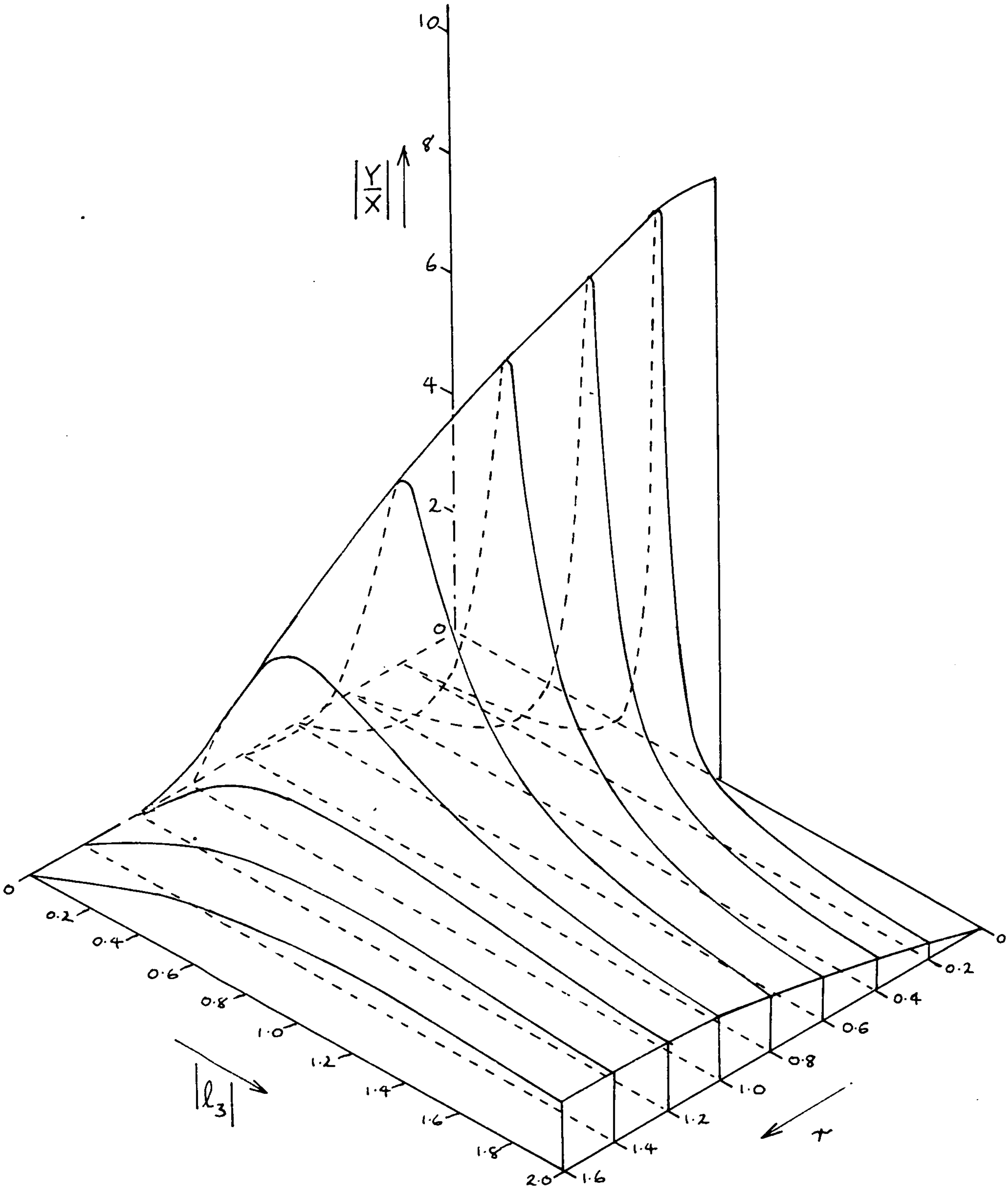

Fig 4.3.3 Variation of $\left|\frac{Y}{X}\right|$ with $|l_3|$ and r for $\zeta = 0.1$

The phase angle curves for positive ℓ_3 are plotted on figures 4.3.4 - 4.3.6, they show the 180° phase change associated with each peak of the modulus curves. In the case of $\angle\frac{Y}{X_s}$ and $\angle\frac{Y}{X}$ there is a step change of 180° at $\ell_3 = 0$ so that the curves for negative ℓ_3 will differ from those drawn by this amount; the curves for $\angle\frac{X}{X_s}$ are symmetrical about $\ell_3 = 0$.

The main concern here is with the measurement of small rates of turn so we can concentrate on values of $\ell_3 \ll 1$ and $r \doteqdot 1$.

4.4 The effect of inertia or stiffness coupling

Inertia and stiffness coupling can be considered together as they both appear only in the factor $v(1) = (u_s - u_i r^2)$ in equations (4.1.2). If the damping coupling $u_d = 0$, the modifications to the uncoupled results due to u_s or u_i can be assessed by considering equations (4.1.4), (4.1.5) and (4.1.7).

From equation (4.1.4):

$$\frac{Y}{X} = \frac{v(1) + jv(2)}{v(4) + jv(5)} \tag{4.1.4}$$

v(2), v(4) and v(5) [see equations (4.1.2)] will be the same as for the uncoupled case so, considering the modulus and phase angle:

$$\left|\frac{Y}{X}\right| = \sqrt{\frac{v(1)^2 + v(2)^2}{v(4)^2 + v(5)^2}} \tag{4.4.1}$$

$$\text{and } \angle\frac{Y}{X} = \arctan\frac{v(2)}{v(1)} - \arctan\frac{v(5)}{v(4)} \tag{4.4.2}$$

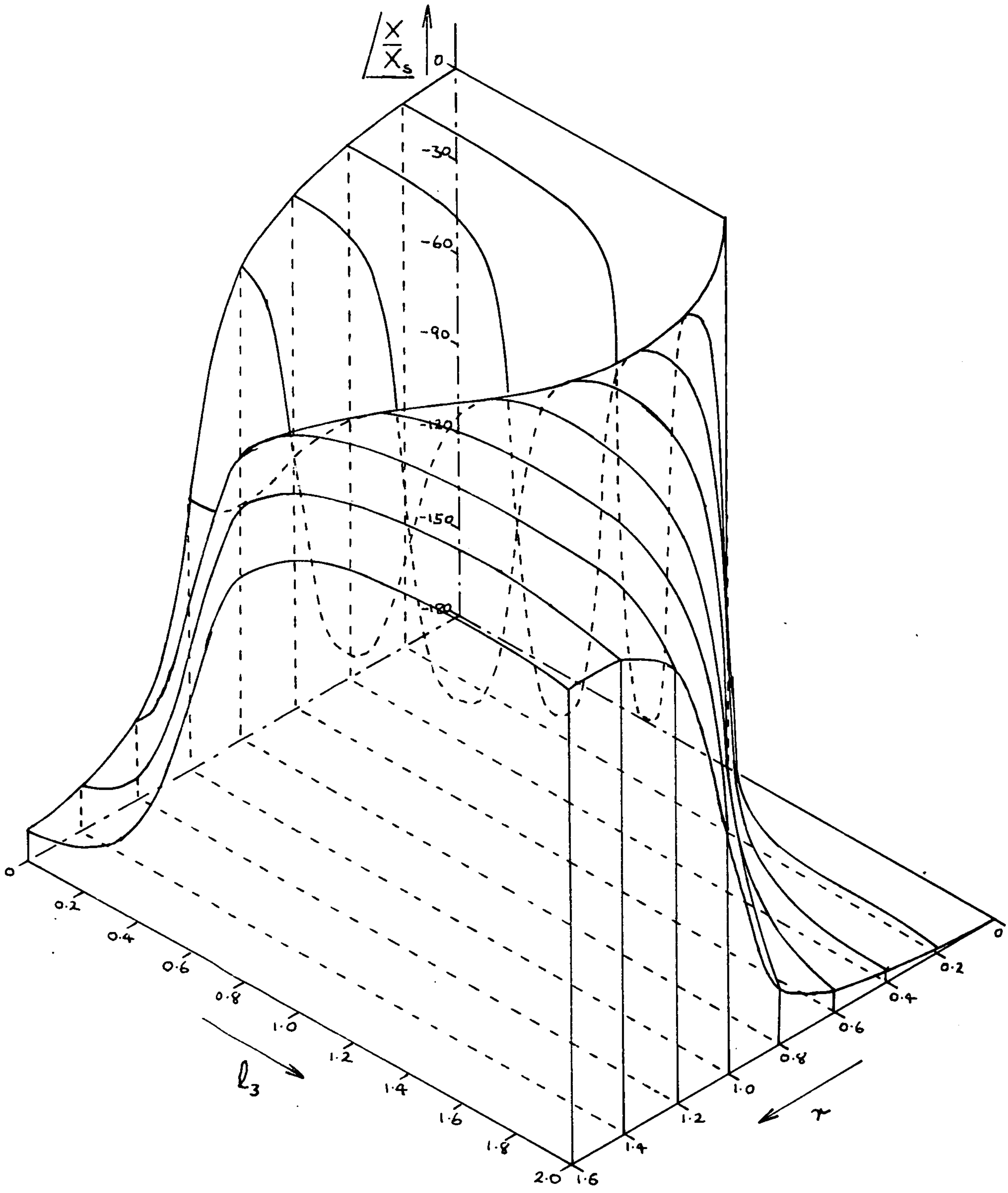

Fig 4.3.4 Variation of $\angle\frac{X}{X_s}$ with l_3 and r for $\zeta = 0.1$

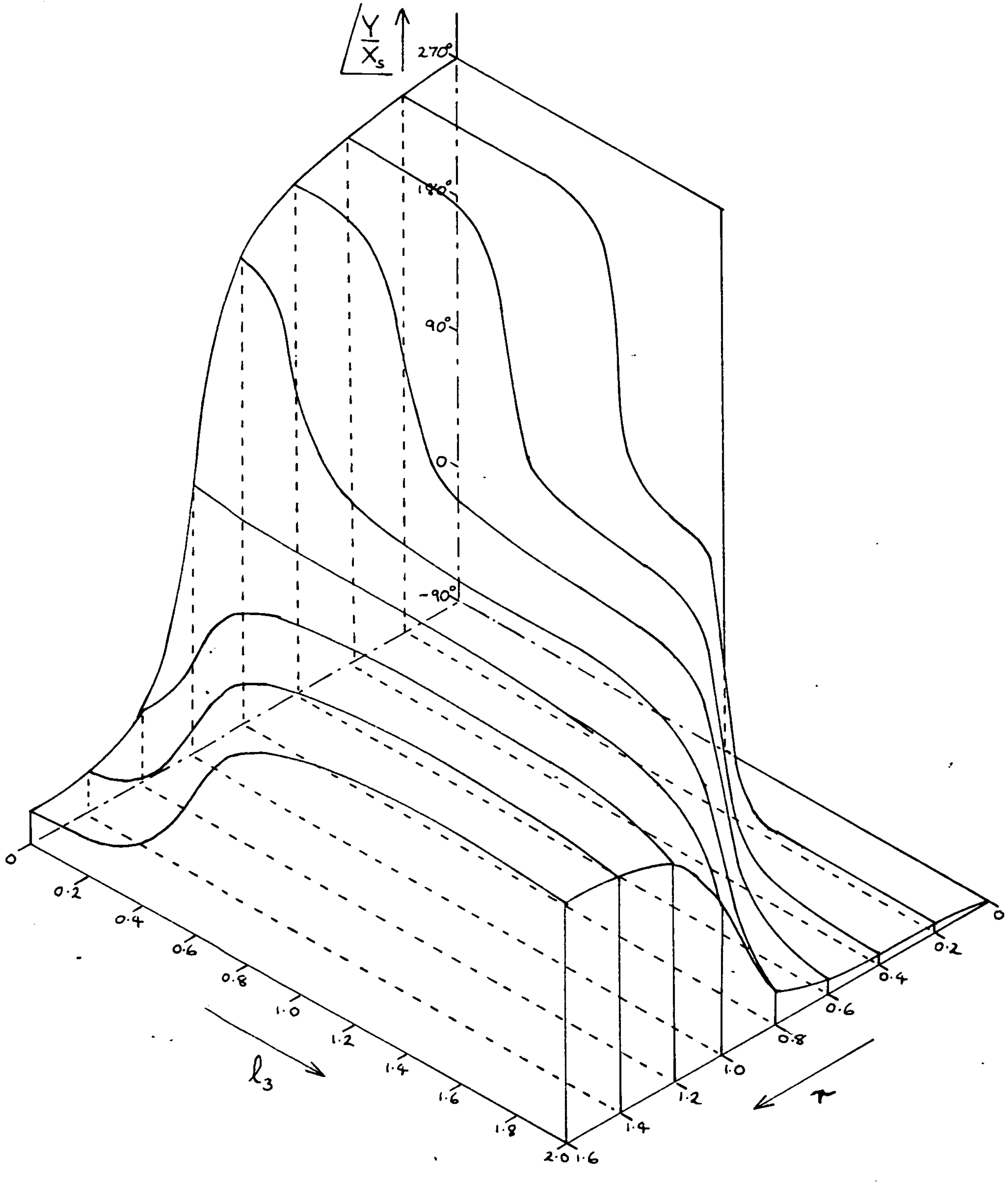

Fig. 4.3.5 Variation of $\angle \frac{Y}{X_s}$ with l_3 and r for $\zeta = 0.1$

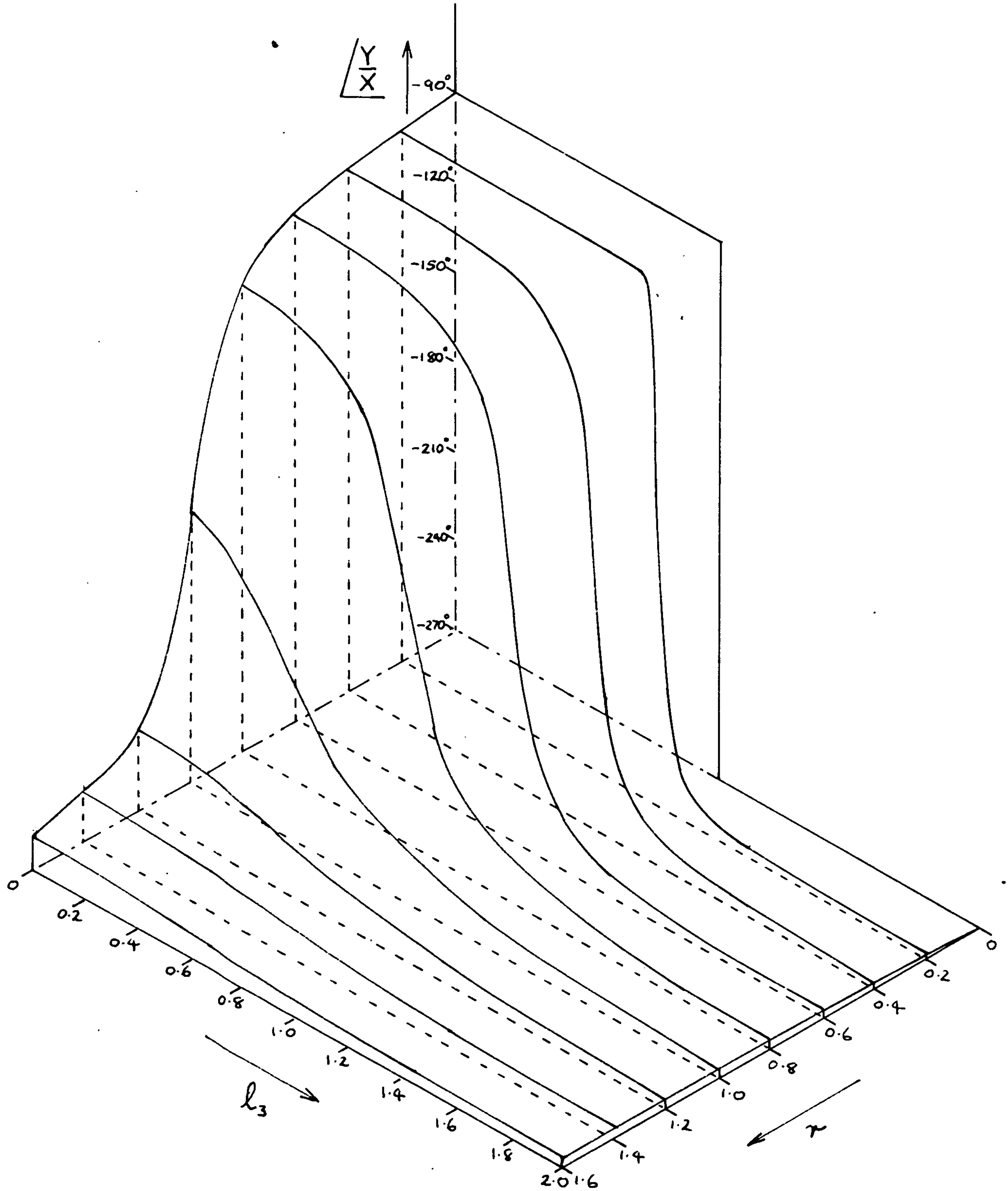

Fig 4.3.6 Variation of $\angle \frac{Y}{X}$ with l_3 and r for $\zeta = 0.1$

Substituting from (4.1.2) into (4.4.1) gives:

$$\left|\frac{Y}{X}\right| = \sqrt{\frac{(u_s - u_i r^2)^2 + (2\,\ell_3 r)^2}{(r^2 + \ell_3^{\,2} - 1)^2 + (2\zeta r)^2}}$$

For $\ell_3^{\,2} \ll 2\zeta r$

$$\left|\frac{Y}{X}\right| \doteqdot \sqrt{\frac{(u_s - u_i r^2)^2 + (2\,\ell_3 r)^2}{(r^2 - 1)^2 + (2\zeta r)^2}} \qquad (4.4.3)$$

$$= \frac{\left|(u_s - u_i r^2)\right|}{\sqrt{(r^2 - 1)^2 + (2\zeta r)^2}} \sqrt{1 + \left(\frac{2\,\ell_3 r}{u_s - u_i r^2}\right)^2}$$

Expanding for $(2\,\ell_3 r)^2 \ll (u_s - u_i r^2)^2$

$$\left|\frac{Y}{X}\right| \doteqdot \frac{\left|u_s - u_i r^2\right|}{\sqrt{(r^2 - 1)^2 + (2\zeta r)^2}} \left\{1 + \frac{2r^2\,\ell_3^{\,2}}{(u_s - u_i r^2)^2}\right\} \qquad (4.4.4)$$

i.e., for constant r, $\left|\frac{Y}{X}\right|$ depends on the square of ℓ_3 and, when $r = 1$:

$$\left|\frac{Y}{X}\right| \doteqdot \frac{\left|u_s - u_i\right|}{2\zeta} \left\{1 + \frac{2\,\ell_3^{\,2}}{(u_s - u_i)^2}\right\} \qquad (4.4.5)$$

Thus, for small values of ℓ_3 and constant r, the coupling has the effect of giving $\left|\frac{Y}{X}\right|$ a finite value when $\ell_3 = 0$ compared with zero in the uncoupled case, and it varies as the square of ℓ_3 compared with the linear relationship:

$$\left|\frac{Y}{X}\right| = \frac{2r\,\ell_3}{\sqrt{(r^2 - 1)^2 + (2\zeta r)^2}} \qquad (4.4.6)$$

in the uncoupled case. This means that the simple method of determining ℓ_3 from $\left|\frac{Y}{X}\right|$ has been lost. However, examining the phase angle $\underline{/\frac{Y}{X}}$, from (4.4.2) and (4.1.2):

$$\underline{/\frac{Y}{X}} \doteqdot \arctan\left[\frac{2\,\ell_3 r}{u_s - u_i r^2}\right] - \arctan\left[\frac{-2\zeta r}{r^2 + \ell_3^{\,2} - 1}\right] \qquad (4.4.7)$$

which, for $\left|2\,\ell_3 r\right| \ll \left|u_s - u_i r^2\right|$ and $\ell_3^{\,2} \ll 2\zeta r$ gives:

$$\left.\begin{aligned}
&\text{if } u_s > u_i r^2 \\
&\angle\frac{Y}{X} \doteqdot \left[\frac{2r}{u_s - u_i r^2}\right]\ell_3 + \arctan\left[\frac{2\zeta r}{r^2 - 1}\right] \\
&\text{and if } u_s < u_i r^2 \\
&\angle\frac{Y}{X} \doteqdot \pi - \left[\frac{2r}{u_i r^2 - u_s}\right]\ell_3 + \arctan\left[\frac{2\zeta r}{r^2 - 1}\right]
\end{aligned}\right\} \quad (4.4.8)$$

i.e., for constant r, $\angle\frac{Y}{X}$ varies linearly with ℓ_3, the slope:

$$\frac{d\angle\frac{Y}{X}}{d\ell_3} = \frac{2r}{u_s - u_i r^2} \quad (4.4.9)$$

being independent of ζ; this compares with the uncoupled case in which there is a 180° step change at $\ell_3 = 0$ and a constant $\angle\frac{Y}{X}$ for $\ell_3 \ll 1$ [cf. equations (3.3.11)]. This means that the phase angle $\angle\frac{Y}{X}$ provides a simple means of determining ℓ_3, for sufficiently small values, when inertia or stiffness coupling is present. Typical curves, derived from the complete equations, of $\left|\frac{Y}{X}\right|$ and $\angle\frac{Y}{X}$ against ℓ_3 for r = 1 are shown on figures 4.4.1 and 4.4.2. It can be seen that, for higher values of ℓ_3, the coupling term v(1) becomes insignificant compared with the other terms and the modulus and phase angle curves approach those for the uncoupled system.

From equation (4.1.5)

$$\left|\frac{Y}{X_s}\right| = \sqrt{\frac{v(1)^2 + v(2)^2}{v(6)^2 + v(7)^2}} \quad (4.4.10)$$

and $$\angle\frac{Y}{X_s} = \arctan\frac{v(2)}{v(1)} - \arctan\frac{v(7)}{v(6)} \quad (4.4.11)$$

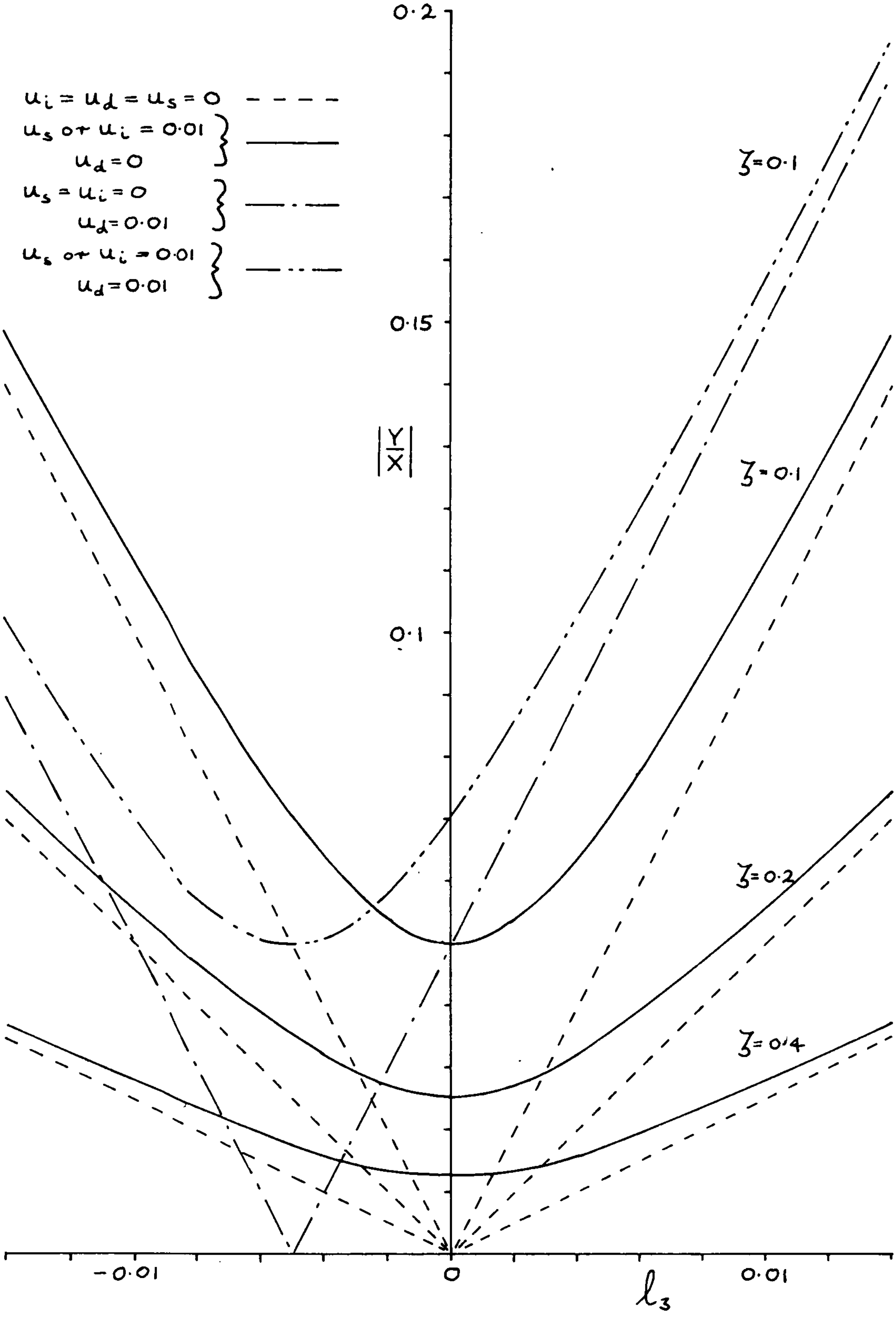

Fig 4.4.1 Variation of $\left|\frac{Y}{X}\right|$ with l_3 for $r = 1$ and various values of u_i, u_d, u_s and ζ

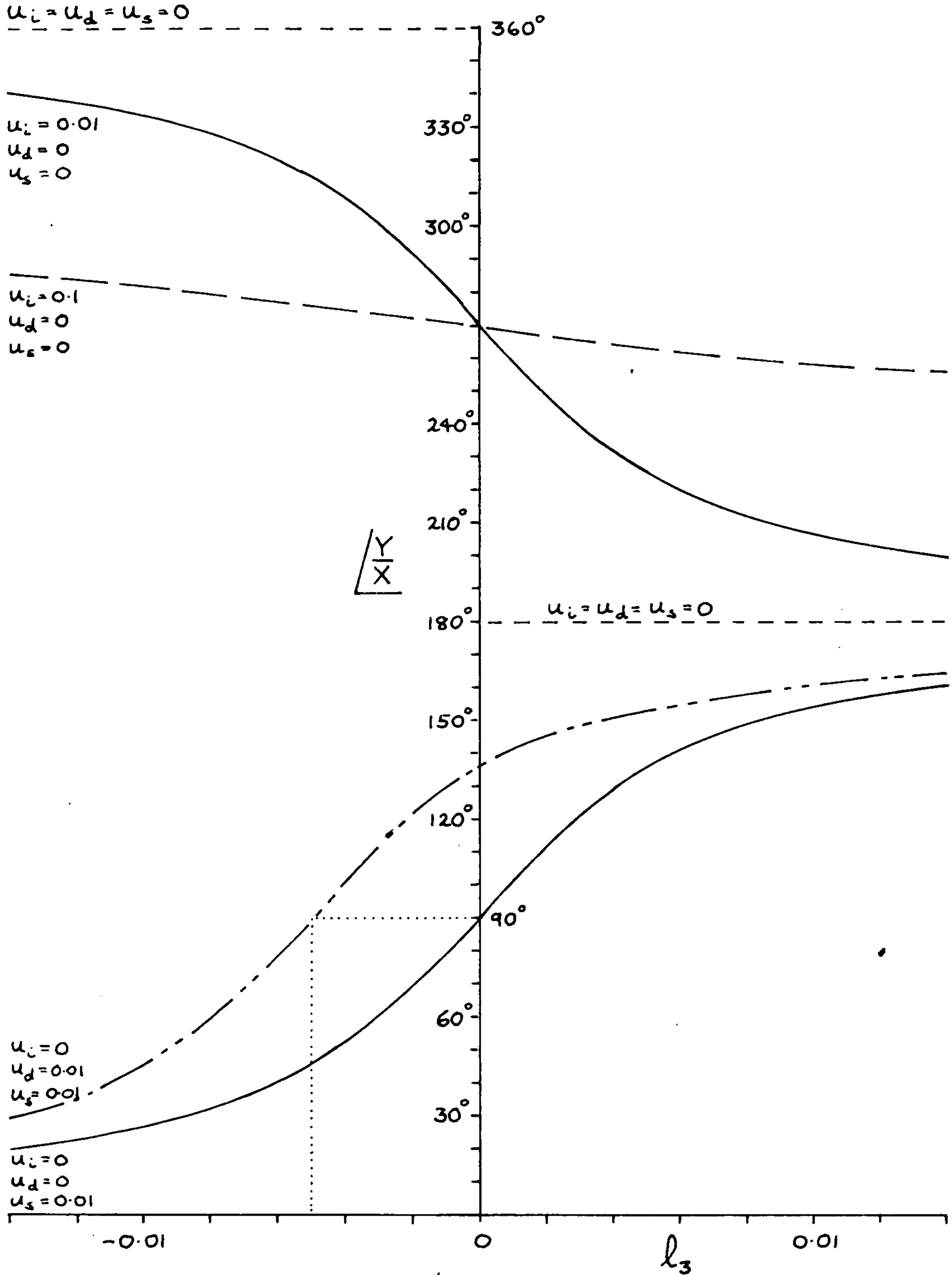

Fig. 4.4.2 Variation of $\angle \frac{Y}{X}$ with l_3 for $r = 1$, various values of u_i, u_d and u_s and all values of ζ

v(6) and v(7) are given by equation (4.1.6) for $u_d = 0$ as:

$$\left.\begin{aligned} v(6) &= (u_s - u_i r^2)^2 + (2\ell_3 r)^2 - (r^2 + \ell_3^2 - 1)^2 + (2\zeta r)^2 \\ v(7) &= -2(r^2 + \ell_3^2 - 1)(-2\zeta r) \end{aligned}\right\} \qquad (4.4.12)$$

If $(2\ell_3 r)^2 \ll (u_s - u_i r^2)^2$:

$$\left.\begin{aligned} v(6) &\doteqdot (u_s - u_i r^2)^2 - (r^2 - 1)^2 + (2\zeta r)^2 \\ v(7) &= 4\zeta r(r^2 + \ell_3^2 - 1) \end{aligned}\right\} \qquad (4.4.13)$$

Substituting into (4.4.10):

$$\left|\frac{Y}{X_s}\right| = \sqrt{\frac{(u_s - u_i r^2)^2 + (2\ell_3 r)^2}{\left[(u_s - u_i r^2)^2 - (r^2-1)^2 + (2\zeta r)^2\right]^2 + \left[4\zeta r(r^2 + \ell_3^2 - 1)\right]^2}}$$

which reduces to:

$$\left|\frac{Y}{X_s}\right| \doteqdot \frac{|u_s - u_i r^2|}{\sqrt{\left[(u_s - u_i r^2)^2 - (r^2-1)^2 + (2\zeta r)^2\right]^2 + \left[4\zeta r(r^2-1)\right]^2}} \left\{1 + \frac{2r^2\ell_3^2}{(u_s - u_i r^2)^2}\right\} \qquad (4.4.14)$$

Thus the coupling has the same effect on $\left|\frac{Y}{X_s}\right|$ as it had on $\left|\frac{Y}{X}\right|$ viz., that for small values of ℓ_3 and constant r, it varies as the square of ℓ_3 and has a finite value at $\ell_3 = 0$ (see figure 4.5.1).

If r = 1:

$$\left|\frac{Y}{X_s}\right| \doteqdot \frac{|u_s - u_i|}{(u_s - u_i)^2 + (2\zeta)^2} \left\{1 + \frac{2\ell_3^2}{(u_s - u_i)^2}\right\} \qquad (4.4.15)$$

From (4.4.11)

$$\angle\frac{Y}{X_s} \doteqdot \arctan\left[\frac{2\ell_3 r}{u_s - u_i r^2}\right] - \arctan\left[\frac{v(7)}{v(6)}\right] \qquad (4.4.16)$$

which, for $|2\ell_3 r| \ll |u_s - u_i r^2|$ gives:

if $u_s > u_i r^2$

$$\angle\frac{Y}{X_s} = \left[\frac{2r}{u_s - u_i r^2}\right]\ell_3 - \arctan\left[\frac{4\zeta r(r^2-1)}{(u_s - u_i r^2)^2 - (r^2-1)^2 + (2\zeta r)^2}\right] \qquad (4.4.17)$$

and if $u_s < u_i r^2$

$$\underline{/\frac{Y}{X_s}} = \pi - \left[\frac{2r}{u_i r^2 - u_s}\right] \ell_3 - \arctan\left[\frac{4\zeta r(r^2-1)}{(u_s - u_i r^2)^2 - (r^2-1)^2 + (2\zeta r)^2}\right] \tag{4.4.18}$$

i.e., for constant r, $\underline{/\frac{Y}{X_s}}$ also varies linearly with ℓ_3, the slope being independent of ζ (see figure 4.5.2).

The effect of damping and inertia coupling on $\frac{X}{X_s}$ for the same low values of ℓ_3 can be determined from the results for $\frac{Y}{X}$ and $\frac{Y}{X_s}$. From (4.4.4) and (4.4.14):

$$\left|\frac{X}{X_s}\right| = \sqrt{\frac{(r^2-1)^2 + (2\zeta r)^2}{\left[(u_s - u_i r^2)^2 - (r^2-1)^2 + (2\zeta r)^2\right]^2 + \left[4\zeta r(r^2-1)\right]^2}} \tag{4.4.19}$$

or, if r = 1:

$$\left|\frac{X}{X_s}\right| = \frac{2}{(u_s - u_i)^2 + 4\zeta^2} \tag{4.4.20}$$

i.e. $\left|\frac{X}{X_s}\right|$ remains constant for constant r.

From (4.4.8), (4.4.9), (4.4.17) and (4.4.18):

$$\underline{/\frac{X}{X_s}} = \underline{/\frac{Y}{X_s}} - \underline{/\frac{Y}{X}}$$

$$= -\arctan\left[\frac{4\zeta r(r^2-1)}{(u_s - u_i r^2)^2 - (r^2-1)^2 + (2\zeta r)^2}\right] - \arctan\left[\frac{2\zeta r}{r^2-1}\right]$$

$$= \arctan\left[\frac{-2\zeta r\left\{(u_s - u_i r^2)^2 + (r^2-1)^2 + (2\zeta r)^2\right\}}{(r^2-1)\left\{(u_s - u_i r^2)^2 - (r^2-1)^2 - (2\zeta r)^2\right\}}\right] \tag{4.4.21}$$

If $r = 1$, $\underline{/\frac{X}{X_s}} = -\frac{\pi}{2}$

again $\underline{/\frac{X}{X_s}}$ is constant for constant r.

For higher values of $|\ell_3|$ the coupling terms are again insignificant and the curves for $\frac{Y}{X_s}$ and $\frac{X}{X_s}$ approach those for the uncoupled case.

4.5 The effect of damping coupling

With damping coupling u_d included, from equations (4.1.2) $v(2) = (u_d - 2\ell_3)r$ but $v(1)$, $v(4)$ and $v(5)$ are unaltered, so that substituting in equation (4.4.1):

$$\left|\frac{Y}{X}\right| = \sqrt{\frac{(u_s-u_i r^2)^2 + (u_d + 2\ell_3)^2 r^2}{(r^2 + \ell_3^2 - 1)^2 + (2\zeta r)^2}} \qquad (4.5.1)$$

For $\ell_3^2 \ll 2\zeta r$

$$\left|\frac{Y}{X}\right| \doteqdot \sqrt{\frac{(u_s-u_i r^2)^2 + (u_d + 2\ell_3)^2 r^2}{(r^2 - 1)^2 + (2\zeta r)^2}} \qquad (4.5.2)$$

therefore the effect is to make $\left|\frac{Y}{X}\right|$ a minimum when $\ell_3 = -\frac{u_d}{2}$ instead of when $\ell_3 = 0$. Close to the minimum, for $(u_d+2\ell_3)^2 r^2 \ll (u_s-u_i r^2)^2$ we can approximate as in equation (4.4.4) to give:

$$\left|\frac{Y}{X}\right| \doteqdot \frac{|u_s-u_i r^2|}{\sqrt{(r^2-1)^2 + (2\zeta r)^2}}\left\{1 + \frac{(u_d + 2\ell_3)^2 r^2}{(u_s-u_i r^2)^2}\right\} \qquad (4.5.3)$$

so that the shape of the $\left|\frac{Y}{X}\right|$ curve and the value of the minimum are unaltered.

In equation (4.4.2):

$$\angle\frac{Y}{X} = \arctan\left[\frac{(u_d+2\ell_3)r}{(u_s-u_i r^2)}\right] + \arctan\left[\frac{2\zeta r}{r^2+\ell_3^2-1}\right] \qquad (4.5.4)$$

As for equations (4.4.7) to (4.4.9), $\angle\frac{Y}{X}$ will vary linearly with ℓ_3 for $|u_d + 2\ell_3| r \ll |u_s - u_i r^2|$, the slope being unaltered.

Typical curves, computed from the complete equations, showing the effect of damping coupling on $\left|\frac{Y}{X}\right|$ and $\angle\frac{Y}{X}$ for $\ell_3 \ll 1$ are shown on figures 4.4.1 and 4.4.2. When $|\ell_3| \gg |u_d|$ the curves will approach those for the uncoupled case.

To evaluate $\frac{Y}{X_s}$ from equation (4.1.5) we have, from equations (4.1.2) and (4.1.6):

$$\left.\begin{aligned} v(6) &= (u_s-u_i r^2)^2-(u_d^{\,2}-4\,\ell_3^{\,2})r^2-(r^2+\ell_3^{\,2}-1)^2+(2\zeta r)^2 \\ v(7) &= 2u_d r(u_s-u_i r^2) - 2(r^2+\ell_3^{\,2}-1)(-2\zeta r) \end{aligned}\right\} \quad (4.5.5)$$

For $2\zeta r \gg |u_d r|$, $|\ell_3 r|$ and $\ell_3^{\,2}$

$$v(6)^2 + v(7)^2 \doteqdot \left[(u_s-u_i r^2)^2-(r^2-1)^2+(2\zeta r)^2\right]^2 + \left[2u_d r(u_s-u_i r^2) + 4\zeta r(r^2-1)\right]^2 \quad (4.5.6)$$

which is constant as ℓ_3 varies, so that, by comparison with equation (4.5.3):

$$\left|\frac{Y}{X_s}\right| = \frac{|u_s-u_i r^2|}{\sqrt{v(6)^2 + v(7)^2}}\left\{1 + \frac{(u_d+2\,\ell_3)^2 r^2}{(u_s - u_i r^2)^2}\right\} \quad (4.5.7)$$

as for $\left|\frac{Y}{X}\right|$ the minumum is at $\ell_3 = -\frac{u_d}{2}$ but its magnitude will differ from the case when $u_d = 0$ due to the u_d term in $v(7)$. [cf. equation (4.4.14)].

$$\underline{/\frac{Y}{X_s}} = \arctan\left[\frac{(u_d+2\,\ell_3)r}{(u_s - u_i r^2)}\right] - \arctan\left[\frac{v(7)}{v(6)}\right] \quad (4.5.8)$$

and as, for the same small values of $|u_d|$ and $|\ell_3|$,

$$\arctan\left[\frac{v(7)}{v(6)}\right] \doteqdot \arctan\left[\frac{2u_d r(u_s-u_i r^2) + 4\zeta r(r^2-1)}{(u_s-u_i r^2)^2 - (r^2-1)^2 + (2\zeta r)^2}\right] \quad (4.5.9)$$

which is constant, then the slope is the same as when $u_d = 0$ but the value at $\ell_3 = -\frac{u_d}{2}$ differs from that when $u_d = 0$ due to the u_d term in $v(7)$. In particular when $r = 1$, from (4.5.9):

$$\arctan\left[\frac{v(7)}{v(6)}\right] = \arctan\left[\frac{2u_d(u_s - u_i)}{(u_s - u_i)^2 + (2\zeta r)^2}\right] \quad (4.5.10)$$

compared with 0 when $u_d = 0$. Typical curves showing the variation of

$\left|\frac{Y}{X_s}\right|$ and $\angle\frac{Y}{X_s}$ with ℓ_3 for r = 1 are shown on figures 4.5.1 and 4.5.2.

From (4.5.1) and (4.5.7), for $2\zeta r \gg |u_d r|$, $|\ell_3 r|$ and ℓ_3^2:

$$\left|\frac{X}{X_s}\right| = \sqrt{\frac{(r^2-1)^2+(2\zeta r)^2}{v(6)^2 + v(7)^2}} \qquad (4.5.11)$$

where $\left[v(6)^2 + v(7)^2\right]$ is given by equation (4.5.6) and, from (4.5.4) and (4.5.8):

$$\angle\frac{X}{X_s} = -\arctan\left[\frac{v(7)}{v(6)}\right] + \arctan\left[\frac{-2\zeta r}{(r^2 - 1)}\right] \qquad (4.5.12)$$

again there is the slight difference from when $u_d = 0$ due to the u_d term in v(7) [cf. equation (4.4.21)].

4.6 The combined effect of u_s, u_d, u_i, r and ζ on the variation of $\frac{Y}{X}$ with ℓ_3

Consider only $\frac{Y}{X}$ for $\ell_3 \ll 1$ and $r = 1 + \delta$ where $|\delta| \ll 1$. Gathering together all the relevant relationships which affect the modulus and phase angle curves as ℓ_3 varies.

(a) Modulus $\left|\frac{Y}{X}\right|$

From the equation (4.5.3) the minimum value, which occurs at $\ell_3 = -\frac{u_d}{2}$, is:

$$\left|\frac{Y}{X}\right|_{min} = \frac{|u_s - u_i r^2|}{\sqrt{(r^2 - 1)^2 + (2\zeta r)^2}}$$

Neglecting small quantities this reduces to:

$$\left|\frac{Y}{X}\right|_{min} \doteqdot \frac{|u_s - u_i - 2u_i\delta|}{2\sqrt{\left(\frac{\delta}{\zeta}\right)^2 + 1}} \qquad (4.6.1)$$

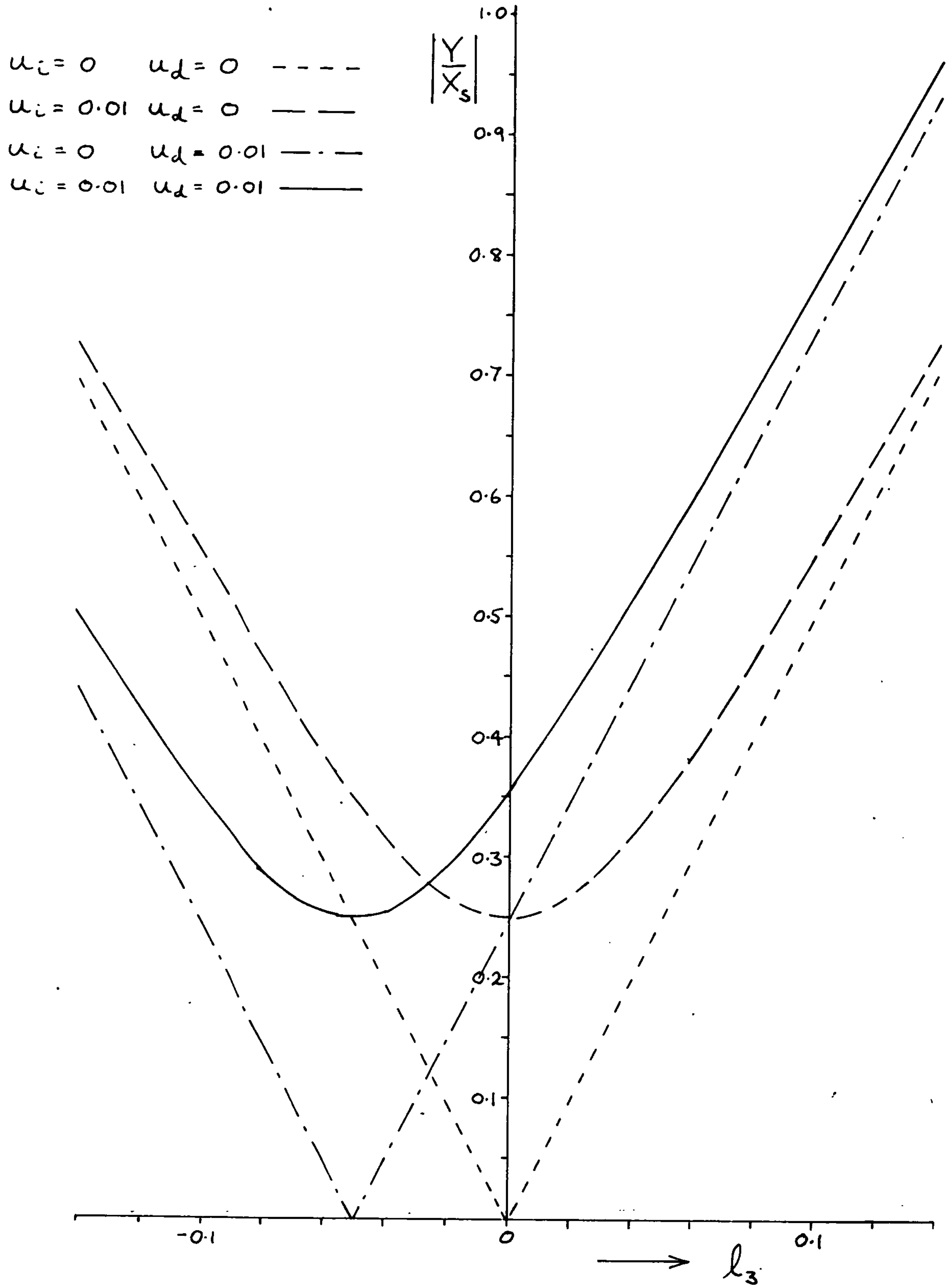

Fig. 4.5.1 Variation of $\left|\frac{Y}{X_s}\right|$ with l_3 for $r = 1$, $\zeta = 0.1$, $u_s = 0$ and various values of u_i and u_d

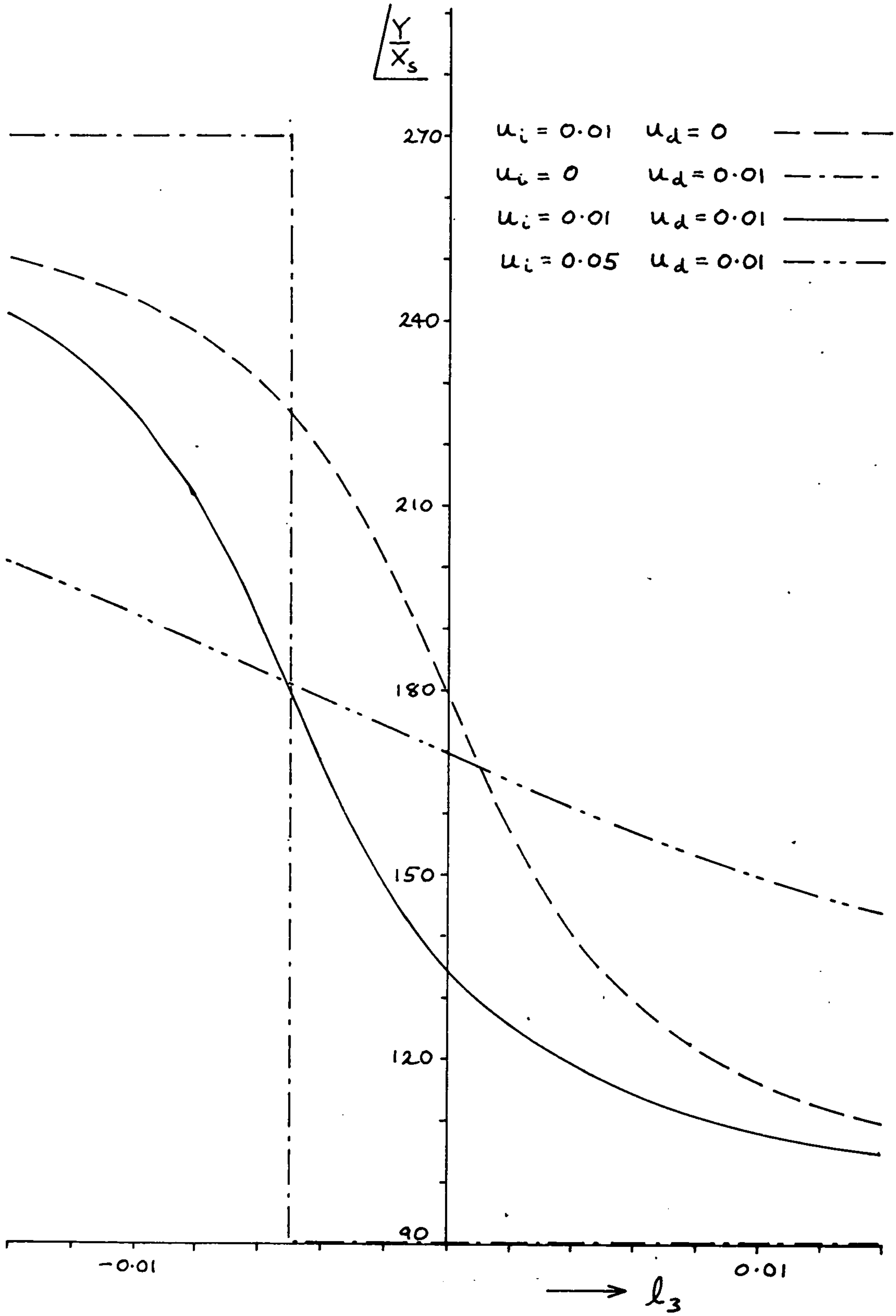

Fig. 4.5.2 Variation of $\angle \frac{Y}{X_s}$ with l_3 for $r = 1$, all values of ζ and various values of u_i and u_d

As $\left|\ell_3\right|$ increases $\left|\frac{Y}{X}\right|$ approaches asymptotically the curve for the uncoupled case which, from equation (3.3.10), is a straight line of slope:

$$\left(\frac{\left|\frac{Y}{X}\right|}{\left|\ell_3\right|}\right)_{\text{asymptote}} = \frac{2r}{\sqrt{(r^2-1)^2 + (2\zeta r)^2}}$$

again neglecting small quantities, this reduces to:

$$\left(\frac{\left|\frac{Y}{X}\right|}{\left|\ell_3\right|}\right)_{\text{asymptote}} \doteqdot \frac{1}{\zeta\sqrt{\left(\frac{\delta}{\zeta}\right)^2 + 1}} \tag{4.6.2}$$

When $\ell_3 = 0$, from equation (4.5.1) neglecting small quantities:

$$\left|\frac{Y}{X}\right|_{\ell_3 = 0} = \sqrt{\frac{\left(\frac{u_s - u_i - 2u_i\delta}{2\zeta}\right)^2 + \left(\frac{u_d}{2}\right)^2}{\left(\frac{\delta}{\zeta}\right)^2 + 1}} \tag{4.6.3}$$

(b) <u>Phase angle $\angle\frac{Y}{X}$</u>

From equation (4.5.4), neglecting small quantities, the maximum slope (at $\ell_3 = -\frac{u_d}{2}$) is:

$$\left(\frac{d\angle\frac{Y}{X}}{d\,\ell_3}\right)_{\ell_3 = \frac{-u_d}{2}} \doteqdot \frac{2}{u_s - u_i - 2u_i\delta} \tag{4.6.4}$$

and the value $\angle\frac{Y}{X}$ at $\ell_3 = -\frac{u_d}{2}$ becomes:

$$\left.\begin{aligned}
&\text{if } u_s - u_i r^2 > 0 \\
&\left(\angle\frac{Y}{X}\right)_{\ell_3 = -\frac{u_d}{2}} \doteqdot \arctan\left[\frac{\zeta}{\delta}\right] \\
&\text{and if } u_s - u_i r^2 < 0 \\
&\left(\angle\frac{Y}{X}\right)_{\ell_3 = -\frac{u_d}{2}} \doteqdot \pi + \arctan\left[\frac{\zeta}{\delta}\right]
\end{aligned}\right\} \tag{4.6.5}$$

and the value $\underline{/\frac{Y}{X}}$ at $\ell_3 = 0$ becomes:

$$\left(\underline{/\frac{Y}{X}}\right)_{\ell_3=0} = \arctan\left[\frac{u_d}{(u_s-u_i-2u_i\delta)}\right] + \arctan\left[\frac{\zeta}{\delta}\right] \quad (4.6.6)$$

Equations (4.6.1) to (4.6.6) can be used to determine the values of $(u_s - u_i - 2u_i\delta)$, u_d, δ and ζ for a particular system. In most cases ζ will be large enough to make $\left(\frac{\delta}{\zeta}\right) \ll 1$ in which case all the denomonators of equations(4.6.1) to (4.6.3) become unity: then ζ can be determined by the modulus asymptotic slope (4.6.2); $(u_s - u_i - 2u_i\delta)$ from the phase angle maximum slope (4.6.4); $\left(\frac{u_d}{2\zeta}\right)$ from the modulus at $\ell_3 = -\frac{u_d}{2}$ (4.6.1); $\left(\frac{\zeta}{\delta}\right)$ from the phase angle at $\ell_3 = -\frac{u_d}{2}$ (4.6.5): the values obtained can be checked from (4.6.3) and (4.6.6) by computing the values of modulus and phase when $\ell_3 = 0$.

4.7 Summary

The most important concept that has been established in this chapter is the linear relationship, independent of ζ, between the phase angle $\underline{/\frac{Y}{X}}$ and ℓ_3 for low values of ℓ_3 when inertia or stiffness coupling is present [see equation (4.4.9)]. This means that the phase angle relationship can be employed to determine very small rates of turn where it is impracticable to use the modulus relationship $\left|\frac{Y}{X}\right|$ with ℓ_3 due to its negligible slope. The non-dependence on ζ should also mean that the damping ratio can be increased to improve the transient response without affecting the sensitivity of the system; however, the value of ζ must still be considered to ensure that the minimum value of Y, approximately given by

$$\left|\frac{Y}{X_s}\right| = \frac{|u_s - u_i|}{(u_s - u_i)^2 + (2\zeta)^2} \qquad (4.7.1)$$

when r = 1, can be detected by the measuring equipment.

It would seem that, in designing a practical system, the value of ζ would be determined by the required transient response and $(u_s - u_i)$ by the minimum signal Y that can be measured, r being made as close to unity as possible for maximum response. It should be possible to adjust the value of $(u_s - u_i)$ by a balancing procedure, either adjusting the mass or the stiffness. If it is not possible to adjust u_d this can be allowed for in the scaling of the instrument.

As far as the experimental work to be discussed here is concerned, the basic idea was not necessarily to produce a practical system but to test the validity of the theoretical results by a design which approximated to the fundamental system, described in section 3.1, as closely as possible.

CHAPTER 5

Experimental apparatus and test procedure

5.1 The sensitive element

In order to approximate to the fundamental system, described in section 3.1, the main requirement is that the motion of the mass should be constrained to the plane Oxy. The simplest way that could be conceived of achieving this was to mount the mass at the centre of a slender rod which had both ends fixed and was under a small tension; the restoring force, and therefore the spring constant, should be reasonably linear provided that the amplitude is small enough to prevent any significant increase in tension at the maximum displacement. A simple load - deflection test carried out with a spring balance, see figure 5.1.1, confirmed this linearity below a deflection of 0.02 in. (the theory for the non-linear vibrations of a comparable system was covered in a paper by Woinowsky - Krieger in 1950).

The sensitive element that was constructed is shown with its principle dimensions on the isometric diagram figure 5.1.2. For clarity only the items affecting the vibrations are shown and all locking nuts and screws are omitted. The mass was $1\frac{1}{2}$" diameter x 1" and made of brass; $\frac{3}{8}$" flats 90° apart were machined for vibration measuring puposes. Attached to the mass for the later experiments was a $5\frac{1}{2}$" long aluminiun strip carrying two $\frac{3}{8}$" diameter dural rods which projected into the two oil dampers as shown (dimensions $1\frac{5}{8}$" x $\frac{3}{4}$" x $2\frac{3}{4}$" deep).

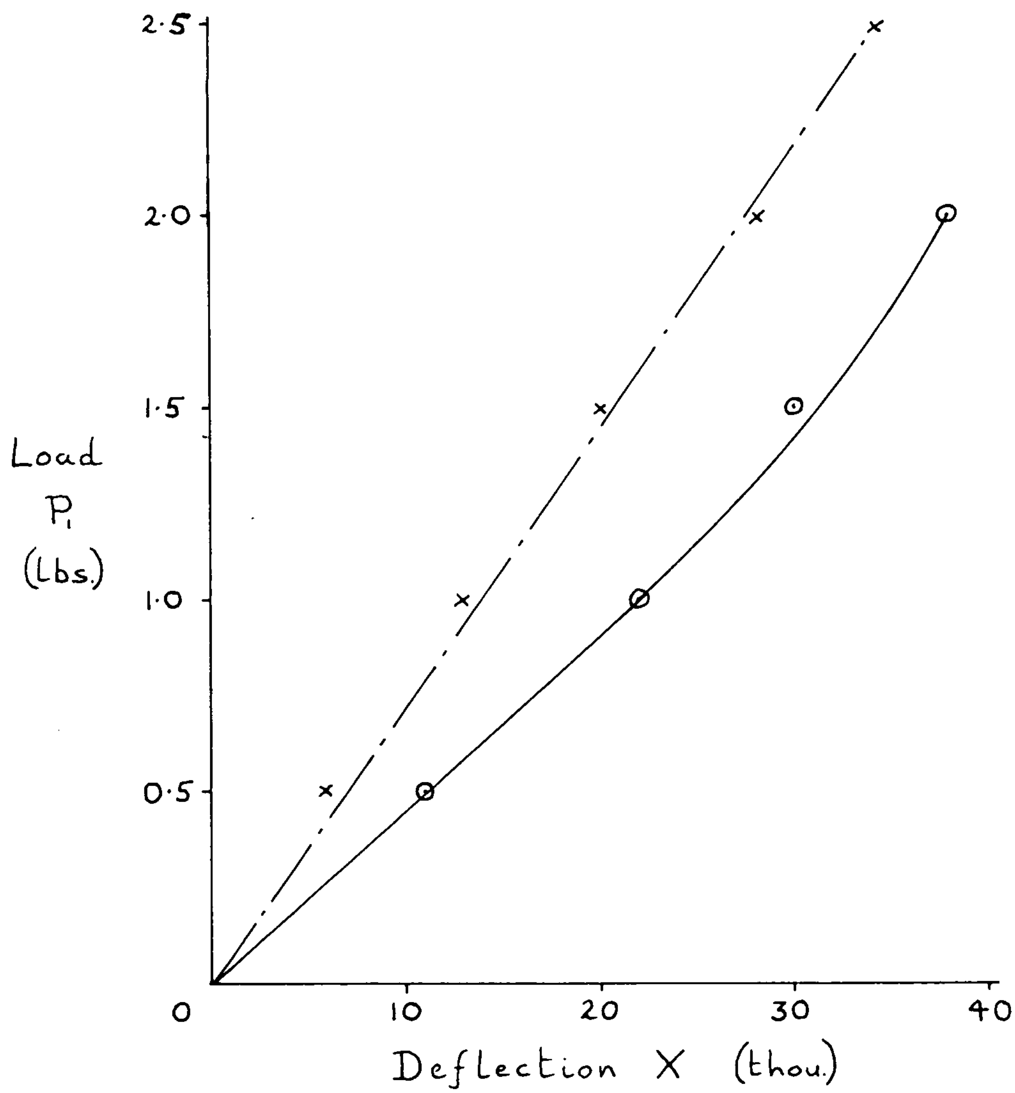

Fig 5.1.1 Load-deflection curve for the sensitive element.

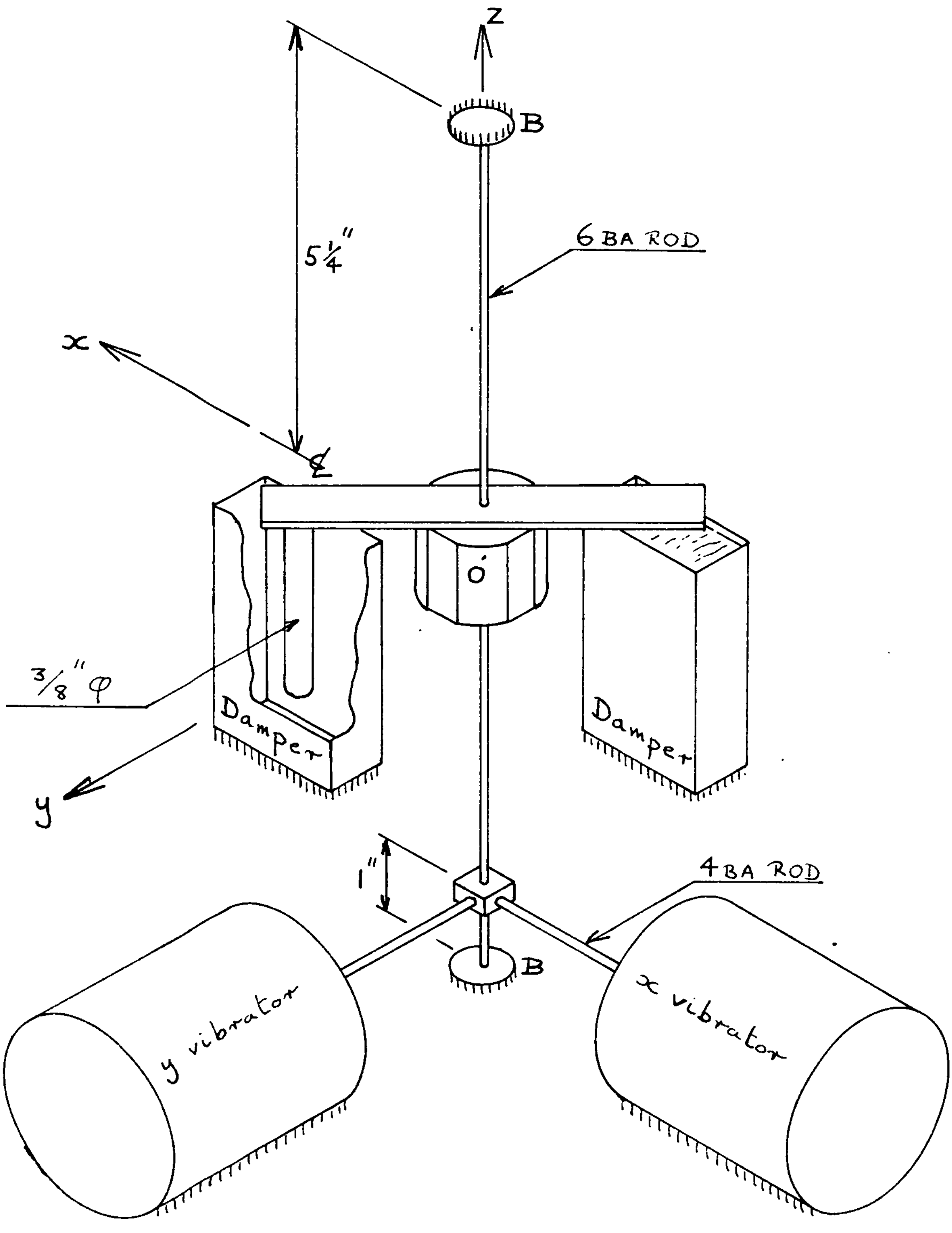

Fig. 5.1.2 Isometric diagram of the sensitive element

The mass was attached at the centre of a 12" long 6BA steel rod which was screwed at both ends B into a stiffened 12" x 4" steel channel section, provision being made for adjusting the tension. The x and y Goodmans V47 electromagnetic vibrators excited the system via 4 BA brass rods which operated in cone bearings on a small block which was attached 1" from the bottom connection on the 6BA rod; the vibrators were located well away from the sensitive mass to minimise the effects of any additional constraints that were introduced.

The photograph, figure 5.1.3, shows the sensitive element before the oil dampers were incorporated; it can be seen that the channel section and vibrators were mounted on a base plate and the complete system was placed on a flexible mounting on the test table; additional support, to prevent toppling, was supplied by a rope attached to the laboratory roof. The flexible mounting was incorporated to prevent, as far as possible, any external vibrations affecting the system.

The photograph, figure 5.1.4, shows a detail of the mass when the dampers were incorporated; the oil vessels could be rotated about their vertical axes to alter the damping characteristics if required.

Fig. 5.1.3 The sensitive element without oil dampers

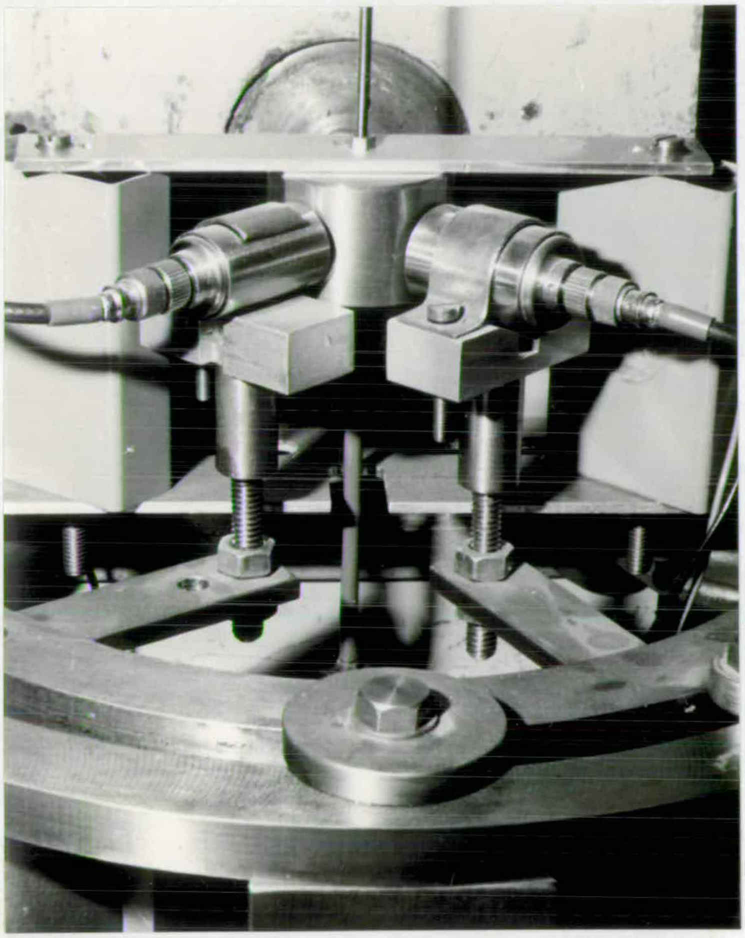

Fig. 5.1.4 Detail of the sensitive element showing the oil dampers

5.2 The Test Table

In order to avoid the difficulties encountered when using the Bryans test table as described in section 2.4, a more rigid turn-table was employed, this was particularly necessary because of the weight of the equipment that had to be rotated. An Elliot milling machine 10" rotary table, with an 80:1 reduction ratio, bolted to a lathe bed gave very good rigidity; it was driven via a 24:1 reduction gear by a Servomex Motor Controller type MC47, the motor is rated at 0.5 H.P. and the speed range is 0 - 10,000 r.p.m. clockwise and anticlockwise. Because of the load on the motor, the maximum speed that could be achieved in this case was 7,000 r.p.m. giving a maximum table speed of $\frac{7,000}{1,920} \doteqdot 3.65$ r.p.m.

No difficulty was experienced with the test table and the set speed was maintained very accurately; clockwise rotation of the motor corresponded to positive rotation of the test table. The table and motor controller are shown on the layout photograph figure 5.2.1 from which it can be seen that the various leads required to the sensitive element were brought in from above without using slip-rings; this limited the number of rotations that could be performed in any one direction but this did not prove much of a handicap except at high table speeds.

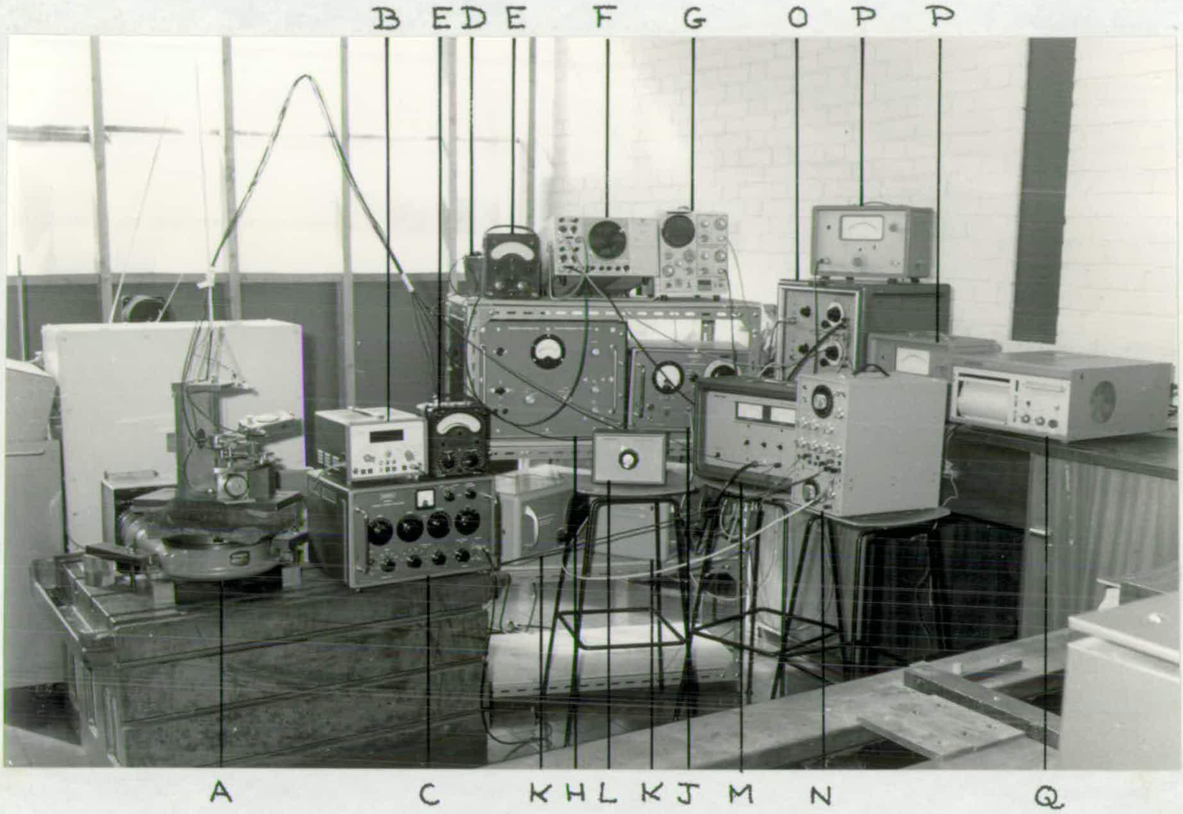

A Sensitive element and turntable

B Advance Counter type TC2A

C Muirhead D-880-A Two Phase L.F. Decade Oscillator

D Southern Instruments Gauge Oscillator M785

E Avometers

F Solartron CD1400 Oscilloscope

G Solartron Solarscope CD1014.2

H Servomex Motor Controller type MC47

J Muirhead D-788-A Low Frequency Analyser

K Goodmans 5VA Power Oscillators

L Wayne Kerr Probe Switch JB731B

M Wayne Kerr Vibration Meter B731B

N Servomex Waveform Generator LF141 and Variable Phase Unit VP142

O Southern Instruments F.M. Pre-amplifier MR513

P Philips GM6012 Valve Voltmeters

Q Honeywell 2106 Visicorder

Fig. 5.2.1 Layout of the equipment for tests A, B and C

5.3 The excitation system

Figure 5.3.1 is a schematic diagram showing the basic equipment controlling the vibration of the sensitive element. The sinewaves required were generated by a Servomex Waveform Generator type LF141 and Variable Phase Unit VP142; to keep the periodic time constant for tests A, B and C, carried out before the dampers were fitted to the sensitive element, it was necessary to lock the LF141 to an accurate frequency generator viz. a Muirhead D-880-A Two Phase L.F. Decade Oscillator. For the majority of the later tests the LF141 and VP142 were replaced by a Hewlett Packard Variable Phase Function Generator model 203A, this had a more stable periodic time so that the D-880-A was not required.

The reference and variable phase sine waves were each amplified by the amplifier section of a Goodmans 5VA Power Oscillator, the amplified reference and variable phase signals respectively being fed, via an Avometer to measure the current, to the x and y Goodmans vibrators on the sensitive element. An Advance 1 Mc/s Timer Counter type TC2A measured the excitation single period across the output of the x amplifier.

Because of the way in which the apparatus was set up the x vibrator lies on the negative x axis and the y vibrator on the positive y axis. In order to make the two applied forces in phase when their currents were in phase the vibrators were connected to their amplifiers in opposite ways (see figure 5.3.1).

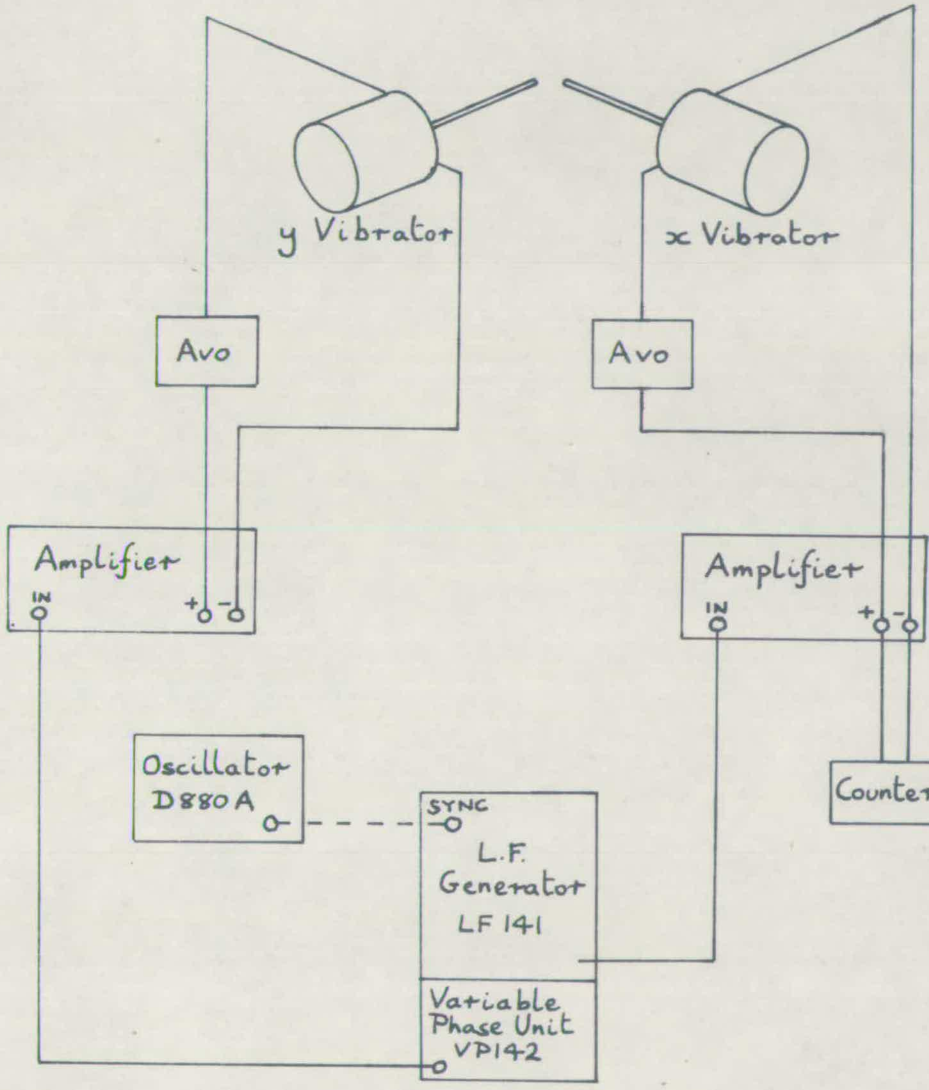

Fig 5.3.1 Schematic diagram of the excitation system

The current supplied to the two vibrators was measured as it should be approximately proportional to the exciting force for the very small amplitudes involved and there was no method available that could be used to measure the force directly.

The photograph, figure 5.2.1, shows the arrangement of the equipment for the first series of tests A, B and C.

5.4 The measuring equipment

Fig. 5.4.1 is a schematic diagram showing the equipment used to monitor and measure the vibrations of the sensitive element.

For the first series of tests A, B and C the x vibrations were measured by two probes viz. a Southern Instruments proximity vibration pick-up G211A and a Wayne Kerr capicitance probe, type ME1, measuring up to 0.1 in. peak to peak. A similar Wayne Kerr probe, type MD1, measuring up to 0.05 in. peak to peak measured the y vibrations.

The G211A pick-up signal was passed through its Gauge Oscillator M785 to the F.M. Pre-amplifier MR513 (all Southern Instruments). The pre-amplifier output was measured by a Philips GM6012 Valve Voltmeter and was displayed against a time base on a Solartron Solarscope CD1014.2 and as the X trace on a Solartron CD1400 oscilloscope set for X-Y operation.

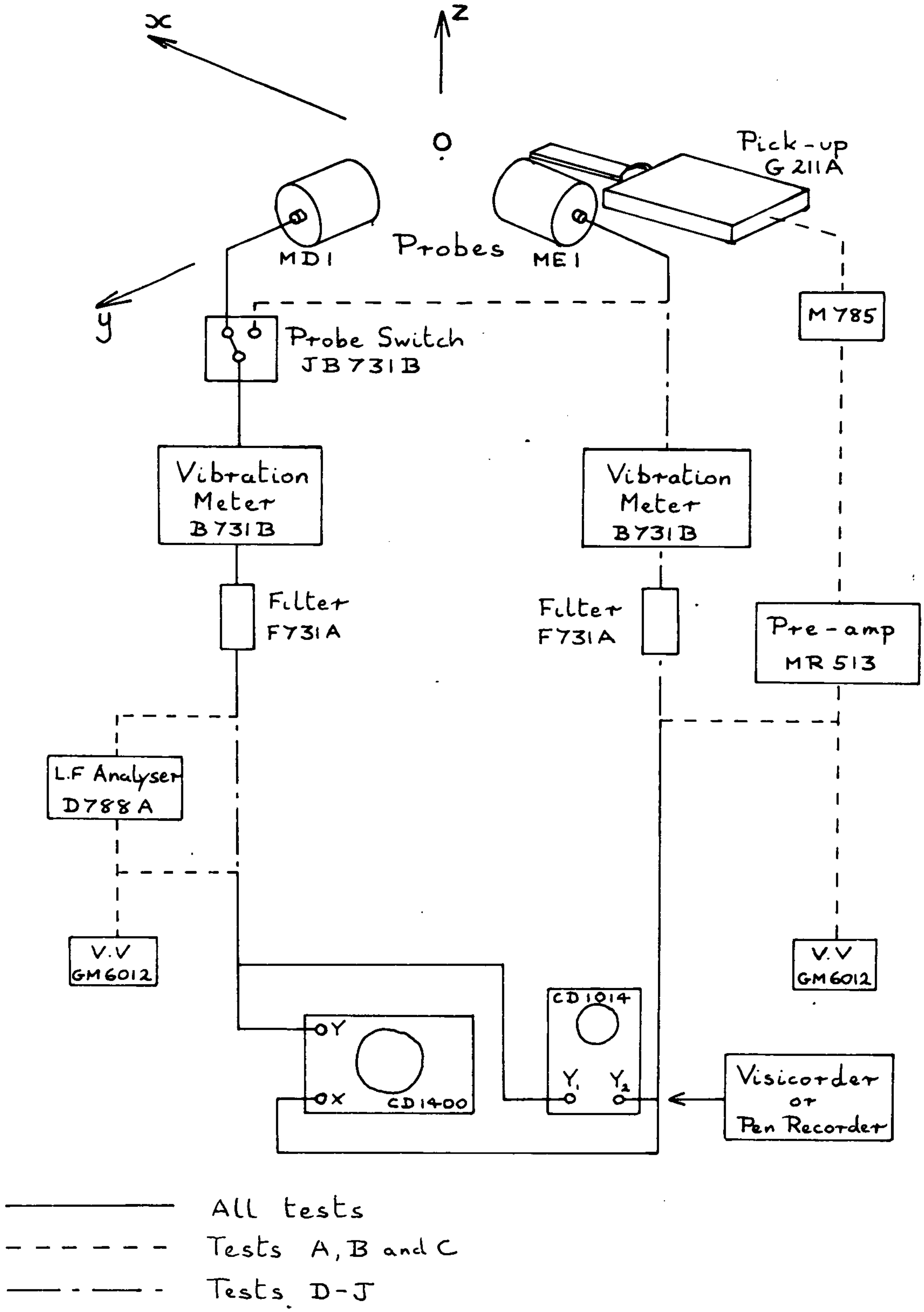

Fig 5.4.1 Schematic diagram of the measuring equipment

The output from the probes MD1 and ME1 was measured by matching Wayne Kerr equipment, the Vibration Meter B731 gave readings of peak to peak amplitude and mean distance of the probe from the mass of the sensitive element and the Probe Switch JB731B selected the required probe; ME1 was only used for calibrating the Valve Voltmeter measuring the G211A pick-up signal so that, for most of the time, the probe MD1 was connected to the Vibration Meter. The output from the Vibration Meter was passed through a Filter F731A to remove the carrier frequency and then through a Muirhead D-788-A Low Frequency Analyser to amplify the signal and remove the small amount of noise. The D-788-A output was measured by another Philips GM6012 Valve Voltmeter and displayed as a second trace on the CD1014.2 and as the Y signal on the CD1400 oscilloscope.

A Honeywell 2106 Visicorder was available for connecting to the MR513 output in order to measure the decrement in the x signal following the switching off of the excitation.

The Southern Instruments equipment gave an output voltage that varied nonlinearly with the distance of the pick-off from the sensitive element mass, this compared with the Wayne Kerr equipment which had very linear characteristics; consequently, when a second Wayne Kerr Vibration Meter became available, it was used to measure the x vibrations and it was possible to reduce the amount of measuring equipment considerably.

Referring to figure 5.4.1, it can be seen that all the Southern Instruments equipment, the Low Frequency Analyser D-788-A and the two Valve Voltmeters GM6012 were not required for the later series of tests. The two Vibration Meters B731B gave direct readings of the peak to peak amplitudes in the x and y directions, removing the necessity for the valve voltmeters, and, although there was some noise and higher harmonics on the output from the y filter F731A which was evident as the output approached zero, it was quite possible to get sufficient accuracy without incorporating the Low Frequency Analyser. In addition it was found more convenient to use a Kelvin and Hughes single channel pen recorder MK5 with its recorder amplifier, in place of the Visicorder, to record the vibrations in a decrement test.

5.5 The Test Procedure

a) Decrement Test

This was carried out with the table stationary by exciting the sensitive element in the x direction at an amplitude of approximately 30 thou. peak to peak and at a frequency close to resonance; the Visicorder or pen recorder was then started and the frequency generator switched off giving a decreasing amplitude waveform trace for evaluating the damping ratio.

b) Frequency response test with the table stationary

i) With only the x vibrator being excited, the excitation frequency was adjusted to give the maximum amplitude in the x direction.

ii) The x vibrator current was adjusted to give a peak to peak amplitude of 30 - 40 thou. in the x direction, measured on the Vibration Meter B731B, in order to keep the spring restraint linear (see fig.5.1.1); this current was then read from the Avometer and maintained constant for the remainder of the test.

iii) The frequency was lowered until the x amplitude was reduced to about 10 thou. peak to peak.

iv) The variable phase section of the waveform generator, which controlled the y vibrator, was adjusted to make the amplitude in the y direction zero, or as small as possible: this was carried out by trial and error noting the variation in the oscilloscope traces, in particular the X - Y trace on the CD1400, as the phase and gain were altered in turn; final adjustments were made by examining the peak to peak y amplitude reading on the Vibration Meter. The y vibrator current was read off from the Avometer and the phase angle between it and the x vibrator current from the Waveform Generator; the excitation single period was read from the Counter and the x peak to peak amplitude from the Vibration Meter (or a Valve Voltmeter suitably calibrated in the case of the earlier tests).

v) The frequency was raised step by step until the x amplitude reached its peak and decreased again to approximately 10 thou. peak to peak. For each frequency the same procedure as detailed in (iv) was carried out.

In test A the x amplitude was not restricted to 40 thou. peak to peak, and the response curve (figure 6.3.1) shows evidence of non-linearity.

c) <u>Response test with the table rotating</u>

i) With the table stationary the desired excitation frequency was obtained using the Counter and the x vibrator current adjusted to give a 30 - 40 thou. peak to peak amplitude. The current and frequency were noted and maintained for the remainder of the test.

ii) The amplitude in the y direction was reduced to zero using the method already described in (b.iv) and the same readings were taken.

iii) The table was rotated at a constant set speed in one direction and the same procedure carried out and readings taken.

iv) The table was rotated at the same speed in the opposite direction and then the speed was increased step by step the same process being repeated each time.

v) Finally, when the maximum required speed readings had been obtained, the system was again tested with the table stationary to note any changes that had taken place during the test.

This procedure applied to all the rotation tests except test B where (i) and (ii) were carried out as detailed above but the y vibrator current and the phase angle were thereafter maintained constant. At each rotation setting Valve Voltmeter readings were taken to give the x and y amplitudes but no equipment was available for measuring the phase angle between the x and y displacements.

5.6 General Comments

Some difficulty was experienced in making the necessary adjustments and taking the readings at high rates of table rotation; the limit on the number of revolutions that was imposed by the method of taking the leads into the sensitive element meant that there was a very short time in which to carry out the required procedure. It was particularly difficult during the early tests, before the dampers were fitted to the sensitive element; any small changes in the excitation frequency or any other factors affecting the sensitive element caused a considerable change in the systems vibration pattern due to operating near a very sharp resonance peak. The presence of the dampers and the improved measuring equipment available for the later tests overcame this difficulty, aided by the increased experience of the operator in adjusting the magnitude and phase of the current to the y vibrator in order to maintain the oscillations in the one plane.

The oil dampers incorporated in the sensitive element were rather crude as they were made from material available at the time but they did have the considerable advantage of being adjustable; rotation of the oil vessels about their vertical axis had a considerable effect on the coupling terms. It was possible to make this adjustment while the sensitive element was vibrating so that, with the table stationary and the x amplitude close to its maximum, the y vibration amplitude could be reduced to a minimum by this means before the tests were carried out.

Before the oil dampers were fitted attempts were made to increase the damping ratio by sleeving the 6BA rod and by using permanent magnet eddy current dampers, but neither of these methods had a significant effect. However electrical damping could be incorporated to give the required damping ratio and presumably would be preferable to oil dampers in a practical system.

CHAPTER 6

Experimental Results

6.1 Object

In order to verify the theoretical equations that have been developed in chapters 3 and 4 three separate series of tests were carried out.

Section 6.3 deals with tests A, B and C which were concerned with the fundamental system with no viscous dampers. Test A examines the response of the non-rotating system to various excitation frequencies near resonance; tests B and C the response of the system at various speeds of rotation using the y vibrator to make Y = 0 when $\ell_3 = 0$ in test B, and to maintain Y = 0 for all values of ℓ_3 in test C (ref. section 3.9).

Section 6.4 deals with tests D and E in which the viscous dampers have been introduced. The aim was to relate the variation in the response of the non-rotating system with frequency to the variation in the response of the system, at a particular frequency, with rate of turn.

Finally section 6.5 deals with tests F, G, H and J which compare the variation in the response of the system with rate of turn at four different frequencies, the other parameters remaining constant.

The readings taken in all tests, except test B, were:

Excitation period p (secs.)

Motor speed (r.p.m.) = 1920 x table speed (r.p.m.)

$$= \frac{1920 \times 60}{p_n} \ell_3 \qquad (6.1.1)$$

x vibrator current (mA)

y vibrator current, magnitude (mA) and phase ($^\circ$) relative to the x vibrator current, required to maintain $Y = 0$

$2|X|$ in thousandths of an inch peak to peak (p. to p. thou.).

The readings, plotted on the figures against excitation period p or motor speed, are:

$$\left.\begin{array}{l} \left|\frac{X}{X_s}\right| \text{ plotted as } \dfrac{2|X|}{\text{x vibrator current}} \left(\dfrac{\text{p. to p. thou}}{\text{amp}}\right) \\ \qquad\qquad\qquad\qquad \text{or } \left(\dfrac{\text{p. to p. thou}}{\text{mA}}\right) \\ \left|\frac{Y_s}{X_s}\right| \doteqdot \dfrac{\text{y vibrator current}}{\text{x vibrator current}} \\ \angle\frac{Y_s}{X_s} = \text{the phase angle between the y and x vibrator} \\ \qquad \text{currents } (^\circ). \end{array}\right\} \quad (6.1.2)$$

6.2 The modified theoretical equations

It is convenient to modify the equations developed in chapters 3 and 4 to put them into a more convenient form for comparison with the experimental results. With the exception of test B, all of the tests described employ the y vibrator to maintain $Y = 0$ for all readings, the ratio $\left|\frac{Y_s}{X_s}\right|$ and the phase angle $\angle\frac{Y_s}{X_s} = \psi$ being measured: the relevant equation, allowing for different parameters in the x and y directions, derived in section 3.10 is:

$$\frac{Y_s}{X_s} = \frac{(-u_i r_2^2 + u_{s2}) + jr_2(u_{d2} + 2\,\ell_{32})}{-(r_1^2 + \ell_{31}^2 - 1) + j(2\zeta_1 r_1)} \qquad (3.10.5)$$

where subscripts 1 and 2 refer to directions Ox and Oy respectively.

For the experimental conditions of r close to unity, and ℓ_3, u_i, u_d and u_s very small, dropping the subscript 2 for simplicity, let

$$r_1 = \frac{p_{n1}}{p} = 1 + \delta_1, \qquad (\delta_1 \ll 1) \qquad (6.2.1)$$

and $$r_2 = \frac{p_n}{p} = 1 + \delta \qquad (\delta \ll 1) \qquad (6.2.2)$$

where $\begin{cases} p = \frac{2\pi}{\omega} & \text{the periodic time of the excitation} \\ p_{n1} = \frac{2\pi}{\omega_{n1}} & \text{the undamped periodic time in direction Ox} \\ p_n = \frac{2\pi}{\omega_{n2}} & \text{the undamped periodic time in direction Oy} \end{cases}$

so that $$(-u_i r_2^2 + u_{s2}) \doteqdot u_s - u_i - 2u_i\delta$$
$$= u_s + u_i - \frac{2u_i p_n}{p} \qquad (6.2.3)$$

then equation (3.10.5) becomes:

$$\frac{Y_s}{X_s} \doteqdot \frac{(u_s + u_i - \frac{2u_i p_n}{p}) + j(u_d + 2\,\ell_3)}{-(2\delta_1) + j(2\zeta_1)} \qquad (6.2.4)$$

so that $$\left|\frac{Y_s}{X_s}\right| = \frac{1}{2\zeta_1}\sqrt{\frac{\left(u_s+u_i-\frac{2u_ip_n}{p}\right)^2+(u_d+2\ell_3)^2}{1+\left(\frac{\delta_1}{\zeta_1}\right)^2}} \qquad (6.2.5)$$

and $$\angle\frac{Y_s}{X_s} = \arctan\left(\frac{u_d+2\ell_3}{u_s+u_i-\frac{2u_ip_n}{p}}\right) - \arctan\left(\frac{\zeta_1}{-\delta_1}\right)$$

$$= -180^\circ + \arctan\left(\frac{u_d+2\ell_3}{u_s+u_i-\frac{2u_ip_n}{p}}\right) + \arctan\left(\frac{\zeta_1}{\delta_1}\right) \qquad (6.2.6)$$

Equations (6.2.5) and (6.2.6) can be used to determine the variation in $\left|\frac{Y_s}{X_s}\right|$ and $\angle\frac{Y_s}{X_s}$ either with ℓ_3 for a particular value of p or with p for $\ell_3 = 0$. In addition, from the first of equations (3.10.2), for $\ell_{31} = 0$ and Y = 0:

$$\left|\frac{X}{X_s}\right| \doteq \frac{1}{\sqrt{(r_1^2-1)^2+(2\zeta_1 r_1)^2}} \qquad (6.2.7)$$

i.e. the same as the response of a simple single degree of freedom system to forced excitation. Taking the approximation (6.2.1), for r close to unity:

$$\left|\frac{X}{X_s}\right| \doteq \frac{1}{2\sqrt{\delta_1^2+\zeta_1^2}} \qquad (6.2.8)$$

and ζ_1 can be estimated from the value of δ_1 at which

$$\left|\frac{X}{X_s}\right| = \tfrac{1}{2}\left|\frac{X}{X_s}\right|_{max} \doteq \tfrac{1}{2}\left(\frac{1}{2\zeta_1}\right)$$

In equation (6.2.8) this gives $\zeta_1 = \pm\frac{\delta_1}{\sqrt{3}}$

or $$\zeta_1 = \frac{1}{\sqrt{3}}\left(\frac{p_b-p_a}{p_b+p_a}\right) \qquad (6.2.9)$$

where p_a and p_b are the excitation periodic times when

$$\left|\frac{X}{X_s}\right| = \frac{1}{2}\left|\frac{X}{X_s}\right|_{max}$$

Equations (6.2.5), (6.2.6) and (6.2.9) will be the ones used in this chapter; the relevant expressions derived in section 4.6 are only modified by the inclusion of the subscript 1 on δ and ζ, the replacement of $(u_s - u_i - 2u_i\delta)$ by the more convenient $(u_s + u_i - \frac{2u_i p_n}{p})$ and the additional angle π in the phase angle due to measuring $\angle\frac{Y_s}{X_s}$ instead of $\angle\frac{Y}{X}$ [ref. equation (3.9.10)]

To compare the theoretical and experimental results for these tests, the equations (6.2.5), (6.2.6) and (6.2.9) were used to determine the values of ζ_1, p_{n1}, (u_s+u_i), $u_i p_n$ and u_d from the experimental curves by equating specific theoretical and experimental values, the theoretical curves could then be drawn for comparison with the experimental readings. The specific values that were equated depended upon the object of the test; in tests D and E the equating was carried out from the experimental readings for $\ell_3 = 0$ and thus enabled the theoretical curves for $\ell_3 \neq 0$ to be constructed; in tests F-J the precedure outlined in section 4.6 was carried out on the experimental curves for varying ℓ_3.

The effect of Earths rate is neglected in the calculations, its component about the Oz axis is approximately $6.96 \times 10^{-4} \sin 56^{\circ} \doteqdot 5.8 \times 10^{-4}$ r.p.m. which is of the order of one hundredth of the lowest rate that could be measured with the present apparatus.

6.3 Tests A, B and C - very low damping

A trace of the decrement, following the switching off of the excitation, indicated a damping ratio ζ_1 of the order of 2×10^{-3}

Test A

The variation in the response of the system with excitation period p for $\ell_3 = 0$; the x vibrator current was maintained constant at 45mA.

The experimental readings are shown on figure 6.3.1; the graphs show evidence of the non-linear stiffness with the bend-over near resonance on the magnitude curves for $2|X| > 40$ thou. (cf. figure 5.1.1) and the discontinuities on all the curves at $p \doteqdot 0.0315$ secs. The other interesting point was a tendency for the system to go unstable at the discontinuity, the amplitude increased until the mass hit the proximity pick-offs and it was impossible to maintain $Y = 0$ using the y vibrator. The possible explanation is that the complete system, on its flexible mounting, was oscillating at the exciting frequency, thus leading to the parametric instability discussed in section 3.7 when $\omega' = \omega \doteqdot \omega_n$.

Owing to the non-linearity no calculations are made from these graphs but they will be used for comparison in tests B and C which examine the response of the system to rotation at a particular value of p.

Test B

This test is included to illustrate the alternative method [ref. section 3.9(a)] of using the y vibrator to make $Y = 0$

when $\ell_3 = 0$ and measuring the rotation by means of the ratio $\left|\frac{Y}{X}\right|$ which should vary linearly with angular velocity ℓ_3. From equation (3.10.4) the slope for very small values of ℓ_3, using the substitution (6.2.2) is:

$$\frac{\left|\frac{Y}{X}\right|}{|\ell_3|} = \frac{2r_2}{(r_2{}^2-1)^2 + (2\zeta_2 r_2)^2} \doteqdot \frac{1}{\sqrt{\delta^2 + \zeta^2}} \qquad (6.3.1)$$

The constants for this test were:

$$\left.\begin{array}{ll} x & \text{vibrator current 49mA} \\ y & \text{vibrator current 6.5mA} \end{array}\right\} \left|\frac{Y_s}{X_s}\right| = 0.133$$

$$\angle\frac{Y_s}{X_s} = -212^\circ$$

$p = 0.03173$ secs. (frequency 31.5 Hz)

The readings of $\left|\frac{Y}{X}\right|$ shown on figure 6.3.2 lie reasonably well on straight lines of slope $\pm\ 6.4 \times 10^{-5}$ per motor r.p.m. From equation (6.1.1), taking $p_n \doteqdot 0.0315$ secs (from test A):

$$\frac{\left|\frac{Y}{X}\right|}{|\ell_3|} = 6.5 \times 10^{-5} \times 3.64 \times 10^6 = 232$$

Assuming $\zeta = \zeta_1 \doteqdot 2 \times 10^{-3}$, in equation (6.3.1) this gives:

$$\delta = \pm\sqrt{\left(\frac{1}{232}\right)^2 - 4 \times 10^{-6}} = \pm\ 0.0038$$

Comparing the constants $\left|\frac{Y_s}{X_s}\right|$ and $\angle\frac{Y_s}{X_s}$ with the test A results on figure 6.3.1, it is apparent that $p = 0.03173$ secs. is below resonance. So $\delta = -\ 0.0038$ which, from equation (6.2.2), gives $p_n = 0.0316$ secs.

Test C

The variation in the response of the system to angular velocity about Oz. With p = 0.03171 secs., the y vibrator was used to maintain Y = 0 and the x vibrator current was constant at 44mA making $2|X| = 37$ thou. p.to p. The experimental values of $\left|\frac{Y_s}{X_s}\right|$ and $\angle\frac{Y_s}{X_s}$ for various values of motor r.p.m. are shown on figure 6.3.3.

From equation (6.1.1) taking $p_n = 0.0316$ secs:

$$\text{Motor speed} = 3.64 \times 10^6 \ell_3$$

Comparing with equation (6.2.6) the phase angle curve indicates that:

$$u_d + 2\ell_3 = 0 \text{ when } \ell_3 = -\frac{420}{3.64 \times 10^6} = -1.15 \times 10^{-4}$$

$$\text{i.e. } u_d = \underline{2.3 \times 10^{-4}}$$

and the maximum slope:

$$\frac{d\angle\frac{Y_s}{X_s}}{d\ell_3} = \frac{2}{u_s + u_i - \frac{2u_i p_n}{p}} = \frac{-27}{1000} \times \frac{\pi}{180} \times 3.64 \times 10^6$$

$$\text{i.e. } u_s + u_i - \frac{2u_i p_n}{p} = \underline{-1.16 \times 10^{-3}}$$

also $\angle\frac{Y_s}{X_s} = -214^\circ$ when $\ell_3 = -1.15 \times 10^{-4}$ giving:

$$-214^\circ = -180^\circ + 180^\circ + \arctan\left(\frac{\zeta_1}{\delta_1}\right)$$

$$\text{i.e. } \left(\frac{\zeta_1}{\delta_1}\right) = \underline{-0.675}$$

Comparing with equation (6.2.5), the asymptotic slope of the modulus curve:

$$\frac{1}{\zeta_1\sqrt{1+\left(\frac{\delta_1}{\zeta_1}\right)^2}} = 9.1 \times 10^{-5} \times 3.64 \times 10^6 = 331$$

hence $\zeta_1 = \underline{0.0017}$

and $\delta_1 = \underline{-0.0025}$ (giving $p_{n1} = 0.03163$ secs.)

Substituting these values into equations (6.2.5) and (6.2.6) gives:

$$\left|\frac{Y_s}{X_s}\right| = \frac{1}{0.0034}\sqrt{\frac{1.34 \times 10^{-6} + (2.3 \times 10^{-4} + 2\,\ell_3)^2}{3.2}}$$

and

$$\underline{/\frac{Y_s}{X_s}} = -34^\circ + \arctan\left(\frac{2.3 \times 10^{-4} + 2\,\ell_3}{-1.16 \times 10^{-3}}\right)$$

$$= -214^\circ - \arctan\left(\frac{2.3 \times 10^{-4} + 2\,\ell_3}{1.16 \times 10^{-3}}\right)$$

These curves are plotted on figure 6.3.4 which also shows the experimental readings; these follow the theoretical phase angle curve very well, which might be expected as the phase angle was used to calculate the majority of the constants, however there is also very reasonable agreement in the case of the modulus curve, the main discrepancy being for positive values of ℓ_3 which would seem to indicate a slightly lower value of u_d.

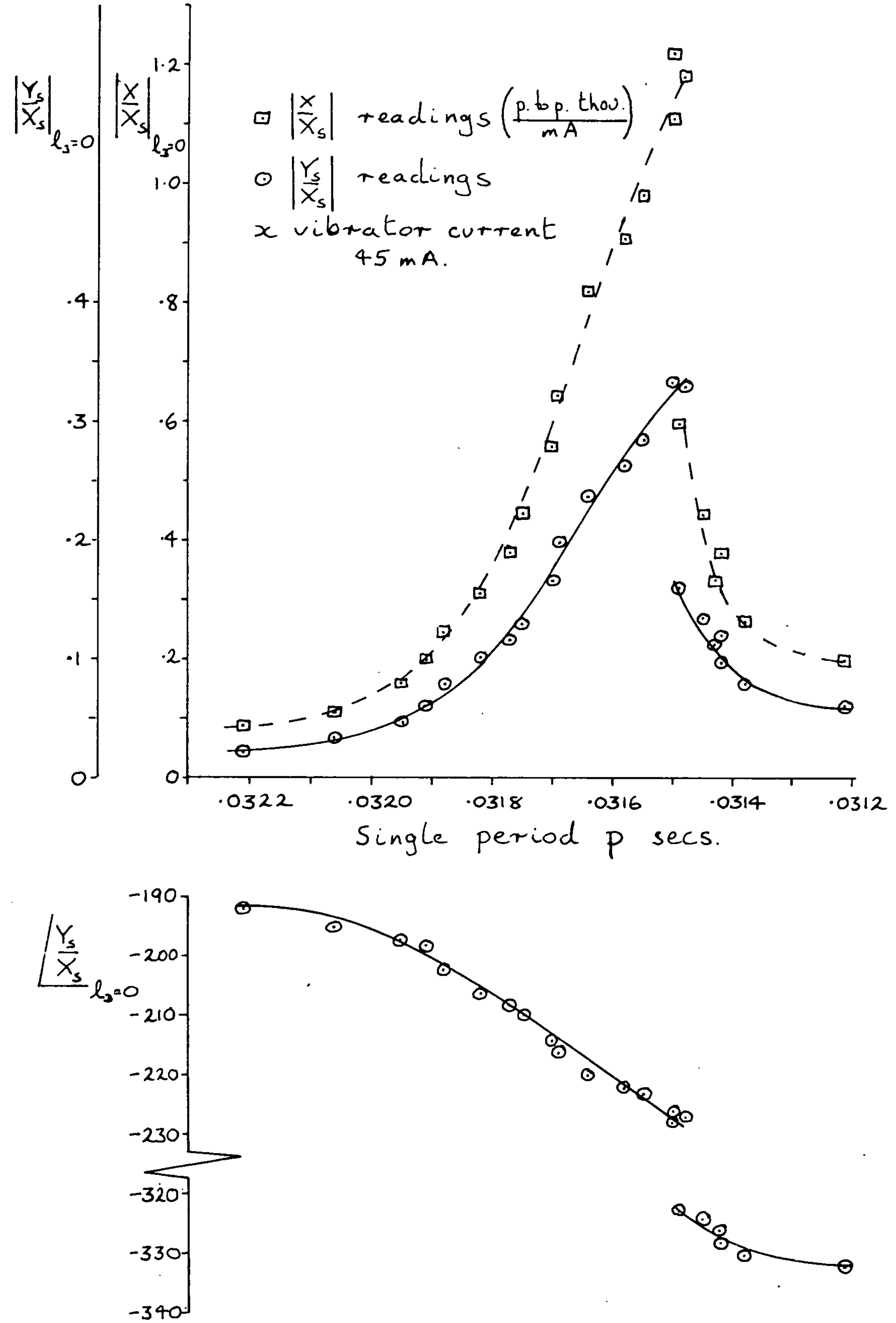

Fig 6.3.1 Test A; Experimental variation of $\left|\frac{Y_s}{X_s}\right|$, $\angle\frac{Y_s}{X_s}$ and $\left|\frac{X}{X_s}\right|$ with single period p secs. for $l_3=0$

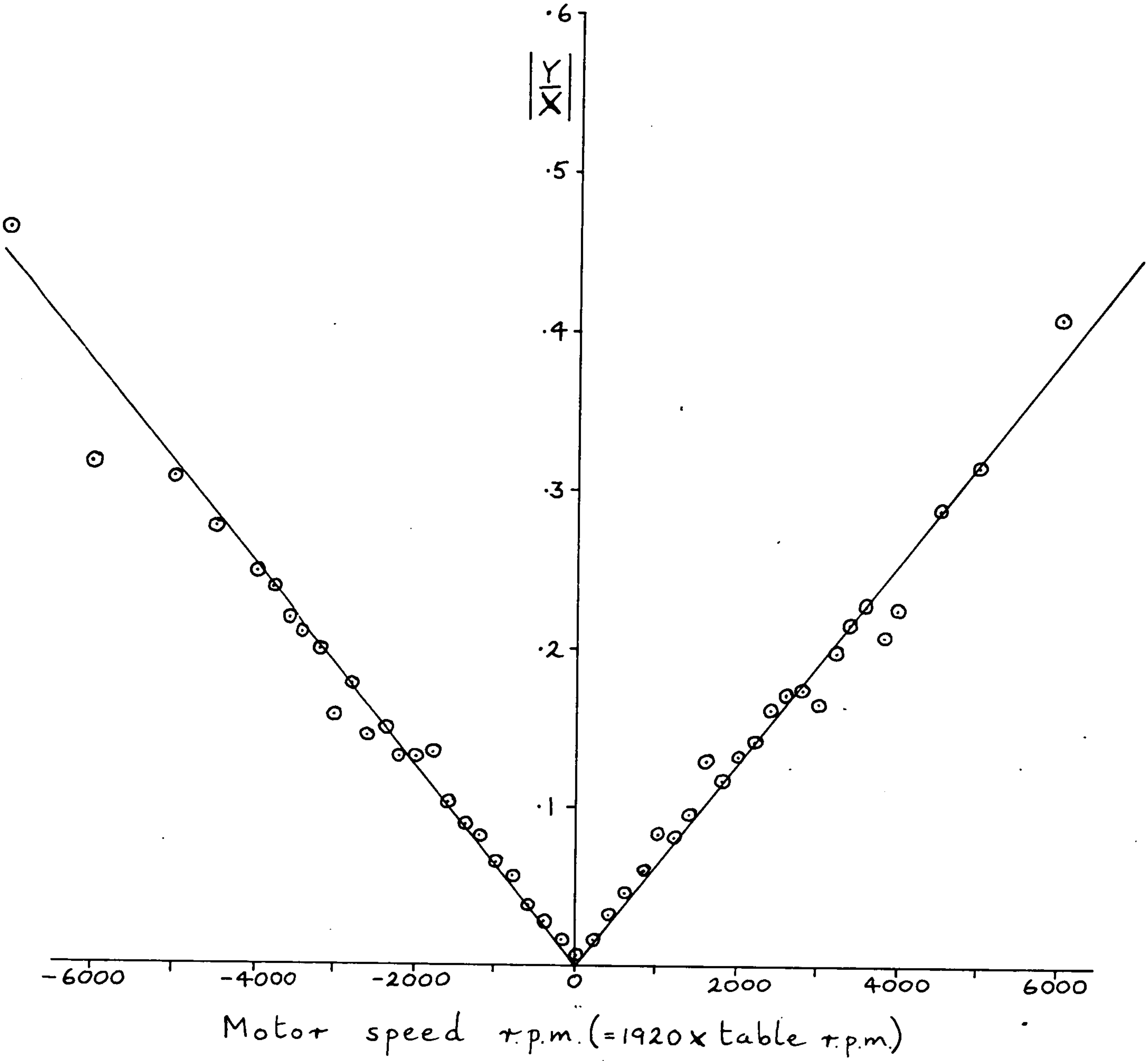

Fig 6.3.2 Test B; Experimental variation of $\left|\frac{Y}{X}\right|$ with motor speed ($= 3{\cdot}64 \times 10^6\, l_3$) for $p = {\cdot}03173$ secs.

o Test B readings x vibrator current 4·9 mA
                      y vibrator current 6·5 mA

$\angle \frac{Y_s}{X_s} = -212°$

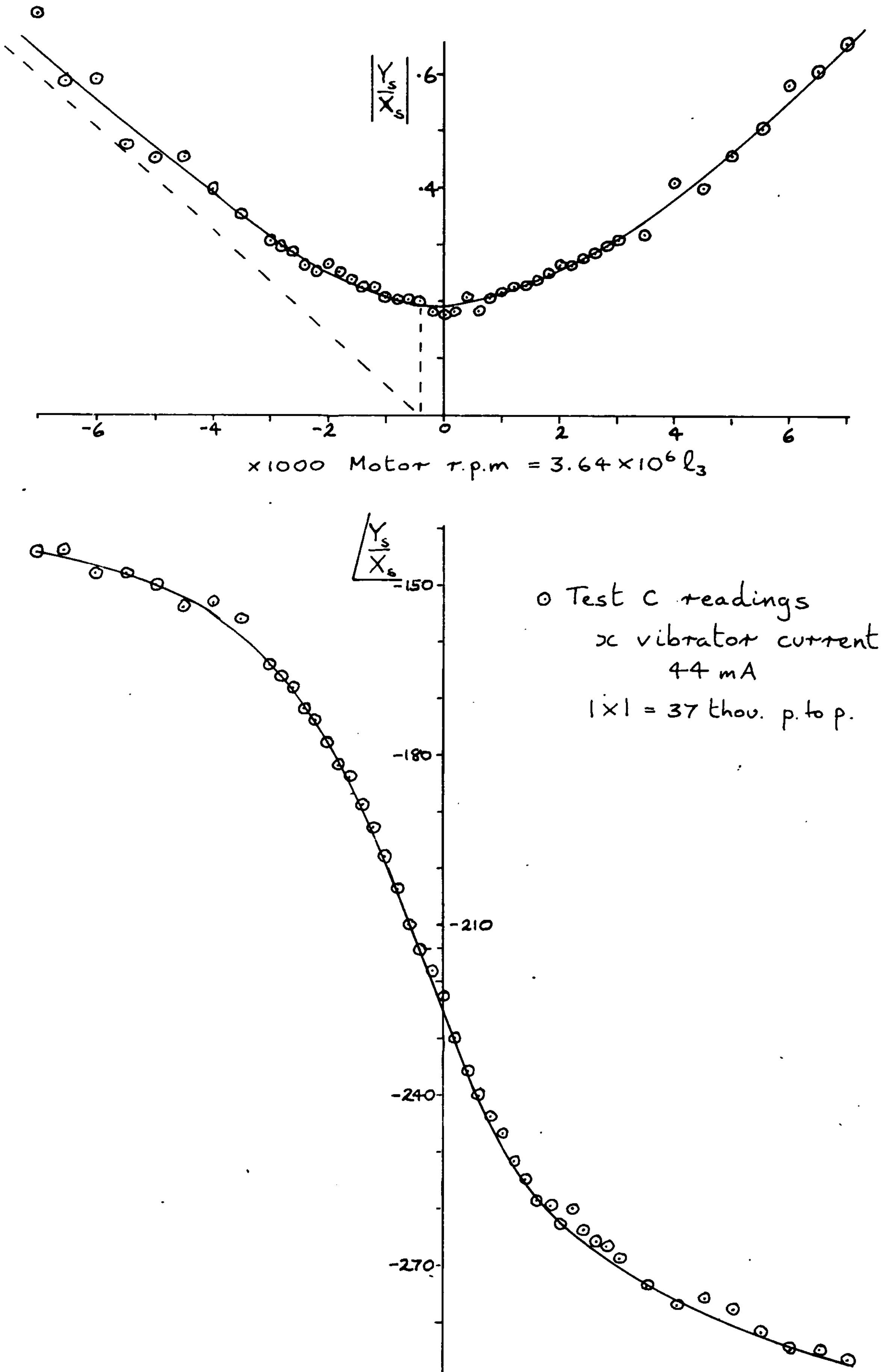

Fig 6.3.3 Test C; Experimental variation of $\left|\frac{Y_s}{X_s}\right|$ and $\angle\frac{Y_s}{X_s}$ with motor r.p.m (= 1920 x table r.p.m) for p = ·03171 secs.

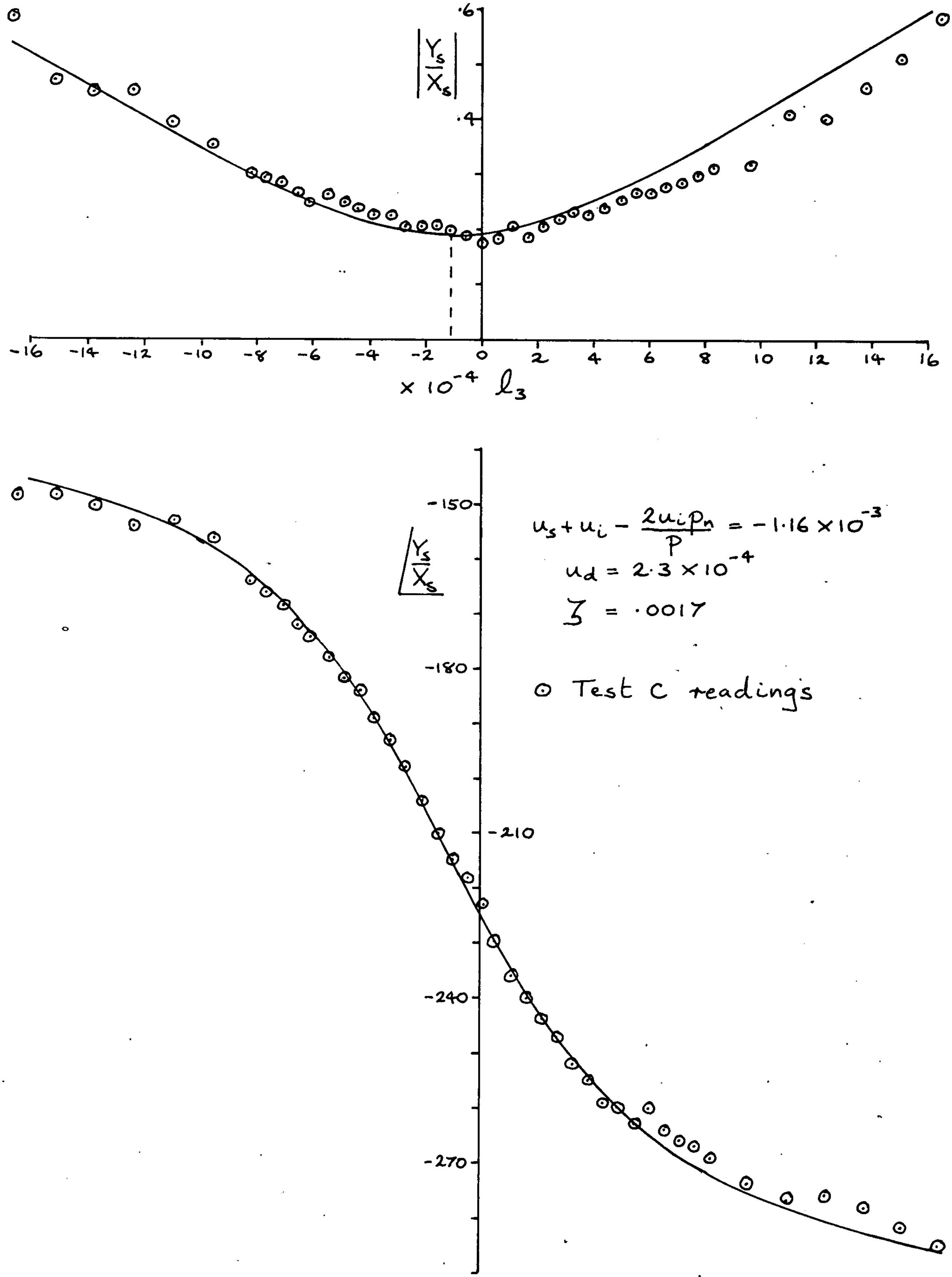

Fig. 6.3.4 Test C; Comparison of the experimental readings with the theoretical curves of $\left|\frac{Y_s}{X_s}\right|$ and $\angle\frac{Y_s}{X_s}$ against l_3

6.4 Tests D and E - viscous dampers incorporated

D and E refer to the system with two different sets of values of the parameters ζ_1, u_i, u_d and u_s; tests D1 and E1 examine the variation in the response of the non-rotating system with excitation period p; tests D2 and E2 examine the variation in the response of the system with angular velocity about Oz for a particular value of p. The aim was to determine the values of the constants from tests D1 and E1 and hence to compute the expected variation with ℓ_3 for a particular value of p for comparison with the experimental readings in tests D2 and E2.

Tests D

A decrement trace, following a switch-off of the excitation, indicated a reduction in $|X|$ of $\frac{2}{5}$ over 6 cycles, i.e. $e^{-12\pi\zeta_1} = 0.4$ giving $\zeta_1 = 0.0243$.

Test D1 was conducted with an x vibrator current of 500mA and the experimental readings and curves, as p was varied, are shown: $\left|\frac{Y_s}{X_s}\right|$ on figure 6.4.1; $\underline{/\frac{Y_s}{X_s}}$ on figure 6.4.2; $\left|\frac{X}{X_s}\right|$ on figure 6.4.3.

From figure 6.4.3, using equation (6.2.9):

$$\zeta_1 = \frac{1}{\sqrt{3}}\left(\frac{0.032 - 0.02955}{0.032 + 0.02955}\right) = \underline{0.023}$$

which compares very well with the figure $\zeta_1 = 0.0243$ obtained from the decrement test. Also the peak value of $\left|\frac{X}{X_s}\right|$ indicates, comparing with equation (6.2.8), that $\delta_1 = 0$ when $p = p_{n1} = 0.0306$ secs., i.e. from equation (6.2.1):

$$\delta_1 = \frac{0.0306}{p} - 1$$

Taking $\zeta_1 = 0.023$, $\arctan\left(\frac{\zeta_1}{\delta_1}\right)$ can now be evaluated and hence, from figure 6.4.2 and equation (6.2.5), $\arctan\left(\frac{u_d}{u_s+u_i-\frac{2u_ip_n}{p}}\right)$; the variation of this angle with p is plotted on figure 6.4.4 and indicates that $\left(u_s+u_i-\frac{2u_ip_n}{p}\right) = 0$ when p = 0.03162 secs., i.e. $u_s + u_i = \frac{2}{0.03162}\,u_ip_n$

Taking the values of $\arctan\left(\frac{u_d}{u_s+u_i-\frac{2u_ip_n}{p}}\right)$ and $\left|\frac{Y_s}{X_s}\right|$ when p = 0.03078 secs., the excitation period used for test D2, from figure 6.4.4:

$$\arctan\left[\frac{u_d}{u_ip_n\left(\frac{2}{0.03162}-\frac{2}{0.03078}\right)}\right] = -124.5^\circ$$

i.e. $u_d = -2.52\,u_ip_n$

and from figure 6.4.1 and equation (6.2.5):

$$0.104 = \frac{1}{0.046}\sqrt{\frac{\left[\left(\frac{2}{0.03162}-\frac{2}{0.03078}\right)u_ip_n\right]^2+\left[-2.52u_ip_n\right]^2}{1.065}}$$

$$\left.\begin{aligned} \text{i.e. } u_ip_n &= \underline{1.61 \times 10^{-3}}\\ \text{giving } u_d &= \underline{-4.06 \times 10^{-3}}\\ \text{and } u_s+u_i &= \underline{10.2 \times 10^{-2}} \end{aligned}\right\} \qquad (6.4.1)$$

In equations (6.2.5) and (6.2.6), for $\ell_3 = 0$, these figures give:

$$\left|\frac{Y_s}{X_s}\right| = \frac{1}{0.046}\sqrt{\frac{\left[3.22 \times 10^{-3}\left(\frac{1}{0.03162}-\frac{1}{p}\right)\right]^2 + 16.5 \times 10^{-6}}{1+\left(\frac{\delta_1}{\zeta_1}\right)^2}}$$

$$\underline{/\frac{Y_s}{X_s}} = -180^\circ + \arctan\left[\frac{-4.06 \times 10^{-3}}{3.22 \times 10^{-3}\left(\frac{1}{0.03162}-\frac{1}{p}\right)}\right] + \arctan\left(\frac{\zeta_1}{\delta_1}\right)$$

These curves are plotted to a base of δ_1 on figures 6.4.5 and 6.4.6 which also show the experimental readings for comparison. There is very good agreement for negative δ_1 but some discrepancy for positive δ_1, which suggests that p_{n1} is possibly slightly higher than 0.0306 secs.

The constants for test D2 were : x vibrator current 500mA making $2|X| = 40$ thou. peak to peak; excitation period p = 0.03078 secs. From equation (6.1.1), taking $p_n \doteqdot 0.0306$ secs:

$$\ell_3 \doteqdot \frac{\text{Motor speed (r.p.m.)}}{3.75 \times 10^6}$$

The readings of $\left|\frac{Y_s}{X_s}\right|$ and $\angle\frac{Y_s}{X_s}$ are shown to a base ℓ_3 on figures 6.4.7 and 6.4.8 and compared with the theoretical curves derived by substituting the values (6.4.1) and p = 0.03078 secs. ($\delta_1 = -0.0059$) in equations (6.2.5) and (6.2.6) viz:

$$\left|\frac{Y_s}{X_s}\right| = \frac{1}{0.046}\sqrt{\frac{7.7 \times 10^{-6} + (-4.06 \times 10^{-3} + 2\ell_3)^2}{1.065}}$$

$$\text{and } \angle\frac{Y_s}{X_s} = -75.5^\circ + \arctan\left(\frac{-4.06 \times 10^{-3} + 2\ell_3}{-2.78 \times 10^{-3}}\right)$$

$$= -255.5^\circ - \arctan\left(\frac{-4.06 \times 10^{-3} + 2\ell_3}{2.78 \times 10^{-3}}\right)$$

These graphs indicate a very good agreement between the derived curves and the experimental points; it will be noted that the value $\ell_3 = -\frac{u_d}{2}$ giving minimum $\left|\frac{Y_s}{X_s}\right|$ could not be achieved (it corresponds to an angular rate of approximately 4 r.p.m.)

Tests E

Following the same analysis as that for tests D. The decrement trace indicated a reduction in $|X|$ of $\frac{20}{56}$ over 5 cycles i.e.
$e^{-10\pi\zeta_1} = \frac{20}{56}$ giving $\zeta_1 = 0.0328$.

In test E1 the x vibrator current was 600mA; the readings are again shown on figures 6.4.1, 6.4.2. and 6.4.3.

From figure 6.4.3, using equations (6.2.9):

$$\zeta_1 = \frac{1}{\sqrt{3}}\left(\frac{0.03265 - 0.02915}{0.03265 + 0.02915}\right) = \underline{0.0327}$$

(cf. 0.0328 from the decrement test).

Also the peak value of $\left|\frac{X}{X_s}\right|$ occurs at $p = p_{n1} = 0.0307$ secs. giving, from equation (6.2.1):

$$\delta_1 = \frac{0.0307}{p} - 1$$

Taking $\zeta_1 = 0.0328$, $\arctan\left(\dfrac{u_d}{u_s + u_i - \dfrac{2u_i p_n}{p}}\right)$ is evaluated as before and plotted to a base p on figure 6.4.4, indicating that $\left(u_s + u_i - \dfrac{2u_i p_n}{p}\right) = 0$ when $p = 0.03028$ secs.

$$\text{i.e. } u_s + u_i = \frac{2}{0.03028}\, u_i p_n$$

From the values at $p = 0.0308$ secs., the excitation period used for test E2:

$$\arctan\left[\frac{u_d}{u_i p_n\left(\dfrac{2}{0.03028} - \dfrac{2}{0.0308}\right)}\right] = -15^\circ$$

i.e. $u_d = -0.298\, u_i p_n$

$$\text{and } 0.021 = \frac{1}{0.0656}\sqrt{\frac{\left[\left(\dfrac{2}{0.03028} - \dfrac{2}{0.0308}\right)u_i p_n\right]^2 + \left[-0.298\, u_i p_n\right]^2}{1.01}}$$

$$\left.\begin{aligned} \text{i.e.}\quad u_i p_n &= \underline{1.2 \times 10^{-3}} \\ \text{giving}\quad u_d &= \underline{-3.56 \times 10^{-4}} \\ \text{and}\quad u_s + u_i &= \underline{7.9 \times 10^{-2}} \end{aligned}\right\} \qquad (6.4.2)$$

In equations (6.2.5) and (6.2.6), for $\ell_3 = 0$, these figures give:

$$\left|\frac{Y_s}{X_s}\right| = \frac{1}{0.0656}\sqrt{\frac{\left[2.4 \times 10^{-6}\left(\frac{1}{0.03028} - \frac{1}{p}\right)\right]^2 + 12.7 \times 10^{-8}}{1 + \left(\frac{\delta_1}{\zeta_1}\right)^2}}$$

and

$$\angle\frac{Y_s}{X_s} = -180^{\circ} + \arctan\left[\frac{-3.56 \times 10^{-4}}{2.4 \times 10^{-3}\left(\frac{1}{0.03028} - \frac{1}{p}\right)}\right] + \arctan\left(\frac{\zeta_1}{\delta_1}\right)$$

These curves are plotted on figures 6.4.5 and 6.4.6 and it can be seen that the experimental results lie very close to them.

The constants for test E2 were: x vibrator current 600mA making $2|X| = 33$ thou. peak to peak; excitation period $p = 0.0308$ secs. Again:

$$\ell_3 \doteqdot \frac{\text{Motor speed (r.p.m.)}}{3.75 \times 10^6}$$

The readings of $\left|\frac{Y_s}{X_s}\right|$ and $\angle\frac{Y_s}{X_s}$ are compared on figures 6.4.7 and 6.4.8 with the theoretical curves derived from equations (6.2.5) and (6.2.6) for this value of p ($\delta_1 = -0.0033$) and values (6.4.2) viz:

$$\left|\frac{Y_s}{X_s}\right| = \frac{1}{0.0656}\sqrt{\frac{1.77 \times 10^{-6} + (-3.56 \times 10^{-4} + 2\ell_3)^2}{1.01}}$$

$$\text{and } \angle \frac{Y_s}{X_s} = -84.5^\circ + \arctan\left(\frac{-3.56 \times 10^{-4} + 2\ell_3}{1.33 \times 10^{-3}}\right)$$

There is a reasonable agreement between the derived curves and the experimental points, although the discrepancy in $\left|\frac{Y_s}{X_s}\right|$ for positive ℓ_3 suggests that the numerical value of u_d should be greater.

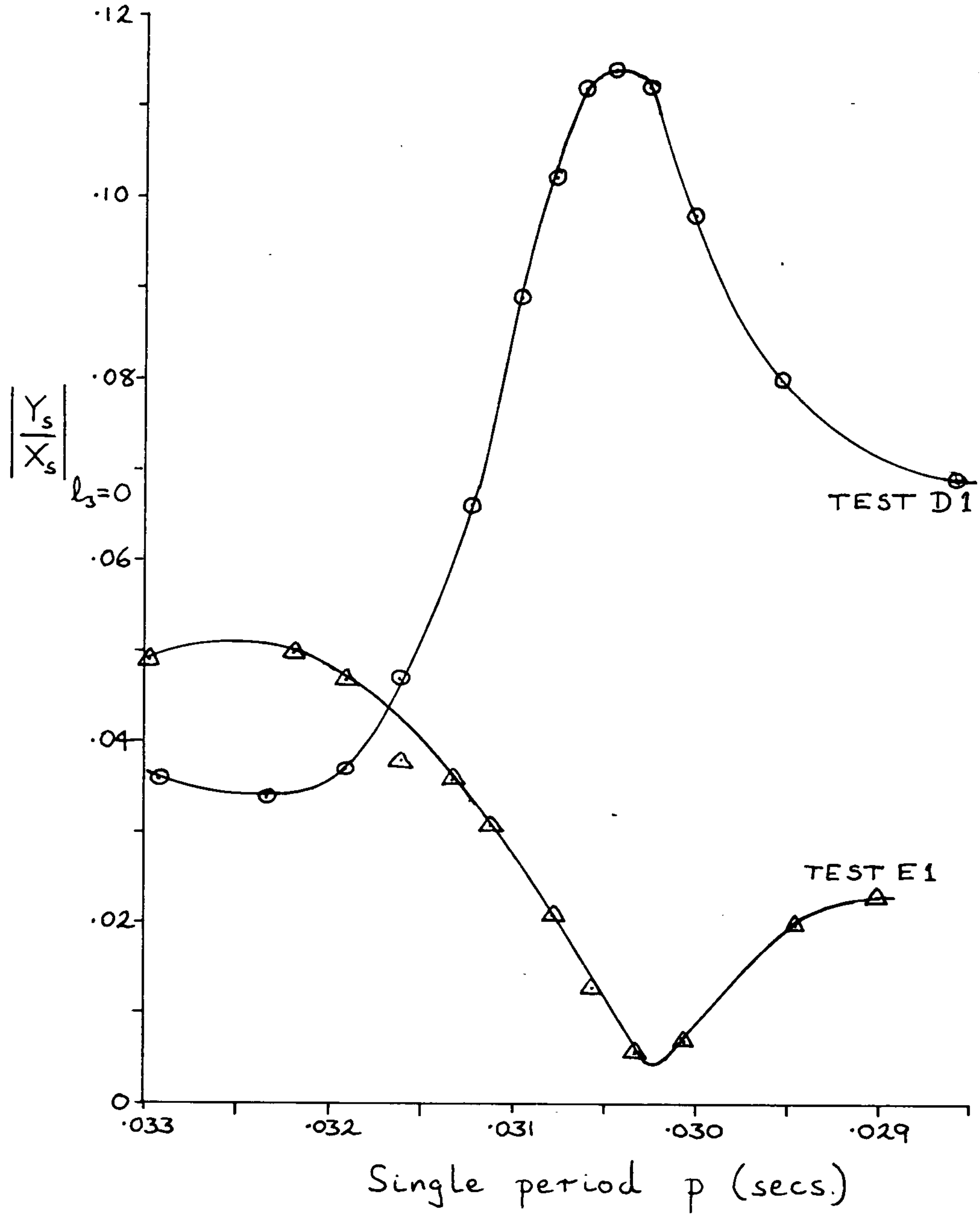

Fig 6.4.1 Experimental variation of $\left|\frac{Y_s}{X_s}\right|$ with single period p (secs) for $l_3=0$

○ Test D1 readings × vibrator current 500 mA.

△ Test E1 readings × vibrator current 600 mA.

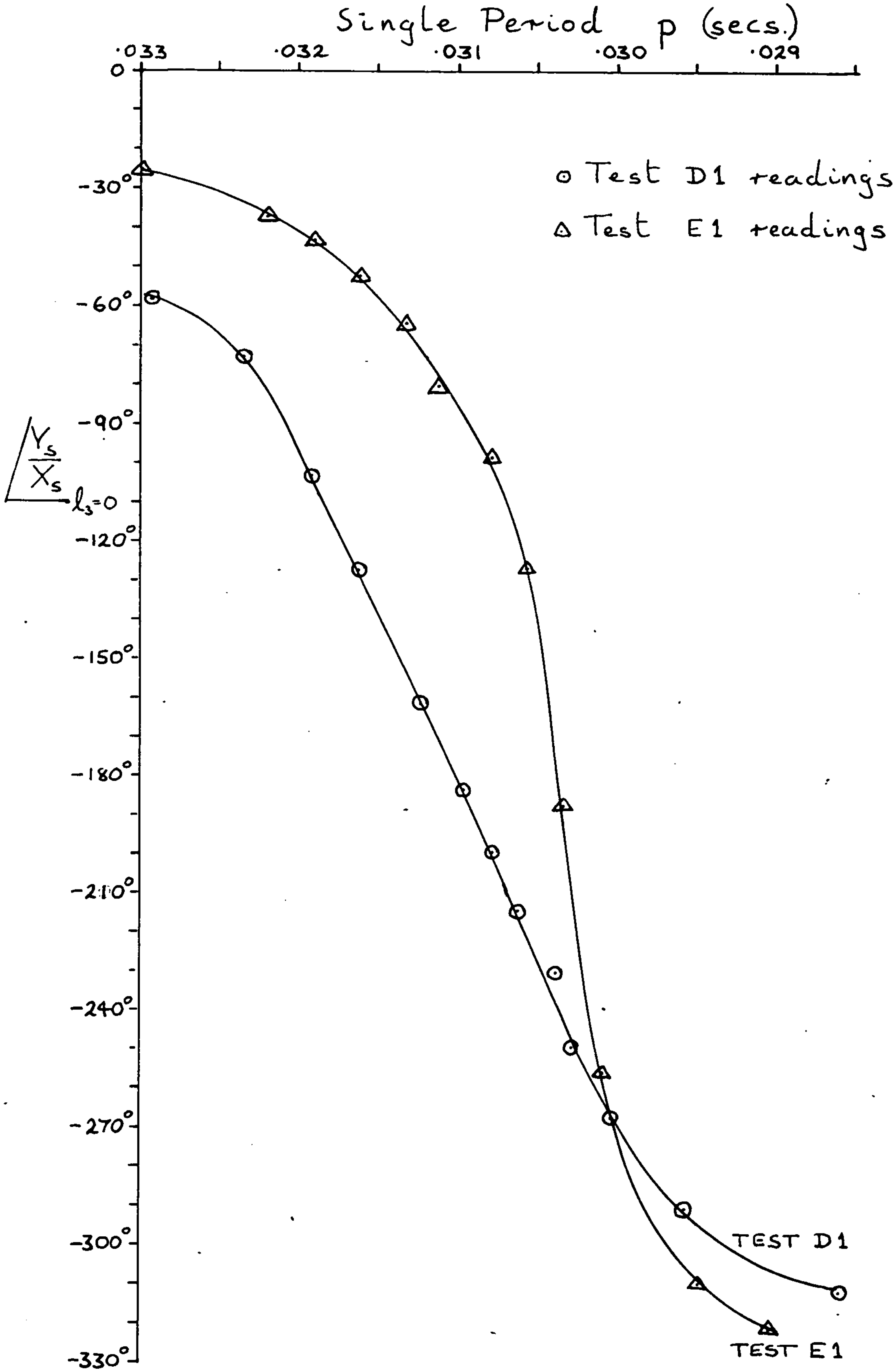

Fig 6.4.2 Experimental variation of $\angle \frac{Y_s}{X_s}$ with single period p (secs) for $l_3 = 0$

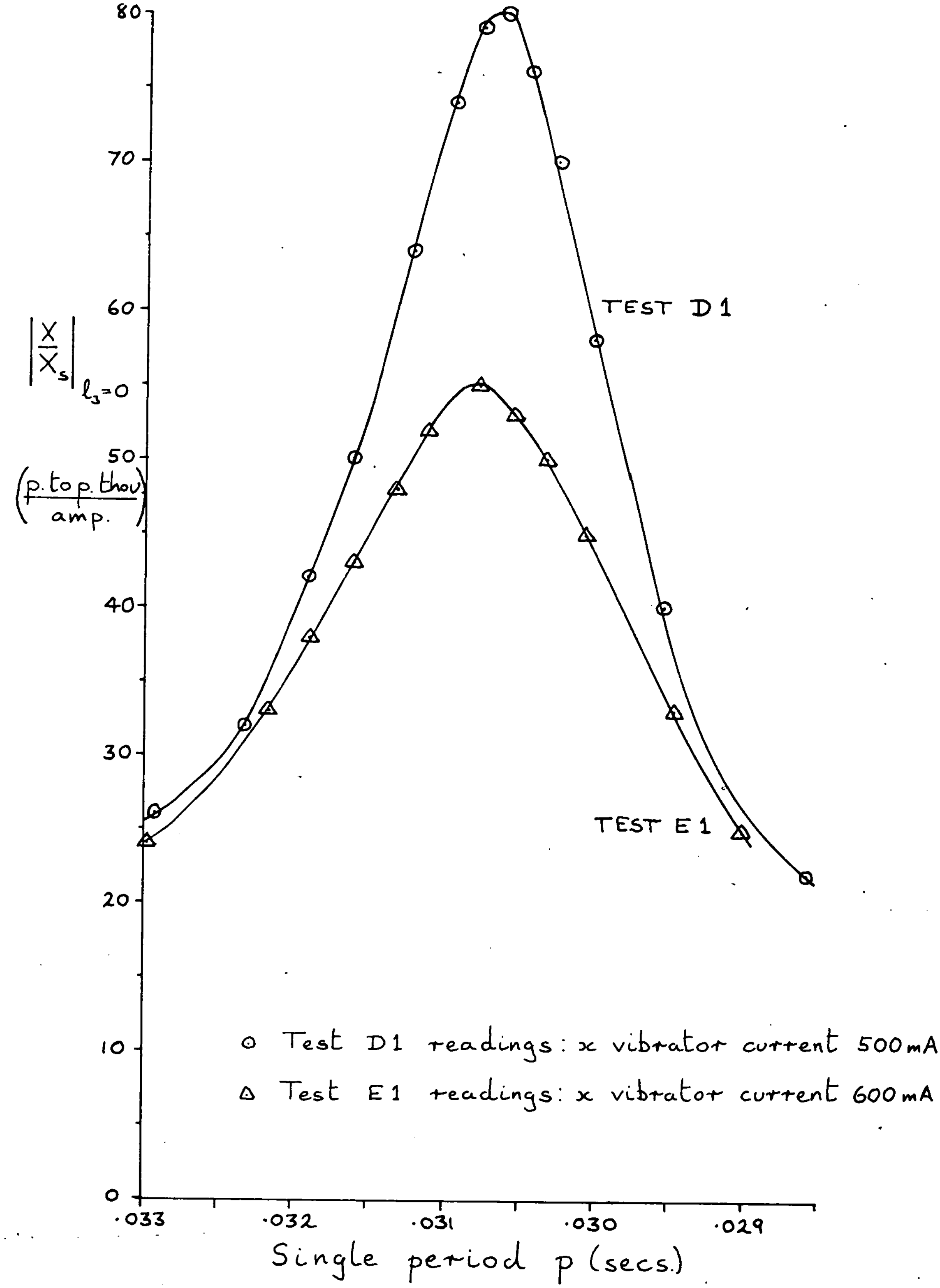

Fig. 6.4.3 Experimental variation of $\left|\frac{X}{X_s}\right|$ with single period p (secs) for $l_3 = 0$

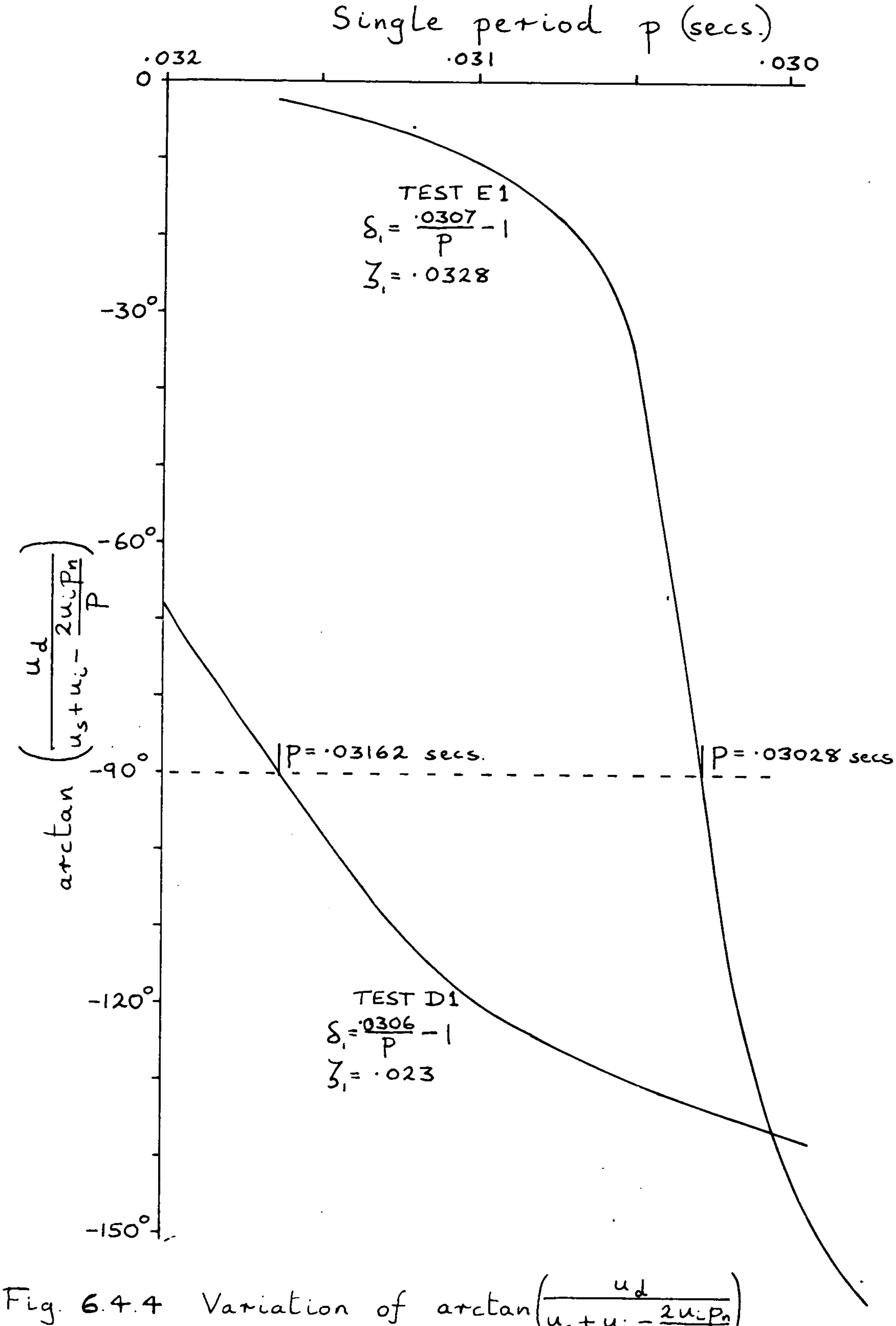

Fig. 6.4.4 Variation of $\arctan\left(\dfrac{u_d}{u_s+u_i-\frac{2u_ip_n}{p}}\right)$ $\left[= \angle\dfrac{Y_s}{X_s} + 180° - \arctan\left(\dfrac{\zeta_1}{\delta_1}\right)\right]$ with single period p (secs) derived from fig 6.4.2

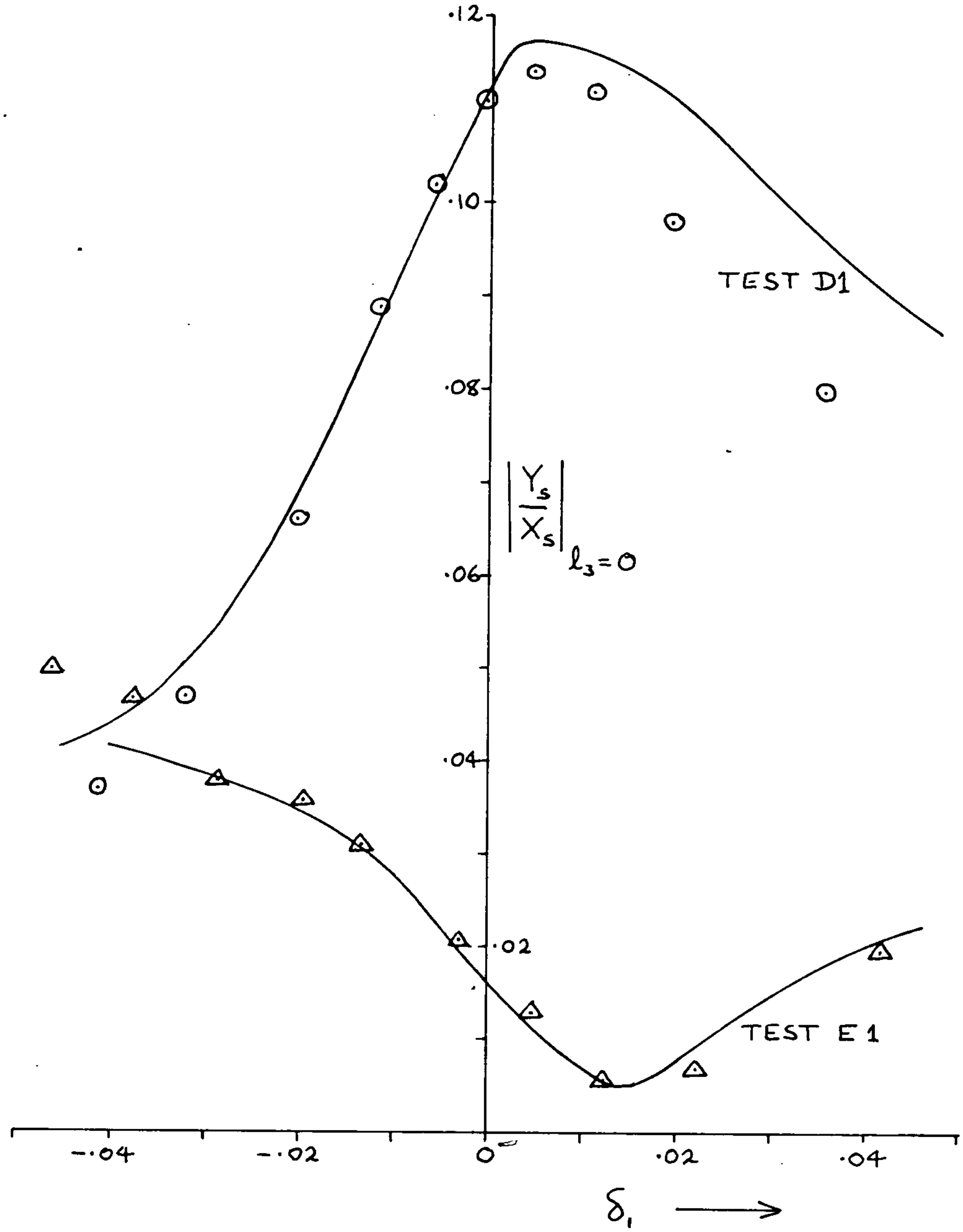

Fig. 6.4.5 Comparison of the experimental readings with the theoretical curves of $\left|\frac{Y_s}{X_s}\right|$ against $\delta_1 = \tau_1 - 1$ for $l_3 = 0$

⊙ Test D1 readings $\delta_1 = \dfrac{0.0306}{P} - 1$

△ Test E1 readings $\delta_1 = \dfrac{0.0307}{P} - 1$

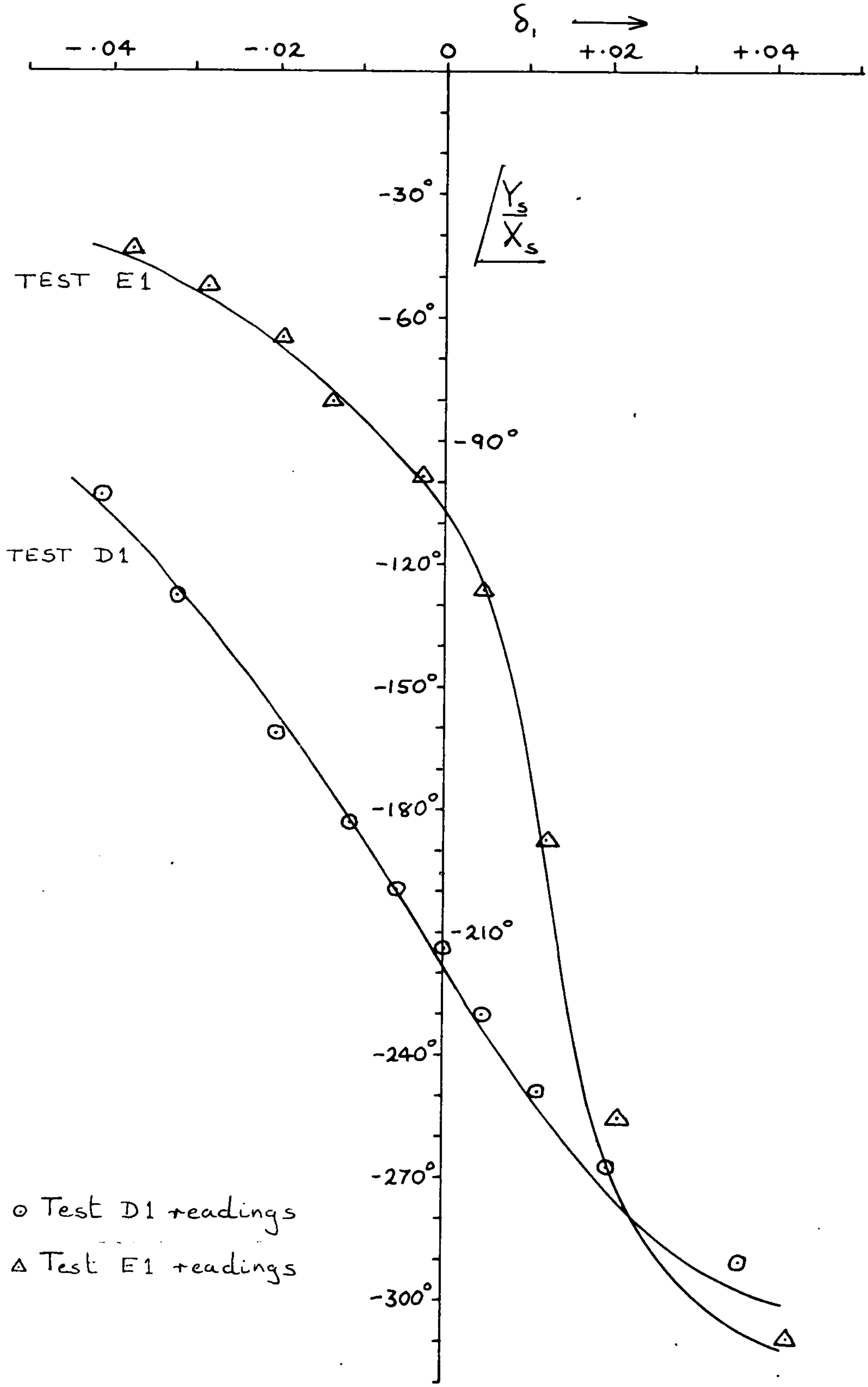

Fig. 6.4.6 Comparison of the experimental readings with the theoretical curves of $\angle \frac{Y_s}{X_s}$ against $\delta_1 = r_1 - 1$ for $l_3 = 0$

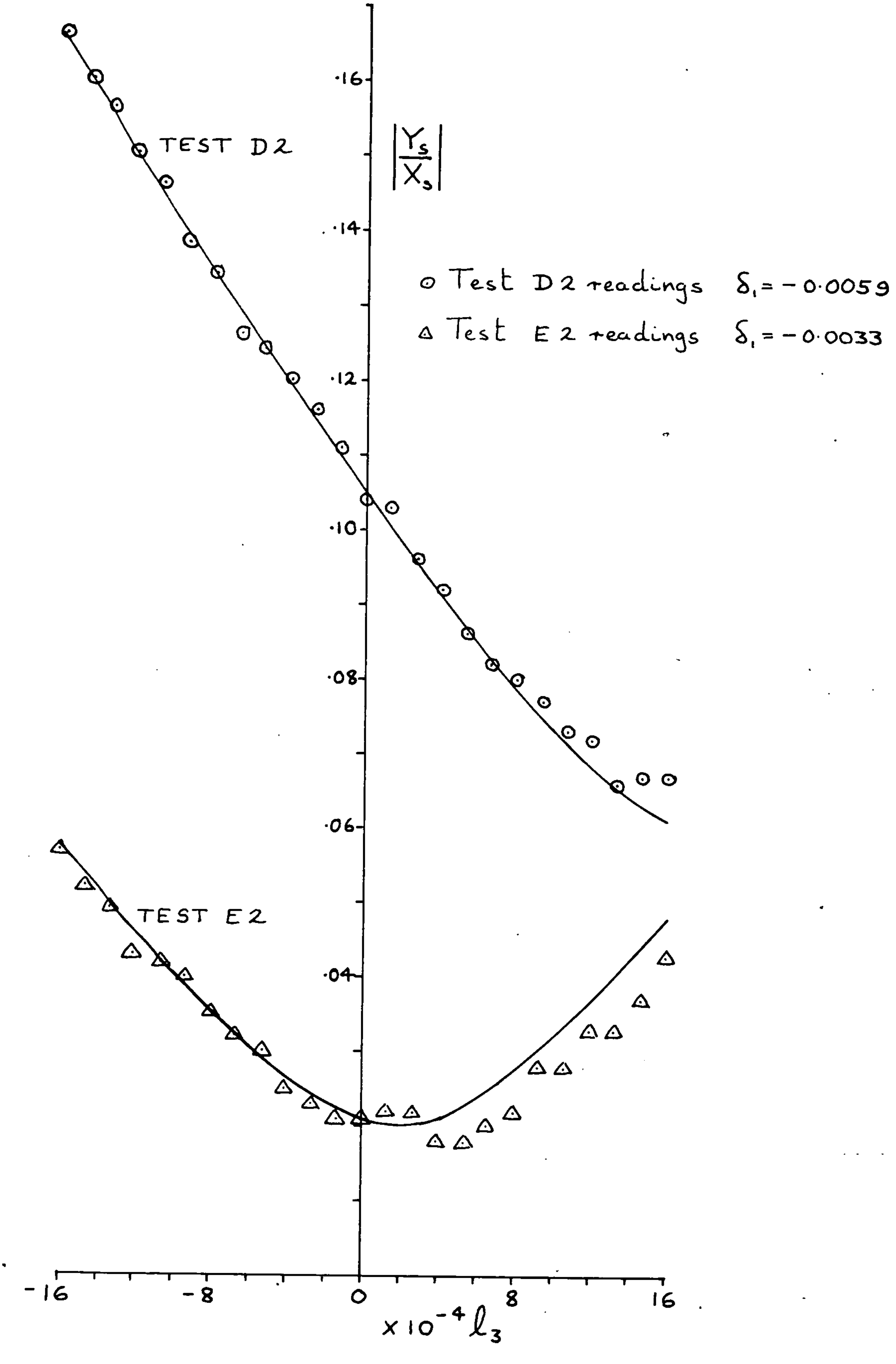

Fig. 6.4.7 Comparison of the experimental readings with the theoretical curves of $\left|\frac{Y_s}{X_s}\right|$ against l_3

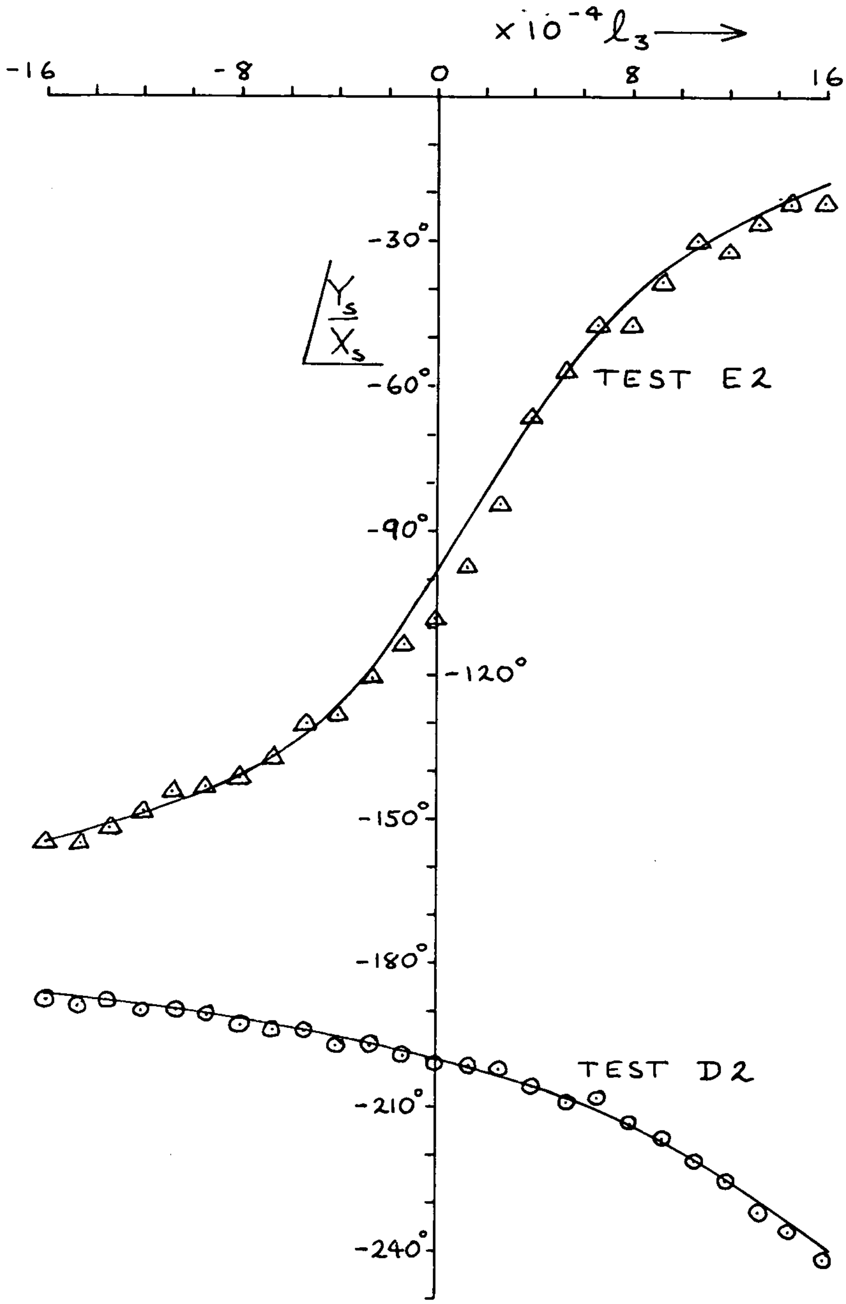

Fig 6.4.8 Comparison of the experimental readings with the theoretical curves of $\angle \frac{Y_s}{X_s}$ with l_3

○ Test D2 readings $\delta_1 = -0.0059$

△ Test E2 readings $\delta_1 = -0.0033$

6.5 Tests F, G, H and J

An interesting point that emerged from tests D and E was the possibility of adjusting the apparatus to give a change in the sign of $(u_s + u_i - \frac{2u_i p_n}{p})$ at a value of p close to resonance. As the maximum slope of the phase angle $\angle \frac{Y_s}{X_s}$ curve as ℓ_3 varies is inversely proportional to this quantity [ref. equations (5.2.6) and (4.6.4)] it must also change sign and become infinite when $p = \frac{2u_i p_n}{u_s + u_i}$.

These tests were aimed at demonstrating this point and investigating the variation in the response of the system with ℓ_3 for four different values of p spanning the change in sign of $(u_s + u_i - \frac{2u_i p_n}{p})$.

The constants for the four tests were:

Test	Excitation period p (secs).	x vibrator current (mA)	$2\lvert X \rvert$ thou. peak to peak
F	0.03071	700	29
G	0.03041	700	30
H	0.03000	700	26.5
J	0.02951	700	22

and the experimental readings and curves for $\left|\frac{Y_s}{X_s}\right|$ and $\angle \frac{Y_s}{X_s}$ for various motor speeds are shown on figures 6.5.1 and 6.5.2 respectively.

The modulus curves all have a minimum at a motor speed of approximately 800 r.p.m. which makes $u_d = -\frac{2 \times 800}{3.75 \times 10^6} = \underline{-4.27 \times 10^{-4}}$

(6.5.1)

this assumes that $p_{n1} \doteqdot 0.0306$ in equation (6.1.1).

For test H the modulus curve is approximately linear and there is a step change in the phase angle which, as $p = 0.03$ secs., indicates that:

$$u_s + u_i = \frac{2u_i p_n}{0.03} \tag{6.5.2}$$

$$\text{i.e. } u_s + u_i - \frac{2u_i p_n}{p} = 2u_i p_n \left(\frac{1}{0.03} - \frac{1}{p}\right)$$

This quantity can now be evaluated for the other three tests and compared with the maximum slope of the phase angle curve $\dfrac{1}{u_i p_n\left(\frac{1}{0.03} - \frac{1}{p}\right)}$ to give $u_i p_n$. Taking the average value:

$$\underline{u_i p_n = 1.3 \times 10^{-3}} \tag{6.5.3}$$

which, substituted in equation (6.5.2) gives:

$$\underline{u_s + u_i = 8.66 \times 10^{-2}} \tag{6.5.4}$$

The remaining constants ζ_1 and p_{n1} are evaluated by comparing the asymptotic slope of the modulus curves, which is $\dfrac{1}{\zeta_1\sqrt{1 + \left(\frac{\delta_1}{\zeta_1}\right)^2}}$ from equation (6.2.5), with the phase angle at $\ell_3 = -\frac{u_d}{2}$ which is, from equation (6.2.6):

$$-180^\circ + \arctan\left(\frac{\zeta_1}{\delta_1}\right) \quad \text{if} \left(u_s + u_i - \frac{2u_i p_n}{p}\right) > 0$$

$$\text{or} \quad \arctan\left(\frac{\zeta_1}{\delta_1}\right) \quad \text{if} \left(u_s + u_i - \frac{2u_i p_n}{p}\right) < 0$$

Averaging for the four tests:

$$\left.\begin{aligned} \zeta_1 &\doteq \underline{0.043} \\ p_{n1} &= \underline{0.0306} \text{ secs.} \\ \text{i.e. } \delta_1 &= \frac{0.0306}{p} - 1 \end{aligned}\right\} \tag{6.5.5}$$

Substituting the values (6.5.1), (6.5.3) and (6.5.5) into equations (6.2.5) and (6.2.6):

Test F : $p = 0.03071$ secs. ; $\delta_1 = -0.00358$

$$\left|\frac{Y_s}{X_s}\right| = \frac{1}{0.086}\sqrt{\frac{4 \times 10^{-6} + (-4.27 \times 10^{-4} + 2\,\ell_3)^2}{1.007}}$$

$$\angle\frac{Y_s}{X_s} = -85^\circ + \arctan\left(\frac{-4.27 \times 10^{-4} + 2\,\ell_3}{2 \times 10^{-3}}\right)$$

Test G : $p = 0.03041$ secs. ; $\delta_1 = +0.00625$

$$\left|\frac{Y_s}{X_s}\right| = \frac{1}{0.086}\sqrt{\frac{1.37 \times 10^{-6} + (-4.27 \times 10^{-4} + 2\,\ell_3)^2}{1.021}}$$

$$\angle\frac{Y_s}{X_s} = -98^\circ + \arctan\left(\frac{-4.27 \times 10^{-4} + 2\,\ell_3}{1.17 \times 10^{-3}}\right)$$

Test H : $p = 0.03$ secs. ; $\delta_1 = +0.02$

$$\left|\frac{Y_s}{X_s}\right| = \frac{\left|-4.27 \times 10^{-4} + 2\,\ell_3\right|}{0.0947}$$

$$\angle\frac{Y_s}{X_s} = -205^\circ \text{ if } \ell_3 < 2.135 \times 10^{-4}$$

$$= -25^\circ \text{ if } \ell_3 > 2.135 \times 10^{-4}$$

Test J : $p = 0.02951$ secs. ; $\delta_1 = +0.037$

$$\left|\frac{Y_s}{X_s}\right| = \frac{1}{0.086}\sqrt{\frac{2.05 \times 10^{-6} + (-4.27 \times 10^{-4} + 2\,\ell_3)^2}{1.74}}$$

$$\angle\frac{Y_s}{X_s} = -131^\circ + \arctan\left(\frac{-4.27 \times 10^{-4} + 2\,\ell_3}{-1.43 \times 10^{-3}}\right)$$

$$= \; -311^{\circ} - \arctan\left(\frac{-4.27 \times 10^{-4} + 2\,\ell_3}{1.43 \times 10^{-3}}\right)$$

These curves are plotted against ℓ_3 on figures 6.5.3 and 6.5.4 which also show the experimental points demonstrating reasonable agreement, particularly in the case of the phase angle curves. The effect of $(u_s + u_i - \frac{2u_i p_n}{p})$ on the phase angle curves can clearly be seen with the slope becoming infinite at $p = 0.03$ secs. and then changing sign.

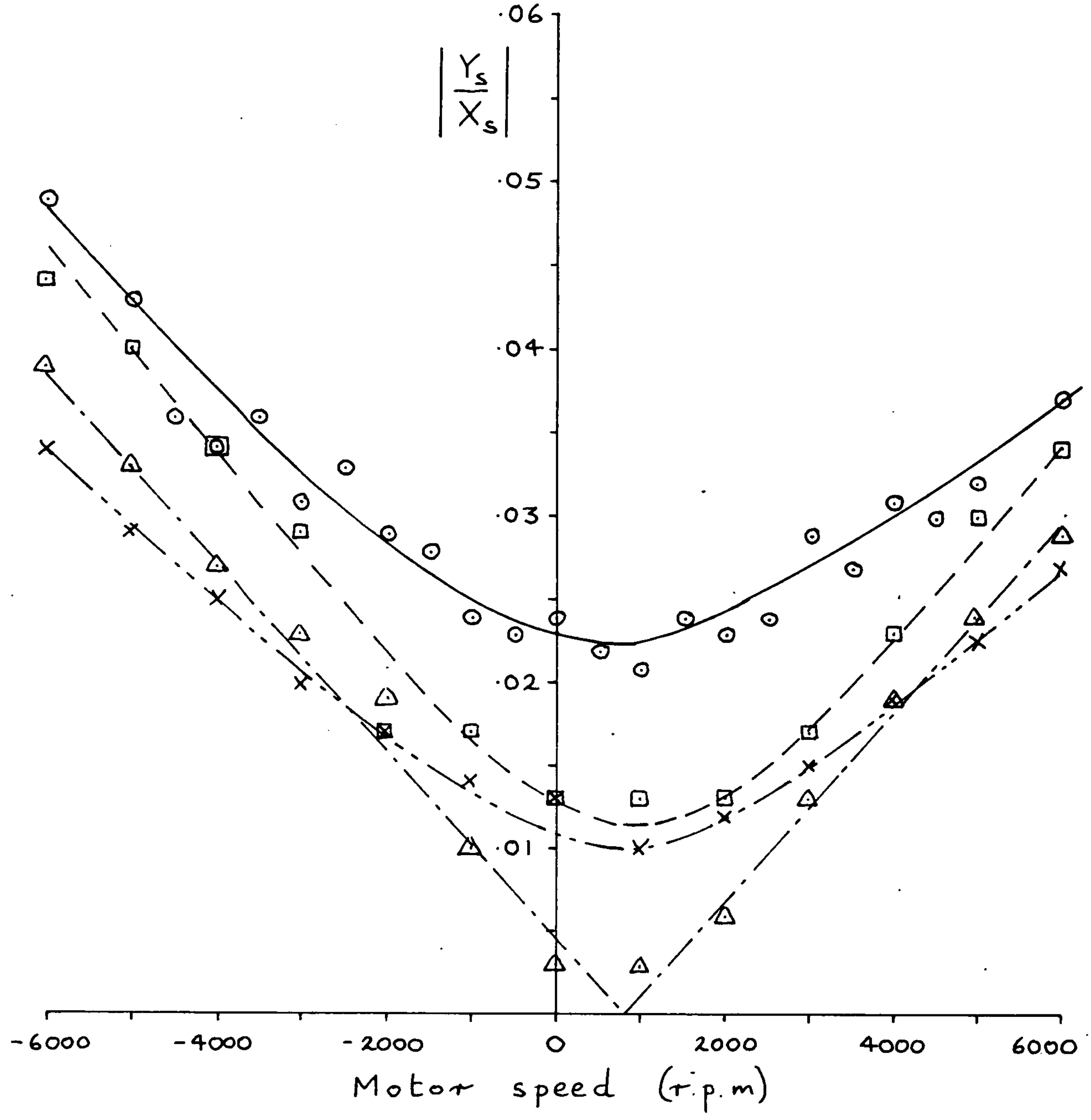

Fig 6.5.1 Experimental variation of $\left|\frac{Y_s}{X_s}\right|$ with motor speed (r.p.m) $[= 1920 \times \text{table speed} = 3{\cdot}75 \times 10^6\, l_3]$ for various values of p : x vibrator current 700 mA

⊙ Test F readings p = 0·03071 secs.

⊡ Test G readings p = 0·03041 secs.

△ Test H readings p = 0·03000 secs.

× Test J readings p = 0·02951 secs.

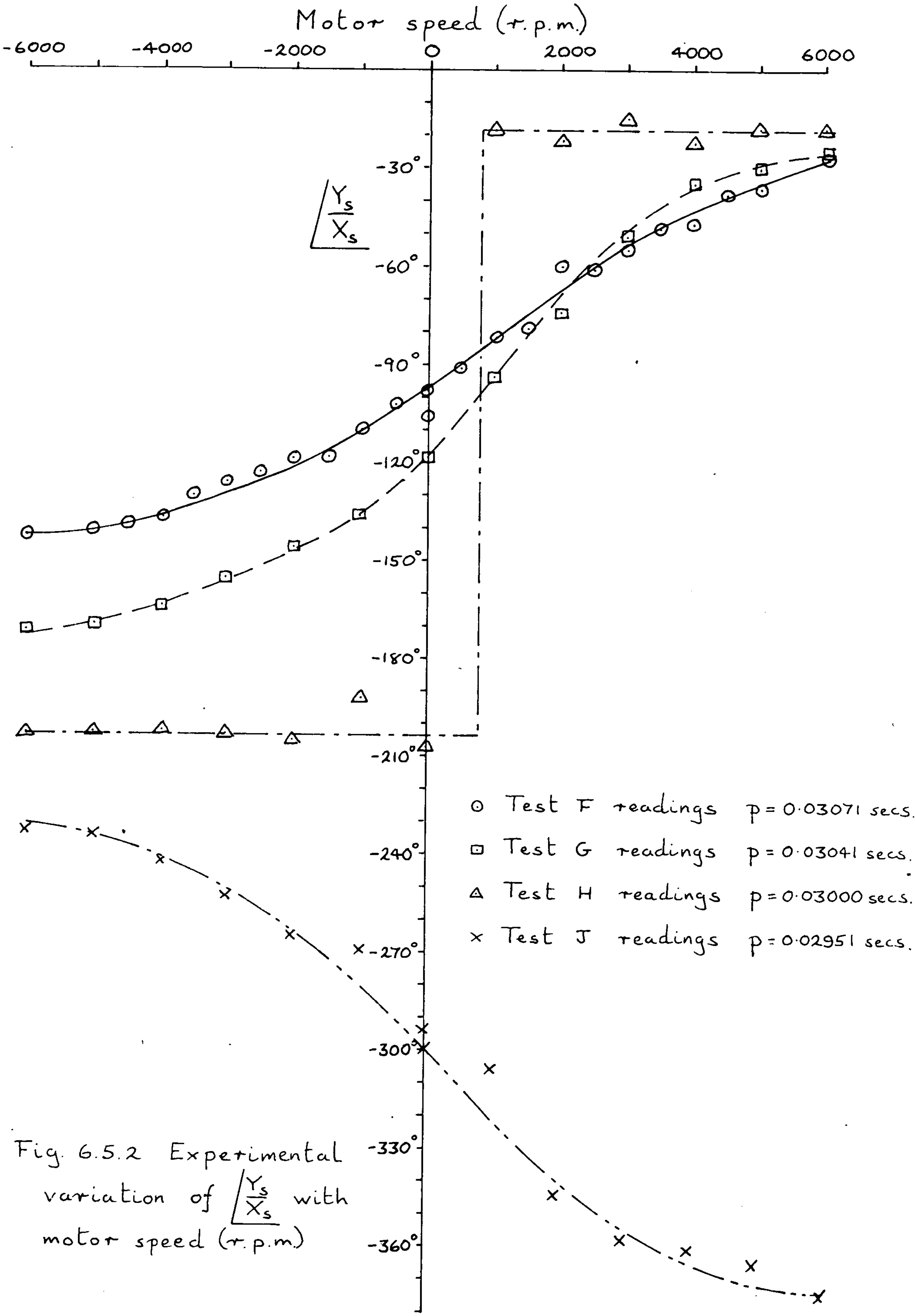

Fig. 6.5.2 Experimental variation of $\angle \frac{Y_s}{X_s}$ with motor speed (r.p.m.)

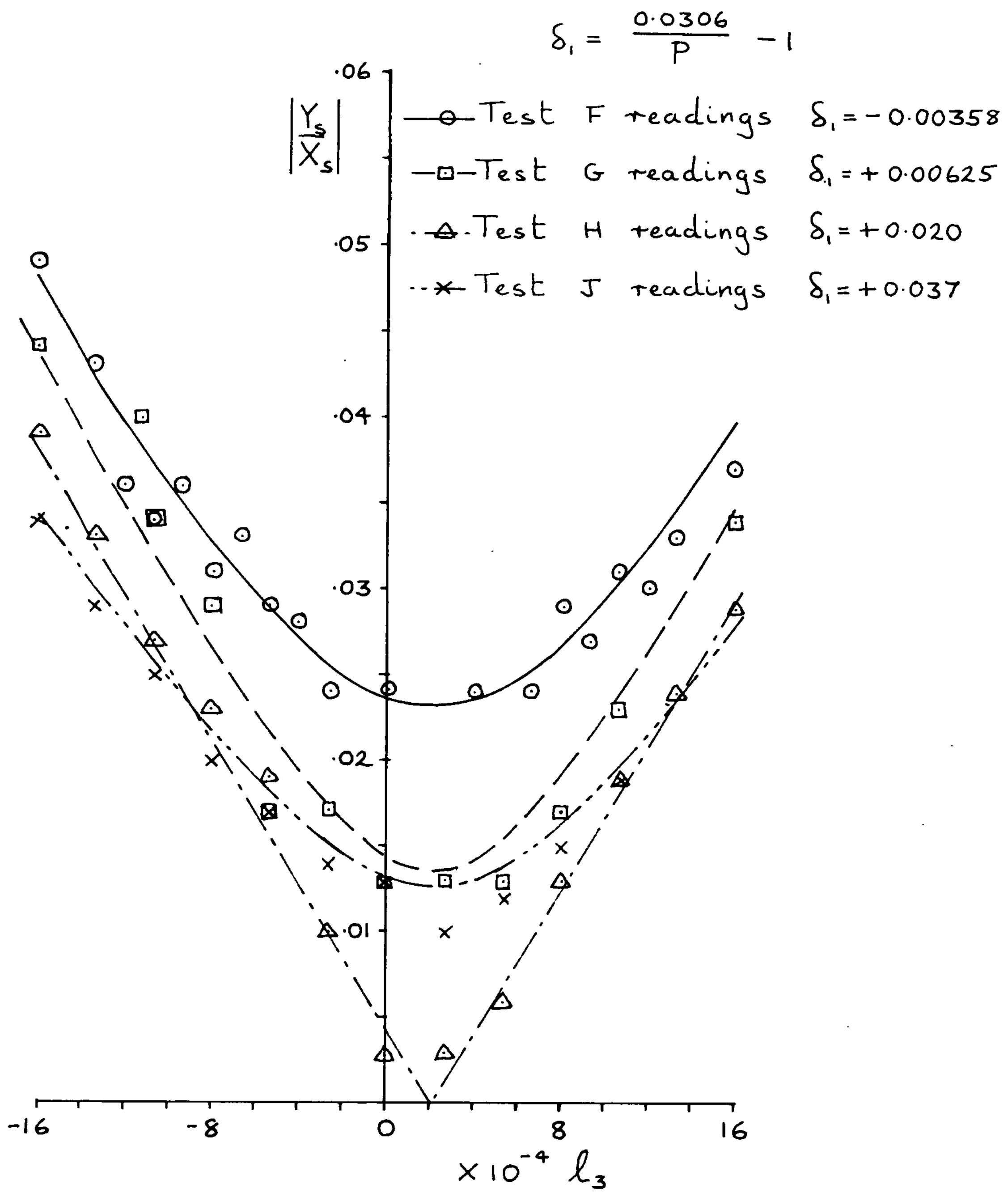

Fig. 6.5.3 Comparison of the experimental results of $\left|\frac{Y_s}{X_s}\right|$ against l_3 with the theoretical curves for

$\zeta = 0.043$ and $u_i p_n = 1.3 \times 10^{-3}$

$u_d = -4.27 \times 10^{-4}$

$u_s + u_i = 8.66 \times 10^{-2}$

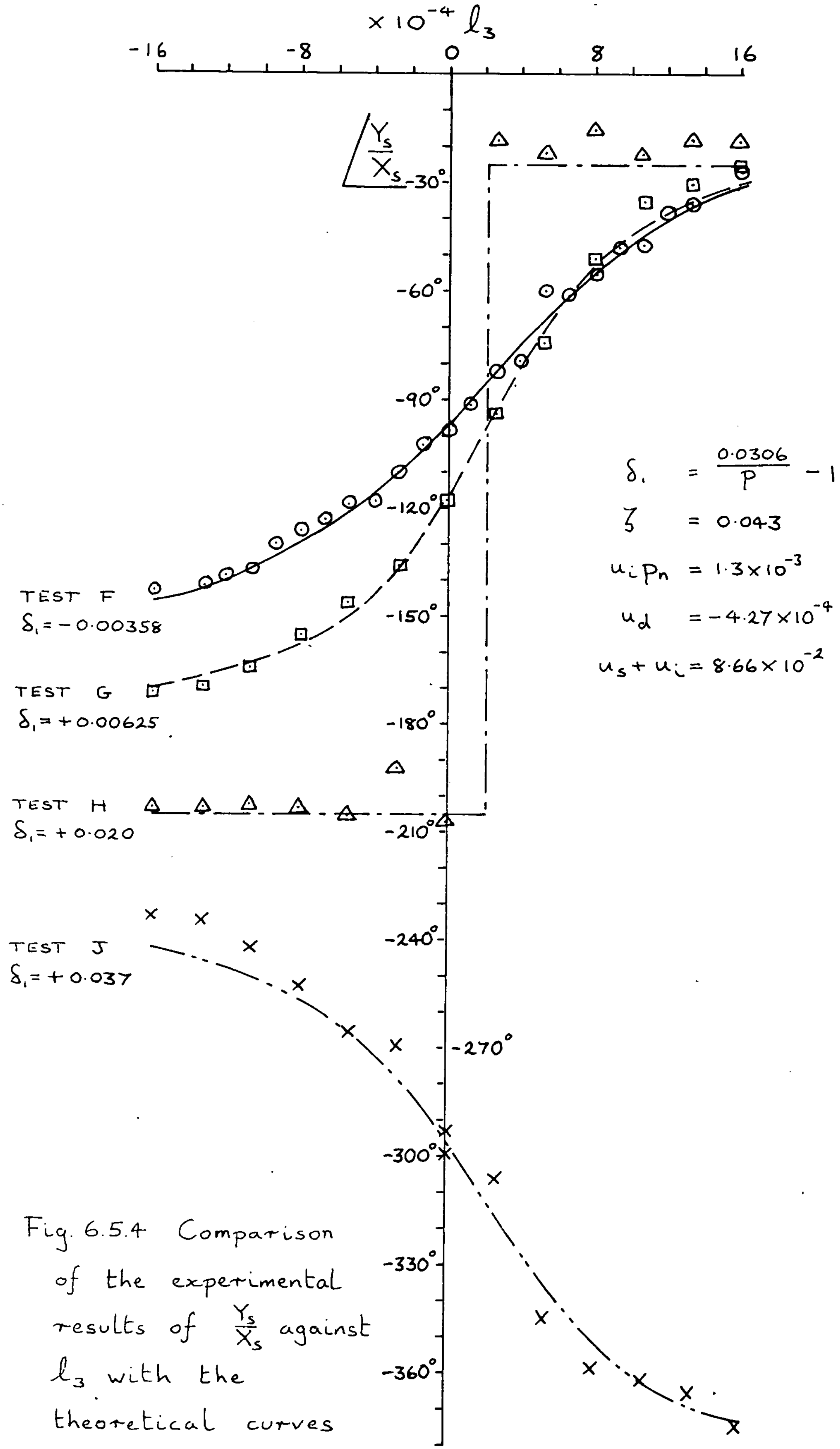

Fig. 6.5.4 Comparison of the experimental results of $\frac{Y_s}{X_s}$ against l_3 with the theoretical curves

6.6 Comments on the experimental results

Different values of damping ratio and natural frequency in the directions Ox and Oy cannot be detected from the experimental results, which determine $(u_s + u_i)$ and $u_i p_n$, however, for particular values of u_s and u_i, the value of p_n obviously affects the performance of the system. Comparing the values of u_s, u_i, u_d, p_n and ζ_1 for tests D, E and F to J by assuming that $p_n = p_{n1}$ gives the following table :

Test	$p_n = p_{n1}$ (secs).	ζ_1	u_s	u_i	u_d
D	0.0306	0.023	4.94×10^{-2}	5.26×10^{-2}	-4.06×10^{-3}
E	0.0307	0.0328	4.0×10^{-2}	3.9×10^{-2}	-3.56×10^{-4}
F–J	0.0306	0.043	4.41×10^{-2}	4.25×10^{-2}	-4.27×10^{-4}

The only alteration made between these series of tests was in the orientation of one of the dampers; the oil and its level were the same in each case and the changes in the value of ζ_1 are presumably due to the differing temperatures in the laboratory. As expected the values of p_{n1} are virtually the same in each case and u_s and u_i are of the same order, the small differences here presumably being due to the different orientations as the small size of the oil vessels, in relation to the moving rods, must have a slight effect on the inertia and stiffness coupling as well as altering the damping coupling.

The presence of damping and stiffness coupling in the experimental system is to be expected but the reason for the inertia coupling is not quite so obvious; the probable explanation is that an unbalance in the mass causes torsional oscillations in phase with the displacement oscillations, these torsional oscillations would then produce forces in the quadrature direction proportional to the linear acceleration.

All the experimental tests were carried out with the natural frequency of the system at around 32 Hz; this frequecny was chosen by trial and error at it was high enough to give stable oscillations and low enough to give a reasonably large amplitude with the spring system linear. The tendency for the system to go unstable at resonance mentioned in test A was not encountered when the damping was raised, this is to be expected since increased damping will reduce the chance of parametric instability.

In general the experimental results fit in very well with the theoretical curves that were developed, any scatter or discrepancy is probably due to small temperature changes in the laboratory which, as has been shown, must have an effect on the damping ratio.

No attempt was made to increase the damping to that which might be required in a practical instrument; as has been stated previously, the object of the experiments was not to produce a practical instrument but to demonstrate the validity of the theoretical equations that were developed in chapters 3 and 4. The good agreement between the experimental and theoretical results confirms the validity of the theory and therefore the fact that the shape of the phase angle curve as ℓ_3 varies is independent of damping. The two alternative methods of employing the y vibrator have been demonstrated, in particular the more attractive method of maintaining the oscillations in one plane and determining the angular velocity from the magnitude and phase relationships between the currents supplied to the two vibrators.

CHAPTER 7

Conclusions

7.1 Summary

The majority of this thesis has been concerned with a fundamental type of vibratory rate sensing device and the theory has been developed in chapters 3 and 4; the steady state and transient response of the system to rotation and acceleration have been considered with the main concentration, in chapter 4, on the response to rotation about the input axis Oz. The possibility of using the phase angle $\angle\frac{Y}{X}$ to measure very small rates of turn, when the variation in the modulus $\left|\frac{Y}{X}\right|$ is negligible, suggests a way of improving the sensitivity of the system. This improved sensitivity can be achieved without affecting the transient response as the shape of the phase angle curve is independent of the damping ratio ζ. A possible method of determining the required system parameters has already been discussed in section 4.7.

The other important concept that has been developed is the method of turning the system into a "null" device by employing an additional vibrator in the direction Oy, in order to maintain the vibrations in the one plane Ozx; the magnitude ratio and the phase angle between the two vibrator currents should provide a read-out that can easily be converted to give the rate of turn.

The experimental tests carried out, which are described in chapter 6, indicated a reasonable agreement between theory and practice; some deviation is only to be expected in a very simple piece of apparatus. Considerable improvement in the accuracy of the device would undoubtedly result from a better method of construction and, in particular, from operating it in a constant temperature environment.

7.2 Considerations in developing a practical instrument

The type of instrument that was constructed suffers from the possible disadvantage of being unbalanced overall as this will induce sinudoidal oscillations of the complete instrument at the operating frequency. The errors that will result have been determined in sections 3.7 and 3.8; sinusoidal variation in $\bar{\Omega}$ at frequency $\omega' = \omega \div \omega_n$ will give output oscillations due to $\Omega'_1 \, \Omega'_2$ and may possibly cause instability (see section 3.7); sinusoidal variation in the acceleration $\bar{A}$ at frequency $\omega \div \omega_n$ will give output oscillations due to A_1 and A_2 [cf. equations (3.8.1)].

The sinusoidal variations in $\bar{\Omega}$ may have been the cause of the instability noted in test A but otherwise any errors due to overall unbalance in the experimental device were too small to have any detectable effect. However in attaining the sensitivity that would be required from a practical instrument these errors may become significant and a balanced system may be required.

The adjustment of the magnitude and phase of the current supplied to the y vibrator would have to be carried out automatically if it was desired to operate a practical system as a "null" device. As there are two quantities that have to be controlled by measuring the y vibration amplitude in order to reduce it to zero, a digital controller employing a hill climbing technique (altering magnitude and phase alternately) would probably be required; this type of controller could also be made to give a read-out of the rate of turn by comparing the magnitude and phase relationships of the vibrator current with the known system characteristics.

Fig. 7.2.1 shows schematically a possible arrangement for a balanced rate of turn indicator. Two identical sensitive elements, similar to the one on which the tests were carried out, are mounted back to back so that they vibrate in the same plane. The vibrations of the two masses A and B are controlled at the same amplitude and frequency, and 180° out of phase; this control could be achieved as shown by taking mass A as a reference and exciting it with the x vibrator (probably an electromagnet) fed from an oscillator via a fixed gain amplifier, the mass B is excited by another x vibrator in a similar manner except that the amplifier gain and phase are controlled to reduce to zero the difference between the feedback signals from the two x pick-offs. The vibrations are maintained in the one plane Ozx by feeding the y pick-off signals into phase and gain controllers which supply the current to the y vibrators. The phase and gain controllers also measure the rate of turn which can be averaged between the two values to give the necessary read-out. The system would have to be damped in the x direction and two possible ways of doing this are by using eddy currents or by applying additional excitation proportional to $\dot{x}$ (measured by the x pick-offs) in the x direction.

It is quite possible that the tuning fork may still be the best answer for a practical balanced system and this could be operated in precisely the same manner. The equations of motion derived for a tuning fork will be similar to the general equations derived in chapter 3 for the fundamental system; in addition to the usual tuning fork equation equating the torques about its input axis there will be an equation equating the exciting force applied to the tines with the forces in the same direction due to the motion of the system. If the fork is to be used as a "null" device the fork would be prevented from oscillating about its input axis by a torque motor, the phase and gain of the current supplied to it giving the required rate of turn.

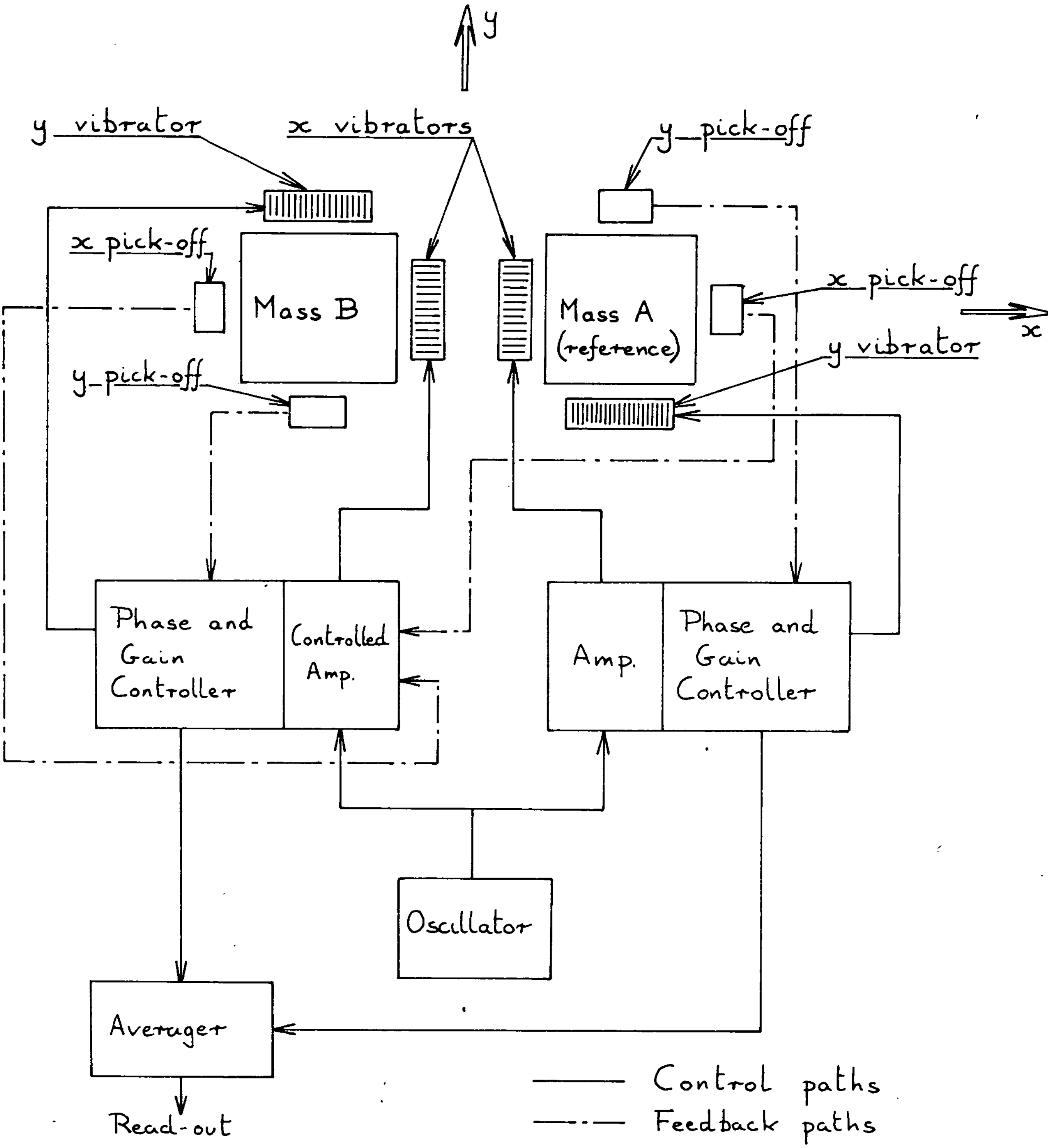

Fig. 7.2.1 A suggested lay-out for a practical rate of turn indicator

PRINCIPAL NOTATION

1	subscript referring to direction Ox
2	" " " " Oy
3	" " " " Oz
$\bar{a}$	$= a_1\bar{i} + a_2\bar{j} + a_3\bar{k}$ absolute acceleration of m with O fixed
$\bar{A}$	$= A_1\bar{i} + A_2\bar{j} + A_3\bar{k}$ absolute acceleration of O
c	viscous damping coefficient
c_d	damping coupling coefficient
c_i	inertia " "
c_s	stiffness " "
$\bar{i},\bar{j},\bar{k}$	unit vectors along Ox, Oy, Oz
j	$= \sqrt{-1}$
k	spring constant
$\bar{\ell}$	$= \ell_1\bar{i} + \ell_2\bar{j} + \ell_3\bar{k} = \frac{\Omega_1}{\omega_n}\bar{i} + \frac{\Omega_2}{\omega_n}\bar{j} + \frac{\Omega_3}{\omega_n}\bar{k}$
ℓ_{31}	$= \frac{\Omega_3}{\omega_{n1}}$; $\ell_{32} = \frac{\Omega_3}{\omega_{n2}}$
m	point mass
Oxyz	rectangular set of axes, origin O
p	$= \frac{2\pi}{\omega}$ excitation period (secs)
p_n	$= \frac{2\pi}{\omega_n}$ undamped natural period
P	amplitude of the exciting force
$\bar{r}$	$= x\bar{i} + y\bar{j} + z\bar{k}$ position vector of m
r	$= \frac{\omega}{\omega_n}$ non-dimensional frequency ratio
t	time (secs)
u_d	$= \frac{c_d}{\omega_n m}$ non-dimensional damping coupling
u_i	$= \frac{c_i}{m}$ " " inertia "

u_s	$= \frac{c_s}{\omega_n^2 m}$ non-dimensional stiffness coupling
x, y, z	rectangular coordinates of $\bar{r}$
$\|X\|$	amplitude of forced vibrations in direction Ox
$\|Y\|$	" " " " " " Oy
$\angle\frac{Y}{X}$	phase lead between the y and x forced vibrations
X_s	$= \frac{P_1}{k_1}$ deflection along Ox due to a static force P_1
Y_s'	$= \frac{P_2}{k_2}$ " " Oy " " " " " P_2
Y_s	$= Y_s' e^{j\psi}$
$\left\|\frac{Y_s}{X_s}\right\|$	$= \frac{Y_s'}{X_s} = \frac{k_1}{k_2}\left(\frac{P_2}{P_1}\right) \doteqdot \frac{P_2}{P_1}$ if $k_1 \doteqdot k_2$
$\angle\frac{Y_s}{X_s}$	$= \psi$ phase lead between the y and x exciting forces
δ	$= r - 1$
ζ	$= \frac{c}{2\sqrt{mk}}$ damping ratio
λ	root of a characteristic equation
ψ	$= \angle\frac{Y_s}{X_s}$
ω	excitation frequency (rads./sec)
ω_n	$= \sqrt{\frac{k}{m}}$ undamped natural frequency
ω'	frequency of oscillation of $\bar{\Omega}$
$\bar{\Omega}$	$= \Omega_1\bar{i} + \Omega_2\bar{j} + \Omega_3\bar{k}$ angular velocity of Oxyz
$\bar{\Omega}'$	$= \Omega_1'\bar{i} + \Omega_2'\bar{j} + \Omega_3'\bar{k}$ amplitude of oscillation of $\bar{\Omega}$

BIBLIOGRAPHY

ARNOLD, R.N. and MAUNDER, L. — Gyrodynamics and its engineering applications. Academic Press 1961.

BARNABY. R.E. CHATTERTON, J.B. and GERING, F.H. — General Theory and Operating Characteristics of the Gyrotron Angular Rate Tachometer. Aeronautical Engineering Review, 1953, 12 No: 11 p.24

BUSH, R.W. and NEWTON, G.C. — Reduction of errorsin vibratory gyroscopes by double modulation. IEEE Trans. on Automatic Control AC-9. 4. p.525 October 1964.

CHATTERTON, J.B. — Some general comparisons between the vibratory and conventional rate gyro. J. of Aeronautical Science. p.33 Sept.1955.

COCHIN, I. — Analysis and Design of the Gyroscope for Inertial Guidance. Wiley 1963.

ETTZEROGLOW, H. — Non-classical gyroscopes : Pt 3 - Vibratory gyros (in French). Doc Air-Espace Vol 86 May 1964.

FEARNSIDE, K. and BRIGGS, P.A.N. — The Mathematical Theory of Vibratory Angular Tachometers. Proc.IEE. Vol.105 C p.155, 1958.

HOBBS, A.E.W. — Some sources of error in the tuning fork gyroscopes. R.A.E Farnborough Tech.Note I.A.P. 1139 April 1962.

HOBBS, A.E.W. — The A5 tuning-fork gyro as a single axis rate and angle detector. R.A.E. Farnborough Tech.Note I.E.E. 34 Sept. 1963.

HUNT, G.H. — The mathematical theory of the output torsion system of tuning-fork gyroscopes. R.A.E. Farnborough Tech.Note I.E.E. 15 Jan. 1963.

HUNT, G.H. — A brief description of tuning-fork gyroscopes No. A5. R.A.E. Farnborough Tech.Note I.E.E. 12 Dec. 1962.

HUNT, G.H. — Damping of the torsion stem of a tuning fork gyroscope. R.A.E. Farnborough Tech.Note I.E.E. 8 October 1962.

HUNT, G.H. and HOBBS, A.E.W. — Development of an accurate tuning-fork gyroscope. Symposium on Gyros. I.Mech.E. Feb. 1965.

HUNT, G.H. and HOBBS, A.E.W. — Some notes on torsion oscillator gyroscopes. R.A.E. Farnborough Tech.Note I.E.E. 32 June 1963.

LANGFORD, R.C. — Unconventional Inertial Sensors. A.I.A.A.Prep; (65-401) 1965

LYMAN, J. — A new rate sensing instrument. Aeronautical Engineering Rev. 1953, 12 No. 11 p.24.

McLEAN, R.F. — An investigation of the characteristics of vibratory rate gyroscopes. M.Sc. Thesis Edin. Univ. 1961

MATHEY, R. — Contribution to the improvement of vibratory gyros: pt.1 - Early development and theory (in French). Doc-Air-Espace Vol.92 May 1965.

MATHEY, R. — Contribution to the improvement of vibratory gyros: pt.2 - Technology and Development at C.S.F. (in French). Doc-Air-Espace Vol. 94 Sept. 1965.

MEREDITH, F.W. — Improvement in or relating to devices for detecting or measuring rate of turn. 1942. U.K. Prov.Patent.Spec. No. 12539/42.

MEREDITH, F.W. — Control of Equilibrium in the Flying Insect. Nature, 1949, 163, p.74.

MORROW, C.T. — Steady State Response of the Sperry Rate Gyrotron. J.Accoust.Soc.Am. January 1955 p.56.

MORROW, C.T. — Response of the Sperry Rate Gyrotron to Varying Rates of Turn. J.Accoust.Soc.Am. January 1955 p.62.

MORROW, C.T. — Zero signals in the Sperry Tuning Fork Gyrotron.
J.Accoust.Soc.Am. 1955. 27 No.3 p.581.

NEWTON, G.C. — Theory and Practice in Vibratory Rate Gyros.
Control Engineering Vol. 10 No.6. June 1963 p. 95.

NEWTON, G.C. — Comparison of Vibratory and Rotating Wheel Gyroscopic Rate Indicators.
Trans. A.I.E.E. Vol.79.II. 1960, p.143.

NEWTON, G.C. — A Vibratory rate gyroscope based on interaction of sonic waves.
I.E.E.E.Trans. on Automatic Control AC-10, 3 p.235 July 1965.

PITT, R.J. — Some performance details of a prototype tuning-fork gyroscope, serial no.K.H.1
R.A.E. Farnborough Tech.Note I.E.E. 10 November 1962.

PRINGLE, J.W.S. — The Gyroscopic Mechanism of the Halteres of the Diptera.
Phil.Trans.Roy.Soc. B. Vol.233 1948.

SLATER, J.M. — Inertial Guidance Sensors.
Reinhold 1964.

SLATER, J.M. — Exotic Gyros - What they offer, where they stand: pt. 1.
Control Engineering Vol.9(11) Nov. 1962 p.92

STRATTON, A. — Gyroscopes for Inertial Naviagtion.
Proc. I. Mech. E. Vol. 178 pt.1 p.1129 1964.

STRATTON, A. and HUNT, G.H. — The sensitivity of vibratory gyroscopes to acceleration.
R.A.E. Farnborough Tech.Note I.E.E.19 March 1963.

WOINOWSKY - KRIEGER, S. — The effect of an axial force on the vibration of hinged bars.
Trans.A.S.M.E. J.Appl.Mech. 1950 p.35.